

MATERIALS CHEMISTRY

FRONTIERS



CHINESE
CHEMICAL
SOCIETY
中国化学会



ROYAL SOCIETY
OF CHEMISTRY

rsc.li/frontiers-materials

REVIEW

[View Article Online](#)
[View Journal](#) | [View Issue](#)



Cite this: *Mater. Chem. Front.*,
2023, 7, 3820

Progress of electrocatalytic urea synthesis: strategic design, reactor engineering, mechanistic details and techno-commercial study

Sourav Paul, Ashadul Adalder and Uttam Kumar Ghorai *

The industrial production of urea is a two step process, involving the reaction of nitrogen and hydrogen to form ammonia followed by the reaction of ammonia with carbon dioxide, so the process is a capital expensive, energy consuming and complex synthesis technique with multiple cycles to increase the production efficiency. On the other hand, electrocatalytic C–N coupling reaction to specifically produce urea by simultaneous activation followed by co-reduction of carbon dioxide (CO_2) and nitrogen sources (N_2 , NO_2^- or NO_3^-) under ambient conditions presents a sustainable and eco-friendly alternative route for urea production by a single step process. However, there are several challenges like adsorption capabilities of the reactants on the substrates followed by activation, vital interaction of the catalyst with intermediates, suppression of the hydrogen evolution reaction and finally effective C–N bond formation to specifically produce urea. In this work we showcase the road map of the electrocatalytic green urea production, with concise yet precise discussion on potential electrocatalysts, electrochemical reactor engineering, mechanistic insight into urea synthesis, and a techno-commercial study and finally conclude with the future prospects of green urea production.

Received 21st April 2023,
Accepted 24th June 2023

DOI: 10.1039/d3qm00433c

rsc.li/frontiers-materials

Department of Industrial and Applied Chemistry, Swami Vivekananda Research Centre, Ramakrishna Mission Vidyamandira, Belur Math, Howrah 711202, India.
E-mail: uttam.indchem@vidyamandira.ac.in, uttaminchem00@gmail.com



Sourav Paul

senior research fellow in the group of Professor Ghorai. His research focuses on the development of two-dimensional nanomaterials for the production of energy and the fixation of nitrogen through the electrocatalytic route.

Mr Sourav Paul was born in Kolkata. He obtained his BSc and MSc degree in industrial chemistry and applied chemistry from Ramakrishna Mission Vidyamandira, University of Calcutta, India, in 2015, and 2017 respectively. Thereafter, he graduated in 2019 with an MTech in Rubber Technology from IIT Kharagpur. For a brief period he was employed as a research associate in the PFIC, Aditya Birla Group. Presently, he is a



Ashadul Adalder

Ashadul Adalder received his MSc in Applied Chemistry from Ramakrishna Mission Vidyamandira, University of Calcutta, India, in 2018. Then he obtained his MTech in Metallurgical Engineering & Materials Science from IIT Bombay. He is presently working as a research fellow in Professor Ghorai's group. His research focuses on 1D–2D hybrid nanomaterials for electrochemical nitrogen and carbon dioxide fixation.

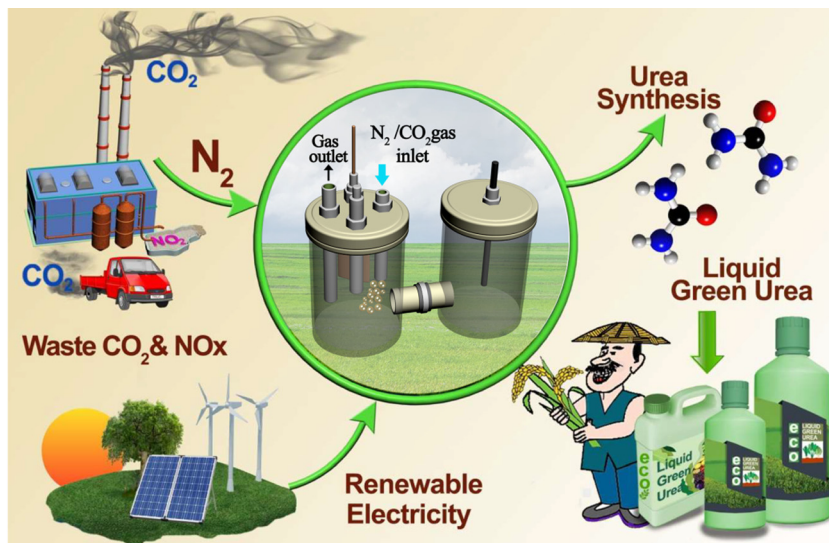


Fig. 1 Various routes for electrochemical urea synthesis via simultaneous carbon dioxide reduction and nitrogenous substrate reduction (N₂ or NO_x).

acidification of water bodies.^{1,2} However the bane can be turned to a boon by converting the carbon dioxide into value added products *via* biological conversion,^{3,4} chemical transformation,^{5,6} chemical–biological hybrid strategies,⁷ electrocatalytic reduction^{8–12} and photocatalytic processes.^{13–17} Recently, carbon dioxide reduction (CO₂RR) has been attracting the attention of the research community due to various factors like: (1) the products generated from electrocatalytic CO₂RR, including hydrocarbons (C₁ methane, C₂ ethene, ethane, C₂₊ products, *etc.*), formic acid, carbon monoxide, acetate, and alcohols (methanol, ethanol, *n*-propanol, *etc.*), are either important chemicals having industrial utility or fuels, which can be used in vehicles, (2) the electrical energy which is used for CO₂RR can be obtained from alternate sources of energy

(like wind, solar, geo-thermal, *etc.*), so it reduces the overall carbon footprint, and (3) the electrocatalytic process of CO₂RR operates under mild conditions and it can be easily controlled, hence it has less process complexity and can be scaled up quite easily.^{18–20} However, the CO₂RR process still suffers from the lack of efficient electrocatalysts, poor energy efficiency, low reaction rate and generation of multiple products and hence from low selectivity. So, to accelerate the field of CO₂RR electrocatalysis, researchers are striving to increase the energy efficiency and selectivity of product formation. To increase the utility of the chemicals produced during CO₂RR, different electrocatalytic coupling reactions can be carried out, to form important classes of compounds like aldehydes, ketones, amides, *etc.* Among them, C–N coupling reactions hold a special place in research owing to the utilization of CO₂ and conversion of nitrogenous compounds (N₂, NO₂[−] or NO₃[−])^{21–23} Although nitrogen is present in abundance in the atmosphere (78%) it cannot be directly utilized by flora and fauna species;^{24,25} there are other nitrogen sources like nitrites and nitrates which are groundwater pollutants, wreaking havoc on human health.²⁶

The strategy to form C–N bonds can provide solutions to a few issues like the energy crisis, carbon footprint reduction and ensuring environmental sustainability, as depicted in Fig. 1. The most desired product produced by this technique is urea, a key player in the fertilizer industry with 155 million tons of global annual production,²⁷ and also having a multi-purpose application in resin synthesis (urea–melamine–formaldehyde),²⁸ pharmaceutical products specifically barbiturates,²⁹ the dermatological industry,³⁰ and reduction of NO_x impurities produced from diesel run vehicle engines.³¹ As urea has a massive impact on the efficient running of modern civilized society, leveraging efficient, sustainable and reliable functioning of urea production is a matter of utmost importance. Presently, industrial production of urea involves preparation



Dr Uttam Kumar Ghorai is an assistant professor at Rama-krishna Mission Vidyamandira, India. He was elected as the Associate of the Indian Academy of Sciences (in 2021), and Young Associate of the Indian National Academy of Engineering (in 2019). He received the Young Engineer Award in 2019 from the Indian National Academy of Engineering, the Young Scientist Platinum Jubilee Award in 2020 from the National Academy of

Sciences, and the BRICS Young Innovator Prize in 2022. His research focuses on the development of catalysts and functional materials for the electrocatalytic production of green ammonia, green urea, and nitric acid.

of ammonia using the Haber–Bosch process followed by the reaction of the produced ammonia with carbon dioxide at high temperature and pressure;³² hence it is a capital expensive, massive energy consuming and complex synthesis process involving multiple cycles to increase the production efficiency of urea. Thus from the sustainability viewpoint the urea production process helps to increase the carbon footprint by burning a humongous amount of fuels; there is already enough evidence that climate change is a huge threat to all life forms, as it approaches the tipping point ensuring irreversible climate change and we need to act in a fast and serious manner.³³ The United Nations Emissions Gap Report of 2020 revealed that the average greenhouse gas emissions increased by 2.6% in 2019 despite the decrease in CO₂ emission by 7% caused by the COVID-19 pandemic and the effect will not outlast 2030 if the entire world does not financially integrate the decarbonization strategy into the existing system.³⁴ Therefore significant research has been carried out to reduce the carbon footprint by developing an energy efficient, economical and environmentally friendly method to produce urea using electrochemical processes,^{22,23,35–37} which generally involve the simultaneous reduction process of carbon dioxide (CO₂RR) and nitrogen sources (NRR).^{9,10,38–52} However, there exist a number of hurdles in the progress of electrochemical urea production which need to be resolved, and these are as follows: (a) the adsorption of the reactants (N₂ and CO₂) to the surface of the electrocatalyst is of a very feeble nature,^{36,37,53} (b) the simultaneous reduction processes (N₂ and CO₂) often compete against one another which results in various types of product formation (like acetamide) other than urea,^{54,55} (c) higher overpotential (difference between the applied potential at the electrode and the thermodynamic potential of CO₂RR at a particular current density) required to cleave the extremely stable N≡N and C=O bonds,⁵⁶ and (d) effectively suppressing the competing HER.^{35–37,57}

In this article, we concisely present the inception and the continuous steady growth of electrochemical green urea

synthesis. The following critical attributes are focused on and thoroughly reviewed; detailed mechanistic insights, understanding the possible reaction pathways, classification of the potential electrocatalysts with decent performance (good urea yield and faradaic efficiency), strategies to suppress the competing reactions, advancement of various types of electrochemical cells, techno-commercial analysis, and the future prospects of electrochemical green urea production.

2. Theoretical advancement and mechanistic insight

2.1 Thermodynamic aspects of N₂ and CO₂ molecules

As the nitrogen molecule is inert in nature it is really difficult to activate nitrogen due to the following reasons: (1) the N≡N triple bond has an exorbitant bond energy of 941 kJ mol⁻¹, so the bonds in N₂ are very difficult to break. Another important aspect is, although acetylene (C₂H₂) has a similar triple bond energy of 962 kJ mol⁻¹, the first bond breaking energy of N₂ is approximately 410 kJ mol⁻¹, which is almost double the first bond breaking energy of C₂H₂ (222 kJ mol⁻¹). Therefore, acetylene has higher reactivity while nitrogen is inert.⁵⁸ (2) Another reason for nitrogen being inert is its non-polar nature along with a high ionization potential (15.58 eV).⁵⁹ (3) The energy difference between the highest occupied molecular orbital (HOMO) and the lowest unoccupied molecular orbital (LUMO) of nitrogen is about 10.82 eV (Fig. 2),⁵⁹ so the electrons would be reluctant to enter the antibonding orbital of the nitrogen molecule. (4) Finally, the nitrogen molecule's affinity towards protons is only 493.8 kJ mol⁻¹; hence the process of hydrogenation is difficult even in the presence of strong acid.

The proton coupled multi-electron assisted nitrogen reduction reactions (NRR) are shown (Table 1) with the equilibrium potentials necessary for various NRR products with either

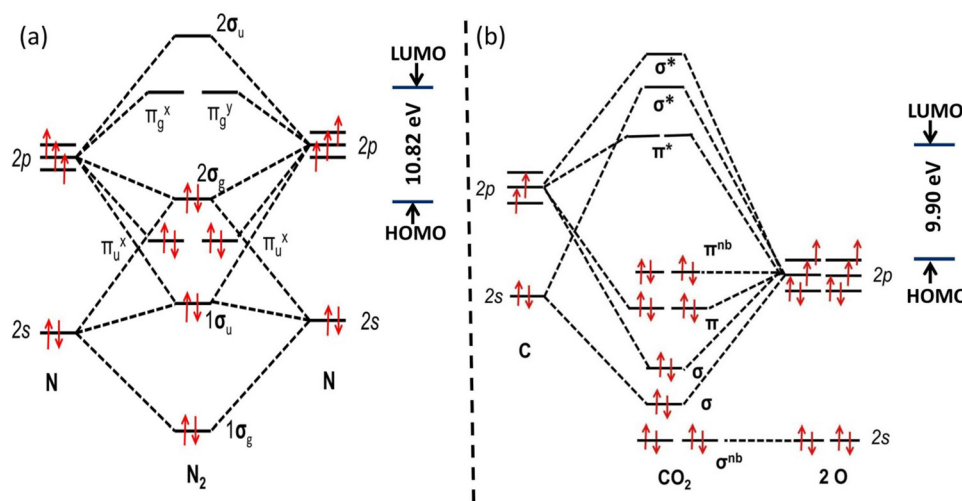


Fig. 2 Molecular orbital diagram of the nitrogen molecule and carbon dioxide molecule (the energy gap of the HOMO and the LUMO is provided for both the molecules).

Table 1 Energy requirements for reducing nitrogen through proton-coupled electron transfer reactions^{60–63}

Chemical reaction	Potential	Equation
$\text{N}_2 + 6\text{H}^+ + 6\text{e}^- \rightleftharpoons 2\text{NH}_3(\text{aq.})$	$E^\circ = +0.092 \text{ V (vs. RHE)}$	(1)
$\text{N}_2 + 6\text{H}_2\text{O} + 6\text{e}^- \rightleftharpoons 2\text{NH}_3 + 6\text{OH}^-$	$E^\circ = +0.092 \text{ V (vs. RHE)}$	(2)
$\text{N}_2 + \text{H}^+ + \text{e}^- \rightleftharpoons \text{N}_2\text{H}$	$E^\circ = -3.2 \text{ V (vs. RHE)}$	(3)
$\text{N}_2 + 2\text{H}^+ + 2\text{e}^- \rightleftharpoons \text{N}_2\text{H}_2(\text{g})$	$E^\circ = -1.10 \text{ V (vs. RHE)}$	(4)
$\text{N}_2 + 4\text{H}^+ + 4\text{e}^- \rightleftharpoons \text{N}_2\text{H}_4(\text{g})$	$E^\circ = -0.36 \text{ V (vs. RHE)}$	(5)
$\text{N}_2 + 4\text{H}_2\text{O} + 6\text{e}^- \rightleftharpoons \text{N}_2\text{H}_4 + 4\text{OH}^-$	$E^\circ = -0.496 \text{ V (vs. RHE)}$	(6)
$\text{N}_2 + \text{e}^- \rightleftharpoons \text{N}_2(\text{aq.})$	$E^\circ = -3.37 \text{ V (vs. RHE)}$	(7)

standard hydrogen electrode (SHE), normal hydrogen electrode (NHE), or reversible hydrogen electrode (RHE). It is found that the potential of NRR is more or less comparable to that of the parasitic HER process. As a matter of fact the major byproduct of NRR in aqueous medium is hydrogen. The NRR process involves many proton–electron transfer reactions, so multiple intermediates are formed. The magnitude of the redox potential is high for the formation of the N_2H intermediate, which means that it is really difficult to add a H atom into the dinitrogen molecule; generally to achieve the purpose drastic reaction conditions are required (eqn (3)). In general, the difficulty lies in the second H atom addition than the third H atom, which is in agreement with the fact that higher redox potential is required for the two electron and four electron transfer process than the reduction by the six electron process (eqn (4)–(6)). Thus, the large magnitude of the negative potentials of the intermediate species clearly indicates the extreme difficulty in executing the process of hydrogenation in the nitrogen molecule.

On the other hand, the carbon dioxide molecule is also difficult to activate due to various reasons: (1) CO_2 is non-polar in nature and has quite a large ionization potential (13.84 eV)⁵⁹ and (2) the large energy gap (9.9 eV) between the HOMO and LUMO of CO_2 does not favor electron transfer processes.⁵⁹

Electrochemical CO_2RR is thermodynamically as well as kinetically inefficient due to large overpotentials, inferior selectivity resulting in poor yield, and direct competition with the hydrogen evolution reaction in aqueous environments. Thermodynamically, the reduction potentials of CO_2 to the products (mentioned above) are within the vicinity of those of the hydrogen evolution reaction (HER; Table 2). To add to the problem, the CO_2 activation energy barrier is quite high and the

reaction pathways include multiple steps of electron transfer, as a result of which the overall CO_2RR kinetics are very sluggish, with poor selectivity and high overpotentials.^{64,65} Therefore, the progress of CO_2RR depends mostly on the electrocatalysts, which can lower the overpotential, speed up the rate of reaction, and improve the selectivity performance.⁶⁶

Generally, the proton-coupled multi-electron reduction reactions (Table 2) are thermodynamically more favorable than one electron reduction of CO_2 (Table 2, eqn (1)). The catalyst eases the transfer of electrons from the electrode surface to CO_2 , thereby lowering the overpotentials, as well as enhancing selectivity. Since the many electron reduction of CO_2 requires protons (Table 2), a Brønsted acid is generally added to the electrolyte to increase the catalytic current and to reduce the overpotential. In aqueous solutions, protons may be provided by water itself or by the intentionally added protic acid.

Thus, thermodynamic analysis shows the bottleneck of the multistep catalytic reactions which involves the formation of many intermediates in the NRR and CO_2RR . The intermediates which are formed during reduction reactions are related to one another *via* energetic means, and the correlations among the various intermediates and their adsorption energies are studied, which are termed as “scaling relations”.⁶⁸ The adverse scaling relation among the adsorption energies of the different intermediates makes it tough to find a catalyst which demonstrates all the energetic reaction steps as thermodynamically descending or of constant nature, for the entire reaction process. In the case of NRR, the binding energy values of NH_2 and N_2H are strangely dependent on one another, and the hostile scaling relation between them results in a minimum overpotential value close to 0.4 V.⁶¹ So far, it is not well understood which is the preferred pathway between sequential proton electron transfer (SPET) and concerted proton electron transfer (CPET) during the NRR process. In the case of metallic electrocatalysts in the solid phase, generally the CPET pathway was often considered as the preferred pathway, although recently conjecture about the SPET pathway is reported.^{69,70} A recent study has shown the role of pH in governing the CPET or SPET pathway for CO_2RR .⁷⁰ However, the majority of the computational research reports on NRR have not taken pH into consideration. The quantum calculation study indicates that the SPET pathway is preferred over CPET, as the activation energy barrier of the latter is higher than that of the former. It is evident that for the CPET pathway, HER is more likely to occur as the proton and electron are transferred in a coupled form of hydrogen atom. On the other hand, in the SPET pathway, first the proton attacks the activated nitrogen molecule, and then the electron is added to the positively charged nitrogen intermediate species.⁷¹ However, more research is required to clearly state the exact preferred pathway between CPET and SPET in electrocatalytic mechanisms for heterogeneous catalysts operating at STP.

2.2 Thermodynamic aspects of nitrate reduction reaction (NO_3RR)

The nitrate reduction reaction (NO_3RR) to ammonia (NH_3) involves extensive variation in the oxidation state of nitrogen,

Table 2 Energy requirements for reducing carbon dioxide through proton-coupled electron transfer reactions. All potentials are reported vs. NHE at pH 7⁶⁷

Chemical reaction	Potential (V vs. NHE)
$\text{CO}_2 + \text{e}^- \rightarrow \text{CO}_2^-$	$E^\circ = -1.90 \text{ V}$
$\text{CO}_2 + 2\text{H}^+ + 2\text{e}^- \rightarrow \text{CO} + \text{H}_2\text{O}$	$E^\circ = -0.53 \text{ V}$
$\text{CO}_2 + 2\text{H}^+ + 2\text{e}^- \rightarrow \text{HCO}_2\text{H}$	$E^\circ = -0.61 \text{ V}$
$\text{CO}_2 + \text{H}^+ + 2\text{e}^- \rightarrow \text{HCO}_3^-$	$E^\circ = -0.43 \text{ V}$
$\text{CO}_2 + 4\text{H}^+ + 4\text{e}^- \rightarrow \text{HCHO} + \text{H}_2\text{O}$	$E^\circ = -0.48 \text{ V}$
$\text{CO}_2 + 6\text{H}^+ + 6\text{e}^- \rightarrow \text{CH}_3\text{OH} + \text{H}_2\text{O}$	$E^\circ = -0.38 \text{ V}$
$\text{CO}_2 + 8\text{H}^+ + 8\text{e}^- \rightarrow \text{CH}_4 + 2\text{H}_2\text{O}$	$E^\circ = -0.24 \text{ V}$
$2\text{H}_2\text{O} \rightarrow \text{O}_2 + 4\text{H}^+ + 4\text{e}^-$	$E^\circ = 0.82 \text{ V}$
$2\text{H}^+ + 2\text{e}^- \rightarrow \text{H}_2$	$E^\circ = -0.41 \text{ V}$

which can exist in more than ten different oxidation states ranging from -3 to $+5$. The electrochemical conversion of nitrate to ammonia involves a complex electron transfer process with varying pathways, so it is very important to understand the underlying mechanism governing the entire process.^{72–81} The NO_3RR process produces a large number of complex products, with varying thermodynamic stability. Hence, the complex thermodynamic relationship among the different oxo and hydrido nitrogen species is addressed by the Frost–Ebsworth (F–Eb) diagram (Fig. 3a);⁸² a reaction can be monitored by the union of two points in the F–Eb diagram. The higher the magnitude of the positive slope, the greater will be the oxidizing potential. A chemical species which is present in a peak above two adjacent points is considered to be unstable, while species present in a peak whose position is below is contemplated as an unstable species. However, when more than three oxidation states are located in a same line in F–Eb diagram, then it represents an equilibrium condition, meaning the reaction will not proceed to completion because the thermodynamic equilibrium has been reached.⁸² It is clearly evident that nitrate is more stable in alkaline medium. Under basic conditions, the NO_3RR process would result in the formation of multiple products like hydroxylamine, nitric oxide, etc., which can decompose into other products. At standard temperature and pressure, nitrogen shows thermodynamic stability in the form of nitrogen and ammonia. From the kinetic aspect, the reduction of nitrate to ammonia is an eight-electron transfer process, while its conversion into nitrogen is a five-electron transfer process (Table 3). Hence, nitrogen is also a competitive side product for the NO_3RR process.

Another very important aspect of the NO_3RR process lies in the variation of the pH level. The Pourbaix diagram (Fig. 3b) reveals that at the respective electrode the catalytic reactions occur at the thermodynamic potentials which proceed towards the decomposition potential of water. Therefore, the pH near the electrode surface varies with the corresponding hydrogen evolution (at the cathode) or oxygen evolution (at the anode), which takes place at the cost of proton consumption or production during electrocatalysis. The factor of current efficiency for NO_3RR is directly dependent not only on nitrate reduction but also on hydrogen evolution.

Table 3 Energy requirements for reducing nitrate through proton-coupled electron transfer reactions. All potentials are reported vs. SHE⁸³

Chemical reaction	Potential (V vs. SHE)
$2\text{NO}_3^- + 12\text{H}^+ + 10\text{e}^- \rightarrow \text{N}_2(\text{aq.}) + 6\text{H}_2\text{O}$	$E^\circ = 1.17$ V
$\text{NO}_3^- + 9\text{H}^+ + 8\text{e}^- \rightarrow \text{NH}_3 + 3\text{H}_2\text{O}$	$E^\circ = -0.12$ V

2.3 Mechanistic aspects of NRR, NO_3RR , CO_2RR and urea formation

2.3.1 Nitrogen reduction reaction (NRR) mechanistic routes. Basically, there are four types of mechanistic pathways through which the electrochemical NRR process takes place: (1) dissociative, (2) associative, (3) enzymatic, and (4) Mars–van Krevelen (MvK) mechanism. In the dissociative pathway, the $\text{N}\equiv\text{N}$ triple bond cleaves into two N atoms and then subsequent protonation occurs to produce NH_3 . In the majority of electrochemical NRR systems, the cleavage of the $\text{N}\equiv\text{N}$ triple bond and the release of the first ammonia molecule as a product occur simultaneously, for the associative pathway. The associative route can be further classified into the distal route and the alternating route. In the distal route, the distally outward nitrogen atom is protonated first followed by the release of the NH_3 molecule, while in the alternating route, the two N atoms are protonated simultaneously.^{57,61,84} In the enzymatic route, the adsorption mode of N atoms on the catalytic surface is side-on rather than end-on. Fig. 4 represents the three mechanistic pathways of ammonia production as discussed above. $^*\text{NH}_2$ is the most important intermediate species with regard to urea formation, as the combination of two $^*\text{NH}_2$ intermediate species with another $^*\text{CO}$ species would result in $^*\text{CO}(\text{NH}_2)_2$ and finally urea formation; $^*\text{NH}_2$ enters the electrolytic medium after desorbing from the catalytic surface. In the Mars–van Krevelen (MvK) mechanism proposed by Skúlason *et al.* specifically for transition metal nitrides, the outermost nitrogen atom of metal nitrides is reduced to NH_3 and the catalyst is subsequently regenerated by reacting with gaseous N_2 .⁸⁵ Theoretical studies suggest that the overpotential for NRR via the MvK mechanism is smaller compared to that via the associative mechanism.⁸⁵

2.3.2 Nitrate reduction reaction (NO_3RR) mechanistic routes. The NO_3RR process involves direct and indirect reaction

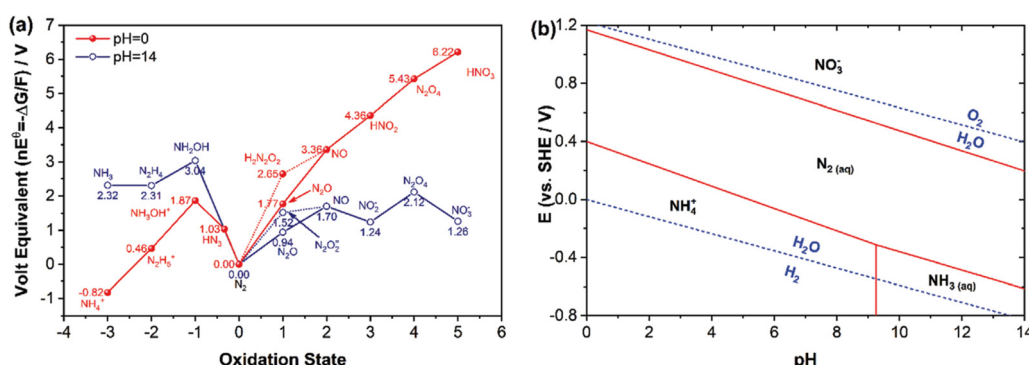


Fig. 3 (a) Frost–Ebsworth diagram of various forms of nitrogen at pH 0.0 and pH 14.0. (b) Pourbaix diagram of nitrogenous forms.⁸² Copyright 2020, John Wiley & Sons, Ltd.

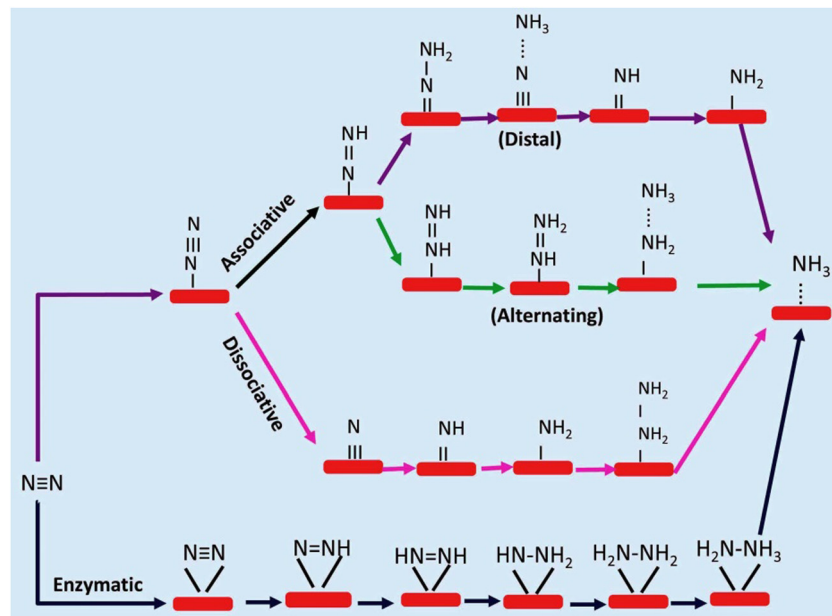


Fig. 4 Schematic representation of the associative route (including distal, alternating), dissociative route, and enzymatic route for the NRR process.

mechanistic routes or the autocatalytic reduction pathway. The direct reaction mechanism requires a low concentration (10^{-6} M NO_3^-) while a high concentration is required for the indirect reaction mechanism (1–4 M NO_3^-).^{86,87} Fig. 5 represents the entire process of nitrate reduction in water. Nitrite is the most important intermediate for the NO_3RR process, as

represented in Table 4.^{88–90} Sequentially, the nitrogen dioxide radical is reduced to NO_2^- which remains adsorbed on the catalytic substrate by a two electron transfer reaction, as shown in Table 4.⁹¹

Various initiators in the catalytic process result in the indirect reaction mechanism where two probable autocatalytic

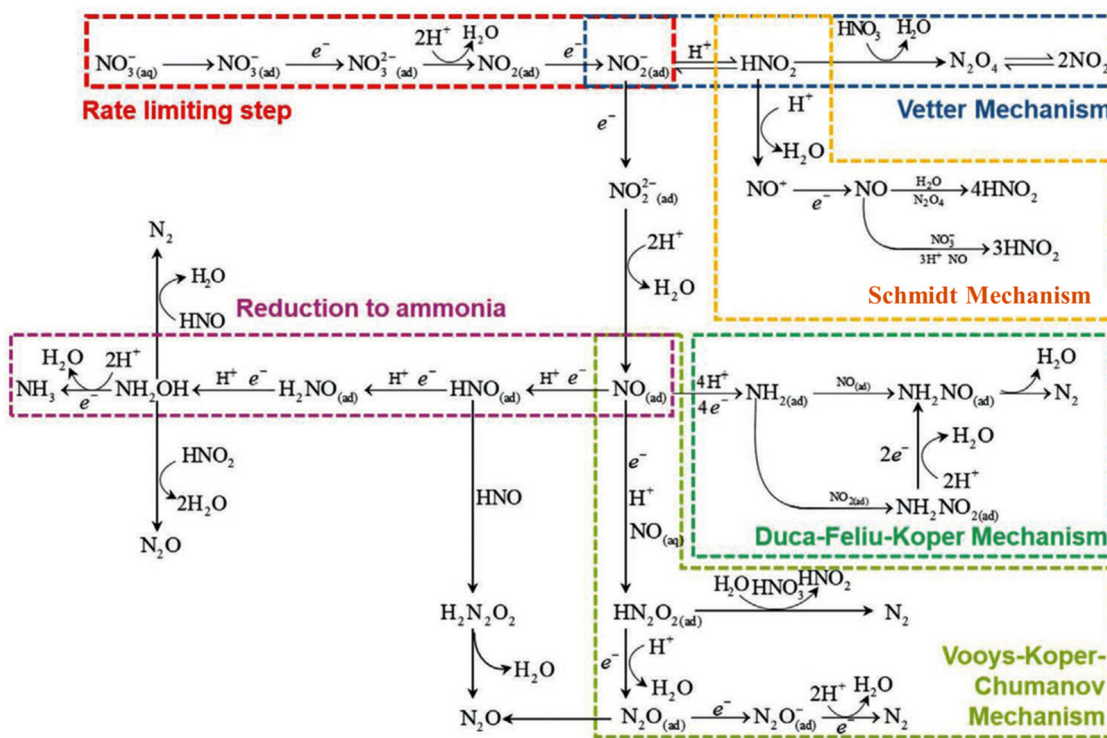


Fig. 5 Schematic representation of the mechanisms and the different processes which occur during electrocatalytic nitrate reduction in aqueous medium.⁸² Copyright 2020, John Wiley & Sons, Ltd.

Table 4 Nitrate to nitrite conversion via the two electron step

Chemical reaction	Potential (V vs. SHE)
$\text{NO}_3^- + \text{e}^- \rightarrow *\text{NO}_3^{2-}$	$E^\circ = -0.89 \text{ V}$
$*\text{NO}_3^{2-} + 2\text{H}^+ \rightarrow \text{NO}_2 + \text{H}_2\text{O}$	
$\text{NO}_2 + \text{e}^- \rightarrow \text{NO}_2^-$	$E^\circ = 1.04 \text{ V}$

mechanisms are proposed, namely, (1) the Vetter mechanism and (2) the Schmidt mechanism. In the Vetter mechanism (Fig. 5) the nitrogen dioxygen radicals as the electrocatalytic active species in the autocatalytic cycle reduce nitrogen dioxide to nitrite ions, which further protonate into nitrous acid in acidic medium; the further propagation step involves the utilization of nitrogen dioxygen radicals, where nitrous acid reacts with nitric acid to produce dinitrogen tetroxide (N_2O_4), which in turn rapidly releases the two electrocatalytically active NO_2 species. In the Schmidt mechanism, the nitrosonium ion (NO^+) plays the role of the electrocatalytic active species in the indirect route or autocatalytic cycle. NO^+ ions are produced from the deprotonation of nitrous acid in acidic medium as shown in Fig. 5; then NO^+ ions readily capture an electron to produce NO_2 .⁹² The two intermediate NO species react with N_2O_4 in aqueous media to generate nitrous acid. By this mechanism, 2 mols of nitrous acid are generated from 1 mol of NO, and the NO^+ ions are generated during the autocatalytic cycle.

The direct reaction route for NO_3RR to NH_3 involves two different routes. The first one involves the modulation of the electrocatalytically active adsorbed hydrogen atom, while the second involves reduction by the electrons supplied by the cathodic surface. In the route involving the adsorbed hydrogen atom (H_{ad}), the electron at first reduces the adsorbed water molecule on the cathodic surface to generate H_{ad} . H_{ad} then converts nitrate to ammonia via the multi-step reduction process which involves various intermediates (NO_2 , NO , N , NH , NH_2).^{72,93} There is the possibility of formation of a bond between adsorbed nitrogen atoms resulting in a nitrogen molecule, which would be detrimental to the production of the vital NH_2 intermediate (an important chemical species for NRR, and urea production); hence to address the concern, theoretical investigations were carried out. The results were quite interesting; the kinetic barrier of the adsorbed N atom is 0.75 eV which is much larger than that of the adsorbed H atom, whose value was around 0.10 eV. Hence, the formation of the N–N bond is kinetically hindered compared to N–H bond formation.⁹⁴ Therefore, as a consequence, the facile adsorption of the hydrogen atom on the catalytic surface can assist the formation of the NH_2 intermediate, which can ultimately facilitate urea formation.

In the case of the electron mediated route (Fig. 5), the first step is conversion of nitrate into nitrite.^{95–98} The second step involves the conversion of the nitrite ion into nitric oxide on the catalytic surface. Nitric oxide (NO) is the most vital intermediate species for the production of nitrogen or ammonia, although there are various routes which result in nitrogen yield. One of the pathways involves the reduction of NO into the nitrogen atom, which combines with another nitrogen atom

and results in the formation of a nitrogen molecule.⁹⁹ Another pathway (Vooys–Kooper–Chumanov mechanism) involves the reaction of NO with dissolved NO in the electrolyte to produce dinitrogen oxide (N_2O) intermediate species.^{100–102} If the adsorbed N_2O does not get desorbed, it gets reduced to a nitrogen molecule.^{103,104} Furthermore, the intermediate NO species are reduced to form azanone (HNO).¹⁰⁵ Another process which is quite similar to the above mentioned mechanism involves dimerization of HNO to yield $\text{H}_2\text{N}_2\text{O}_2$, which is a stable molecule at an appropriate pH level.^{106,107} The conjugate acid of $\text{H}_2\text{N}_2\text{O}_2$ is unstable in nature, and it decomposes to produce N_2O , which further decomposes to form nitrogen.^{99,106} The generation of nitrogen can also occur via the Duca–Feliu–Koper mechanism, as represented in Fig. 5, where NO is reduced and protonated to form NH_2 on the catalytic surface. Then NONH_2 is generated by the Langmuir–Hinshelwood-type reaction, in which NH_2 formally reacts with NO. NONH_2 is thermally not stable; hence it decomposes into nitrogen and water. Furthermore, NH_2 can be produced in the optimized potential window by the direct reduction of nitric oxide.^{108,109}

2.3.3 Carbon dioxide reduction reaction (CO_2RR) mechanistic routes. In general, the CO_2RR process results in a wide spectrum of products (C_1 products, C_2 products, etc.). We would confine our discussion to C_1 product formation only (which includes CO, HCOOH , CH_3OH , CH_4) as it is pertinent from the perspective of urea formation; since different side products can be formed, appropriate strategies need to be adapted in order to reduce them and enhance the urea yield. The initiation of the CO_2RR involves a two electron transfer and two proton reaction phenomenon; at first the CO_2 molecule is adsorbed on the catalytic surface, then it is reduced to form intermediate $*\text{COOH}$ species via the proton coupled electron transfer (PCET) process.^{110–114} Then a proton and an electron react with the carboxylic acid intermediate which results in the formation of H_2O and intermediate $*\text{CO}$ species. Then, in the final step, $*\text{CO}$ gets desorbed from the surface of the electrode. The entire process is shown schematically in Fig. 6. Now, it is very important to realize the adsorption strength of $*\text{CO}$ on the catalytic surface. If $*\text{CO}$ binds very strongly with the catalytic surface, then the electrocatalytic active sites will be poisoned and will not be able to show reducing ability; hence HER will gain the upper hand and dominate the CO_2RR process. On the other hand, if the binding strength of $*\text{CO}$ and the catalytic surface is low, then it means $*\text{CO}$ will be easily desorbed from the catalytic surface. The perfect optimized condition for urea formation is achieved when $*\text{CO}$ binds with intermittent energy (neither very strongly nor in a weak manner); then $*\text{CO}$ formed by CO_2RR would have to react with two intermediate species of $*\text{NH}_2$ produced via the NRR or NO_3RR process, to ultimately produce urea. However, HCOO^- is formed via the $*\text{OCHO}$ intermediate, which has a medium adsorption energy,¹¹⁵ which has a negative impact and reduces the urea yield. It is observed that $*\text{COOH}$ can easily be reduced to $*\text{CO}$. However, the first step of reduction of CO_2 to $*\text{COOH}$ is hindered by the weak binding strength of the catalytic surface and $*\text{COOH}$. The desorption process of the CO molecule from the surface of

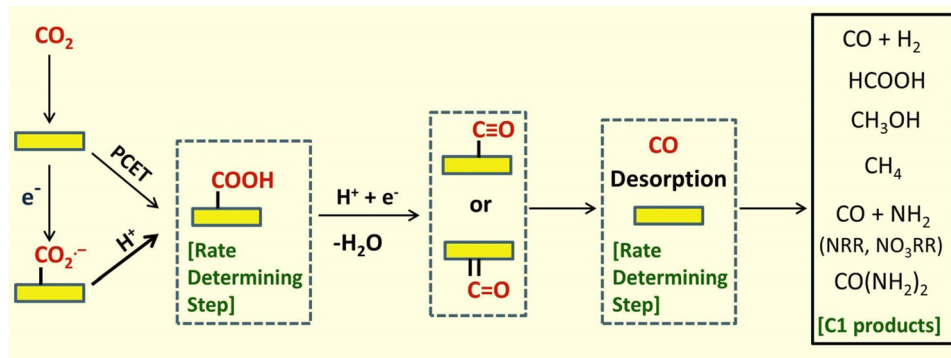


Fig. 6 Schematic representation of the mechanistic route for the electrochemical carbon dioxide reduction reaction to carbon monoxide.

the electrode is also inhibited by the strong binding interaction of *CO with the electrode surface. Hence, these two vital steps are taken as the rate determining step of the CO₂RR process. The other pathway to produce *COOH differs in the manner of the activation of CO₂.^{116–118} The first step of activation of CO₂ does not involve a PCET process, but instead a decoupled electron transfer and proton transfer takes place; initially a CO₂⁻ radical anion is formed on the surface of the electrode. However, the process of direct reduction of CO₂ *via* the one electron transfer process to produce CO₂⁻ requires a large reduction potential (-1.9 V vs. RHE);¹¹⁹ hence, the activation of CO₂ in the first step *via* this process is unfavorable.

2.3.4 Urea formation mechanistic pathway. In order to understand the mechanism of urea production, we have to identify the key intermediates which are formed during the vital C–N coupling reaction, which ultimately leads to urea generation. Basically, there are four mechanistic pathways (shown in Fig. 7) which are as follows: (1) *CO + *NH₂ pathway, (2) *COOH + *NH₂ pathway,¹²⁰ (3) CO₂ + NH₃ pathway,¹²¹ and (4) *CO₂ + *N₂ route.^{35,36} The ammonia resulting from nitrogen

fixation further reacts with CO₂ to produce NH₂COO⁻, which is further converted to carbamate.^{121,122} However, this mechanistic pathway is conjectural as it originates from the cathodic Tafel plot and energy of activation analyses. The first and second pathways have a common intermediate species in the form of *NH₂, which can be produced by the different routes for the NRR process, as discussed previously (Fig. 4).

With regard to the carboxylic intermediate species, it is produced by the CO₂RR process *via* the proton coupled electron transfer process (PCET), from the solution containing CO₂, or by the process of decoupled electron transfer (as discussed in the mechanism of CO₂RR). The vital *CO intermediate species are formed *via* the PCET process, where the attack occurs on the oxygen atom (OH) of the *COOH activated species, which releases water in a facile way.¹²³ *COOH is considered to be the vital intermediate species for the C–N coupling reaction, as found by the *in situ* FTIR investigation in the presence of CO₂ and NO₂⁻, and for reference only CO₂ was taken for the experiment.¹²⁴ However further proof is required to establish the formation of *NH₂ intermediate species and the

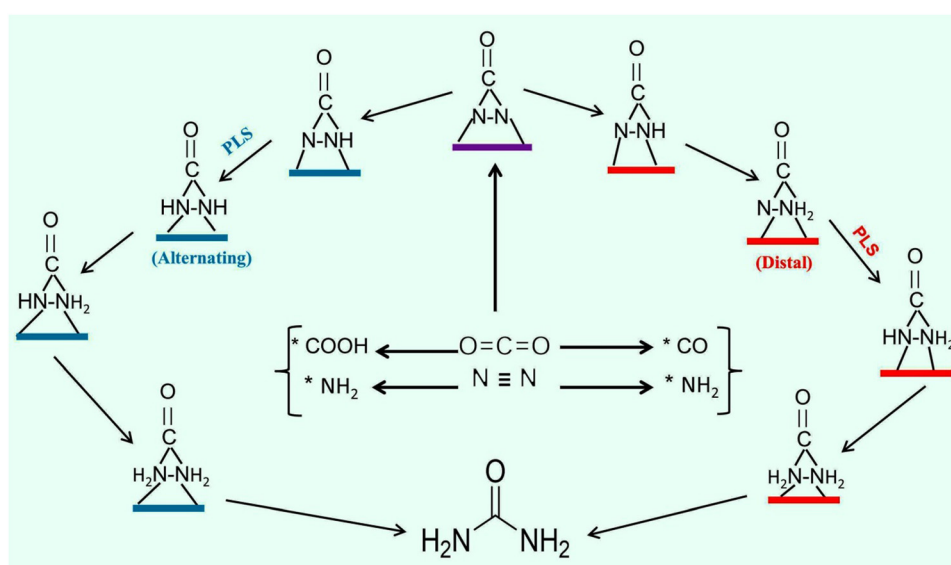


Fig. 7 Schematic representation of the various mechanistic routes for electrochemical urea production.

corresponding coupling with $^{*}\text{COOH}$ species. It was inferred that $^{*}\text{CO}$ would react with $^{*}\text{NH}_2$ to produce urea, as the process is assisted by the reduction of CO_2 to CO , and NO_2^- to NH_3 , although when the control experiment was carried out in the absence of CO_2 or NO_2^- , urea was not formed.²² As CO_2 is more electrophilic in nature, it can easily undergo the coupling reaction with the nucleophilic $^{*}\text{NH}_2$ species. Another important aspect is that the $^{*\text{CONH}_2}$ intermediate formed during urea production is less prone to attack by the $^{*}\text{NH}_2$ species.

As there are various mechanistic models proposed for urea formation *via* different kinds of intermediate chemical species, in order to scientifically investigate and elucidate the mechanistic aspects, we further classify them on the basis of the reactants involved, which follows the different pathways before producing urea.

(a) *Nitrogen gas and carbon dioxide gas as reactants.* The initiation step of urea formation starts with the successful adsorption of N_2 and CO_2 (Fig. 8a-d) on the preferred site of the catalyst substrate;^{35,36} the side on adsorption position enhances electron mobility to the antibonding (π^*) orbitals of N_2 , thereby weakening the $\text{N}\equiv\text{N}$ bond by lowering the bond order of $\text{N}-\text{N}$.³⁵ A parallel reduction reaction of CO_2 to CO generally occurs on the metal center/site (Fig. 8c).³⁶ The working potential range is so optimized for the dual reduction reaction to take place and most importantly the near vicinity of the intermediate activated $^{*\text{C=O}}$ and the $^{*\text{N=N}}$ molecules creates an optimized geometry of complementary molecular orbitals which ultimately results in C-N coupling and finally in

the formation of the vital $^{*\text{NCON*}}$ intermediate (Fig. 8d), the potential determining step from a thermodynamic perspective. The subsequent hydrogenation to the $^{*\text{NCON*}}$ intermediate leads to two probable reaction pathways, namely, distal and alternating.⁵⁶ In the distal mechanistic route, the $(\text{H}^+ + \text{e}^-)$ reacts with the distal N atom, whereas in the alternating mechanistic route the $(\text{H}^+ + \text{e}^-)$ alternatively attacks the N atom on both sides (Fig. 8a and b). The selectivity of the electrochemical urea synthesis is intimately linked with the formation of $^{*\text{NCON*}}$ intermediates. The possible NRR or the unrestrained release of CO would result in a drop in the efficiency of the vital electrochemical C-N coupling reaction and thereby a reduction in selectivity.

(b) *Carbon dioxide gas and nitric oxide gas.* As nitrogen gas has very low solubility in the aqueous phase, in direct electrolytic urea synthesis carbon dioxide gas and nitric oxide gas are employed, as nitric oxide has higher solubility in water.^{125,126} The theoretical study suggests that the urea formation mechanism involves a ten step cascade reaction procedure. The proton coupled electron transfer aids in CO_2 to CO conversion *via* reduction of CO_2 to $^{*\text{COOH}}$ which forms the potential determining step (Fig. 9a), ultimately forming the $^{*\text{CO}}$ intermediate, while the NO reduction reaction takes places through the alternate mechanism *via* the N-atom, where the sequential reaction involving $^{*\text{NO}}$, $^{*\text{NHO}}$, $^{*\text{NHOH}}$, $^{*\text{NH}_2\text{OH}}$, and $^{*\text{NH}_2}$ takes place; after this step, two possible products can form NH_3 or C-N coupling can occur by the reaction of $^{*\text{CO}}$ and $^{*\text{NH}_2}$; among the various intermediates formed ($^{*\text{CO-NO}}$, $^{*\text{CO-NH}_2\text{OH}}$,

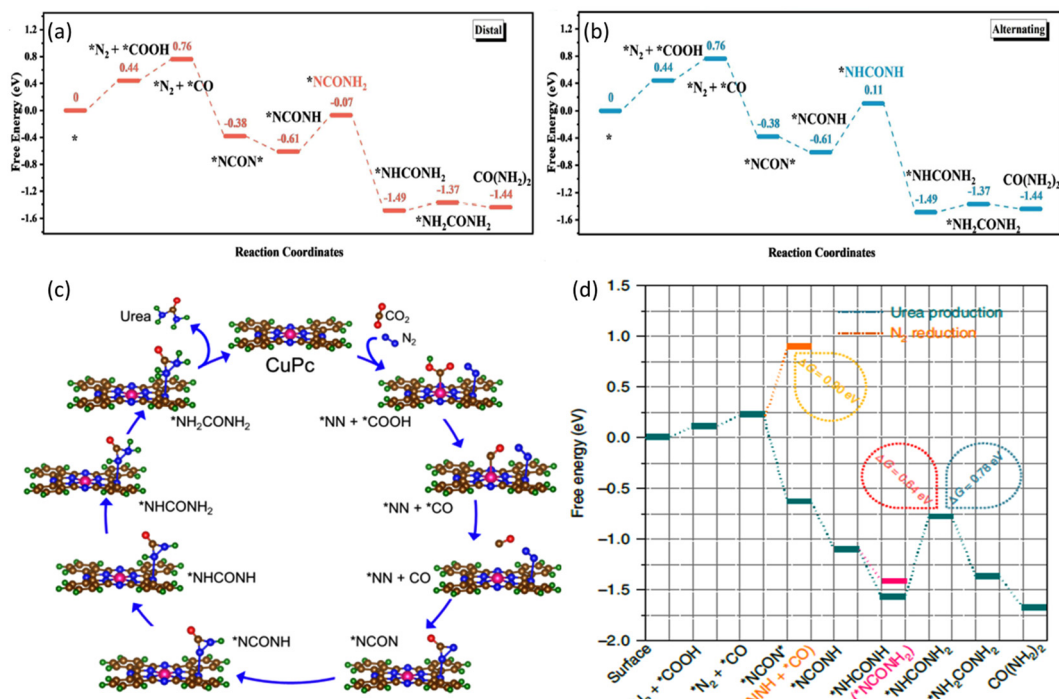


Fig. 8 (a and b) Free energy diagram of urea production and the reaction pathway of $^{*\text{NCON*}}$ formation, illustrating the distal and alternate pathways.⁵⁶ (c) Schematic diagram of urea synthesis by using CuPc.³⁶ Copyright 2022, John Wiley & Sons, Ltd. (d) Free energy plot of the alternating and distal mechanism.³⁵ Copyright 2020, Springer Nature.

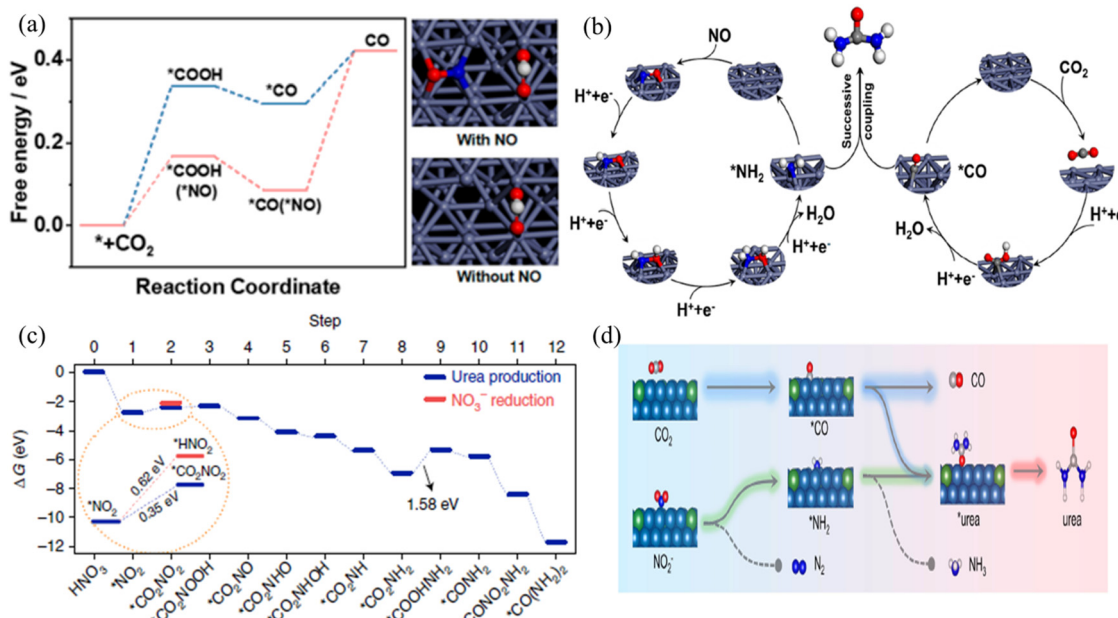
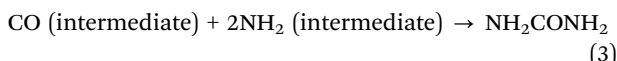
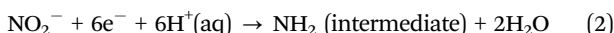


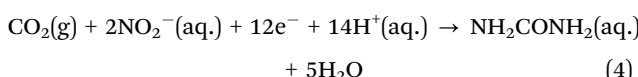
Fig. 9 (a) Free energy diagram of the urea formation mechanism on the surface of Zn using NO and CO₂ as feed gas.¹²⁵ Copyright 2022, American Chemical Society. (b) Schematic representation of the urea formation mechanism on the Zn surface using NO and CO₂ as reactants.¹²⁵ Copyright 2022, American Chemical Society. (c) Diagram of free energy changes of urea synthesis on the (100) facets of In(OH)₃ at 0 V vs. RHE.¹²⁴ Copyright 2021, Springer Nature. (d) Schematic illustration of urea synthesis from CO₂RR and NO₂RR on Te–Pd NCs.⁵⁴ Copyright 2020, American Chemical Society.

and *CO-NHOH), *CO-NH₂ has a lower value of Gibbs free energy which means it is stable than the other transient products, and also simulation suggests that urea formation does not require higher activation energy. It is also observed that the *CO-NH₂ reaction is promoted as the energy of desorption of *CO is reduced in the presence of NO, hence implying a higher rate of urea formation. Thus, the urea sequential step generation by coupling of *CO and *NH₂ is shown in the proposed reaction pathway of electrochemical urea synthesis from NO and CO₂ co-reduction as demonstrated in Fig. 9b.

(c) Mechanistic pathway of biphasic reactants (gas-ions): carbon dioxide in the gas phase and nitrite in the ionic form. The probable mechanism of urea formation by utilizing carbon dioxide and nitrite ions is as follows:¹²⁷



Overall reaction:

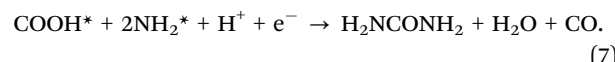


Initially carbon dioxide is reduced in the co-ordinated catalytic site *via* the proton-coupled electron transfer route to produce CO* as an intermediate. On the other hand, NO₂⁻ ions are adsorbed to the catalytic site in a preferred manner (side-on); then the cleavage of the N-O bond followed by bond breaking and proton concerted electron transfer take place and the

reaction progresses *via* proton addition to form NH₂* as an intermediate. Then the tandem reaction route enables C–N coupling, where NH₂* forms a bond to CO*, thus finally resulting in the formation of NH₂CONH₂.

In the context of the free-energy diagram of the lowest energy pathway as shown in Fig. 9c,¹²⁴ the urea synthesis starts from thermodynamically spontaneous reduction of NO₃⁻ (HNO₃) to the *NO₂ intermediate on the In(OH)₃ facets of {100}; an adsorption free energy of -2.48 eV is noticed. In comparison to the spontaneous formation of the *NO₂ intermediate, the protonation step of CO₂ needs an additional energy of 0.38 eV. This causes a higher degree of coverage of *NO₂ on the surface of catalysts during the electrocatalysis process, which hinders the adsorption and reduction of CO₂ on the electrocatalytic surface of In(OH)₃-S.

Other proposed reaction mechanism:¹²⁸

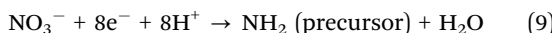
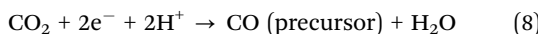


The schematic illustration of the carbon dioxide reduction reaction (CO₂RR) and the nitrite ion reduction reaction (NO₂RR) is represented in Fig. 9d. The reaction pathway is predicted on the basis of the catalytic surface which contains oxygen vacant sites in ZnO. Initially the oxygen atom present in nitrite ions attacks the oxygen vacant sites of the catalyst, and then the nitrite ions are reduced to the NH₂* intermediate *via* multi-step proton coupled electron transfer, and simultaneously carbon dioxide is inserted

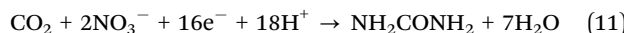
into the vacant sites and transformed into COOH^* by single proton assisted electron transfer and finally the union of NH_2^* and COOH^* intermediates results in urea formation.

Liu *et al.* explored the reaction mechanisms of the main steps of simultaneous electrochemical reduction of CO_2 and $\text{NO}_3^-/\text{NO}_2^-$ for urea formation on the Cu (100) surface as a model catalyst using *ab initio* molecular dynamics simulations. They investigated different combinations of coupling intermediates and explained that the process of selectivity in electrochemical urea synthesis is potential dependent, and clearly elucidated the role of $^*\text{NH}$ and $^*\text{CO}$ as the critical surface intermediates for C–N coupling along the urea pathway at low overpotentials. In the case of higher overpotentials, C–N coupling proceeds with a different mechanism where ammonia is the dominant product; hence the process of urea synthesis has a narrow potential window.^{125,126}

(d) *Carbon dioxide in the gas phase and nitrate ions.* The mechanism of carbon dioxide and nitrate ion reduction reaction can be represented by the following equations:¹²⁹



Overall reaction:



The net reaction involves 18 protons and 16 electrons to form a urea molecule by converting two nitrate ions and a carbon dioxide molecule.

Source of urea synthesis	Advantages	Disadvantages
$\text{CO}_2 + \text{N}_2$	The commercial urea synthesis process requires high temperature and pressure. But the electrochemical urea synthesis process can be carried out at normal temperature and pressure using CO_2 and N_2 gases. This process is environmentally friendly. N_2 is easily available (78% in air) and the overall process is cost-efficient.	The solubility of N_2 in the electrolyte solution is very low (approximately 20 mg L ⁻¹ in aqueous medium at 1 bar pressure and 20 °C temperature).
$\text{CO}_2 + \text{NO}$	The solubility of NO in an aqueous medium is 0.0098 g/100 mL (0 °C) or 0.0056 g/100 mL (20 °C)	Higher levels of nitrogen dioxide can damage a person's respiratory system and increase a

which is better than the solubility of N_2 ; thereby the urea synthesis process is enhanced

person's weakness and the severity of respiratory infections and asthma. Long-term use of high doses of nitrogen dioxide can lead to chronic lung disease

$\text{CO}_2 + \text{NO}_2^-$
Nitrite ion is easily soluble in aqueous medium. Bond breaking energy of NO_2^- ($\text{O}=\text{N}-\text{O}^-$) is less compared to that of NO or N_2 ($\text{N}\equiv\text{N}$, triple bond)

$\text{CO}_2 + \text{NO}_3^-$
Nitrate ion is easily soluble in aqueous medium. The low dissociation energy of the $\text{N}=\text{O}$ bond (204 kJ mol⁻¹) in nitrate compared to that of the $\text{N}\equiv\text{N}$ bond (941 kJ mol⁻¹)¹²⁴

At high concentration nitrite ions are toxic

Excessive nitrate intake can affect the oxygen carrying capacity of blood and can lead to the deadly disease called methemoglobinemia (known as the blue baby syndrome)

We find that the number of protons and electrons transferred throughout the urea production process changes depending on the reactant(s) used. Thus, it appears that the transfer of electrons is the central step in the synthesis of urea; however, we cannot ignore the fact that crucial intermediates like CO^* and NH_2^* are formed in all cases, regardless of the transfer of electrons. The NH_2^* intermediate acts as a base and attacks the positively charged centre of CO^* , triggering the crucial C–N coupling reaction and the formation of the C–N bond, which ultimately results in the formation of urea.

3. Classification of electrocatalysts investigated (to date) for urea generation

Thus to reduce and eliminate the negative impact of urea production on the ecosystem, the researchers are in the search of finding the Holy Grail in the form of an electrocatalyst which can produce urea in an eco-friendly as well as more industry friendly way with large scale production feasibility. To systematically explore the catalytic selectivity, stability, and activity during the electroreduction process to form urea, it is necessary to find a screening strategy in order to find a promising catalyst from the wide spectrum of electrocatalysts which can facilitate a greener route for synthesis with a generous amount of urea yield with decent faradaic efficiency. However, the electrochemical urea synthesis is a nascent field, so from the handful number of potential electrocatalysts for urea production, we can broadly classify them into six categories, namely, (1) metal

borides, (2) metal complexes, (3) metal chalcogenides and chalcogenide borates, (4) metal alloy systems, (5) heterostructured catalysts, and (6) carbon based catalysts.

3.1 Metal borides (MBenes)

The two-dimensional MBenes (Mo_2B_2 , Ti_2B_2 , and Cr_2B_2) are potential candidates due to their ability to suppress surface oxidation and inhibit self-corrosion during electrolysis. Furthermore, the simultaneous coupling of N_2 and CO_2 to form urea occurs in a narrow potential window (-0.49 to -0.65 eV) with decent selectivity and with effective suppression of the competitive ammonia formation by nitrogen reduction reaction.¹³⁰ The electrocatalytic stability under various conditions can be revealed by the plot of surface Pourbaix diagrams of the three MBenes to reveal the most stable surface configurations under different equilibrium potentials and varying pH conditions, as shown in Fig. 10(a–c). It was also observed that the extensive passivation domain in the case of Mo_2B_2 (pH < 7.08) and Cr_2B_2 (pH < 7.22) falls in the potential value

of -0.49 V and -0.52 V, respectively. Structural integrity was preserved under operating conditions for both of them (Mo_2B_2 and Cr_2B_2) because of the elevated barrier of solid–liquid phase transformation. However, a stark difference was noticed in the case of Ti_2B_2 which showed a skewed passivation region (pH < 2.26) at a potential of -0.65 V. Furthermore, at a higher pH value Ti_2B_2 conversion to $\text{Ti}(\text{OH})_3$ takes place, which leads to corrosion, thereby interfering with the process of urea production. Hence, Ti_2B_2 has inferior electrochemical stability.

3.2 Metal complexes

Owing to the unique metal ligand interaction, metal complexes possess the active sites responsible for electrochemical urea synthesis. Copper phthalocyanine (CuPc) upholds its place as an effective catalyst due to the presence of a metal center ($\text{M}-\text{N}_4$) and the pyridinic nitrogen as an active site, which performs the dual role of adsorption and activation of N_2 and CO_2 ; the nanotube morphology of CuPc is shown in Fig. 10d. CuPc has been demonstrated to promote C–N bond formation

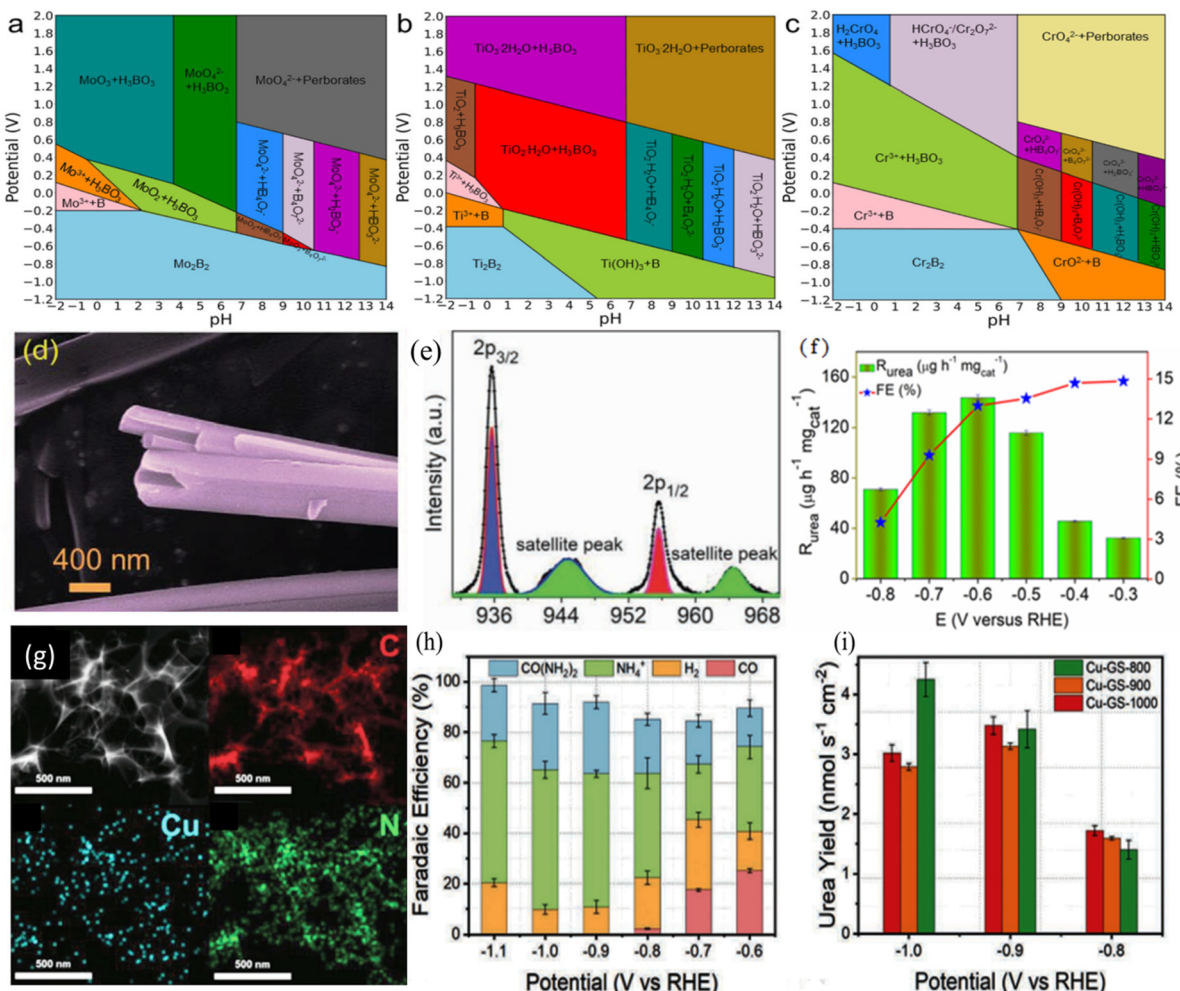


Fig. 10 (a–c) Theoretically predicted Pourbaix diagram of Mo_2B_2 , Ti_2B_2 and Cr_2B_2 respectively.¹³⁰ (d) FESEM image of the copper phthalocyanine nanotube.³⁶ Copyright 2022, John Wiley & Sons, Ltd. (e) High resolution XPS spectra of the Cu 2p doublet.³⁶ Copyright 2022, John Wiley & Sons, Ltd. (f) The urea yield rate and FE with N_2 and CO_2 as feeding gas at different potentials for CuPc NTs.³⁶ Copyright 2022, John Wiley & Sons, Ltd. (g) EDX mapping for Cu SAC annealed at 800 °C. (h–i) Faradaic efficiency and yield rate at varying potentials.¹³⁵

and result in a urea yield of $143.47 \mu\text{g h}^{-1} \text{mg}_{\text{cat}}^{-1}$ and a faradaic efficiency of 12.99% at -0.6 V vs. RHE as shown in Fig. 10f.³⁶ The XPS study revealed the Cu $2\text{p}_{3/2}$ and $2\text{p}_{1/2}$ peaks of copper in CuPc (Fig. 10e). The catalyst can be synthesized on a large scale using a solvothermal route, and hence may have industrial utility.³⁷

Density functional theory is extensively employed to find a catalyst by high throughput screening; single atom catalyst systems are generally anchored on various substrates and then the systems are evaluated for catalytic activity.^{131,132} The single atoms (like iron and cobalt) anchored on boron nitride showed unique asymmetric triple active sites comprised of two boron atoms and the other Fe/Co; the system can enhance the electrochemical urea synthesis by the effective adsorption sites, suppressing the side reaction, and the active sites have optimal binding strength for the intermediates (as confirmed by the charge distribution analysis).¹³³ The volcano plot provides the key to understand about the limiting potential, position of the d-band center, and a descriptor to understand the mechanistic insights into the inherent correlation from the atomistic viewpoint, which takes electronegativity and the number of electrons in the d orbital of metal atoms into consideration. In the case of the transition single atom system (Ti, Cr, Nb, Mo, and Ta) affixed on the borophene nanosheets, an excellent catalytic activity was demonstrated with a relatively low working potential;¹³⁴ by tuning the limiting potential and position of the d band center the thermodynamic and electronic properties of materials can be moderated to improve the overall catalytic performance.

Similarly, the structure of metal complexes can be tuned in order to observe the correlation with activity, like the structure-activity relationship of the copper (Cu) single atom catalyst (SAC) system.¹³⁵ Cu SAC systems have predominant Cu–N₄ and Cu–N_{4-x}–C_x active sites; the former have higher activity for CO₂RR, while both the active sites show activity towards nitrate reduction reaction. Among the three variants of Cu SAC and confined in graphene sheets (due to its fundamental advantages^{136,137}), the variations are with respect to the annealing temperature (800, 900, and 1000 °C). The elemental mapping image (Fig. 10g) reveals the presence of the elements copper, nitrogen, and carbon in the Cu SAC system. The Cu SAC sample annealed at 800 °C showed brilliant performance; the greatest urea yield rate of $4.3 \text{ nmol s}^{-1} \text{cm}^{-2}$ ($1800 \mu\text{g h}^{-1} \text{mg}_{\text{cat}}^{-1}$) was observed at -1.0 V vs. RHE while the highest faradaic efficiency of 28% was obtained at -0.9 V vs. RHE , as shown in Fig. 10(h and i). Recently, an interesting report showed a strategically designed diatomic Fe–Ni catalyst which demonstrated excellent CO₂RR and NO₃RR performance with a urea yield rate of $20.2 \text{ mmol g}^{-1} \text{h}^{-1}$ with a faradaic efficiency of 17.8% due to the effective triggering of the diatomic active sites resulting in the efficient C–N coupling reaction.¹³⁸

Electrocatalysts play a crucial role in electrochemical urea production, which involves the conversion of nitrogen gas and carbon dioxide into urea using renewable electricity. Atom-centered electrocatalysts have gained significant attention due to their potential for enhancing catalytic efficiency and

reducing costs. The advantages and disadvantages of single-atom, dual-atom, and other types of atom-centered electrocatalysts are discussed.

Single-atom electrocatalysts^{22,135}. Advantages: (a) single atoms can exhibit unique electronic properties, such as increased activity due to the presence of unsaturated coordination sites; (b) efficient utilization of metal atoms by using single-atom catalysts maximizes the utilization of metal atoms, reducing the material costs; (c) the single-atom dispersion can provide increased stability against aggregation and sintering compared to nanoparticle catalysts, thereby increasing stability; (d) precise control and tunability can be achieved for single-atom catalysts which offers the potential for fine-tuning the reactivity by controlling the coordination environment of the atom.

Disadvantages: (a) the synthesis of single-atom catalysts can be complex and requires precise control over the coordination and environment to achieve the desired catalytic properties; (b) large-scale production of single-atom catalysts is still challenging and expensive; (c) the performance of single-atom catalysts can be highly sensitive to reaction conditions, such as temperature, pH, and electrolyte composition.

Dual-atom electrocatalysts¹³⁸. Advantages: (a) dual-atom catalysts can exhibit synergistic effects between the two atoms, leading to enhanced catalytic activity and selectivity; (b) the interaction between the two atoms in dual-atom catalysts can improve stability, preventing agglomeration and promoting long-term catalytic performance; (c) dual-atom catalysts offer a wide range of possible combinations, allowing for the exploration of various catalytic motifs and performance optimization.

Disadvantages: (a) synthesizing dual-atom catalysts with controlled atomic arrangements can be challenging, requiring precise control over the reaction conditions; (b) the design principles and mechanisms governing the catalytic performance of dual-atom catalysts are not yet fully understood, limiting their rational design and optimization.

Other types of atom-centered electrocatalysts^{36,54}. Apart from single-atom and dual-atom catalysts, there are other atom-centered electrocatalysts, such as nanoparticles and surface alloys.

Advantages: (a) nanoparticle catalysts and surface alloys have well-established synthesis routes, making them relatively easier to produce on a larger scale; (b) these catalysts can exhibit higher activity compared to bulk materials due to the presence of exposed active sites and increased surface area; (c) the size and composition of nanoparticles and surface alloys can be tailored to optimize catalytic performance.

Disadvantages: (a) nanoparticle catalysts and surface alloys may suffer from particle aggregation and deactivation over prolonged use; (b) achieving precise control over the atomic arrangements in nanoparticle catalysts and surface alloys can be challenging, leading to limited control over their catalytic properties.

In summary, single-atom and dual-atom electrocatalysts offer unique advantages in terms of catalytic activity, atom utilization, and stability. However, their synthesis complexity

and limited scalability pose challenges. Other types of atom-centered electrocatalysts, such as nanoparticles and surface alloys, have more established synthesis methods but may suffer from aggregation and deactivation issues. Further research is necessary to overcome these limitations and harness the full potential of atom-centered electrocatalysts for electrochemical urea production.

3.3 Metal chalcogenides and chalcogenide borates

In this section, four variants of electrocatalysts are discussed, which are as follows: (1) metal oxides (TiO_2 , ZnO), (2) metal hydroxides ($\text{In}(\text{OH})_3$), (3) metal oxyhydroxides ($\text{In}-\text{O}-\text{O}-\text{H}$) and (4) nickel orthoborate ($\text{Ni}_3(\text{BO}_3)_2$).

3.3.1 Metal oxide(s). In this section, three types of transition metal oxide(s) (presently reported) showing electrochemical activity for urea synthesis are discussed.

(a) *Titanium oxide (TiO_2)*. The catalyst has been used to address the persisting problem of the hazardous impact of NO_x on the environment and on our life. A modified electrode

prepared by using a tin-doped indium oxide plate and coated with titanium dioxide treated with Nafion showed a decent performance at $-0.98 \text{ V vs. Ag/AgCl}$ in converting CO_2 in the presence of nitrate ions to urea with a yield of $0.33 \mu\text{moles per hour}$ and a faradaic efficiency of 40% ; however it suffered from a lack of specificity, as the electrocatalyst resulted in different product formation which includes carbon monoxide and ammonia with the yield higher than the urea yield.¹²⁹

(b) *Oxygen vacancy rich TiO_2 doped with copper*. Copper-doped TiO_2 is a synergistic catalyst system to electrochemically synthesize urea with a production rate of $20.8 \mu\text{mol h}^{-1}$ and an excellent FE of 43.1% by co-reducing CO_2 and NO_2^- ions (Fig. 11c). The heteroatom (copper) doped oxygen vacancy (OV) rich anatase TiO_2 is characterized using an XRD study (shown in Fig. 11b); TiO_2 (OV) plays the role of a synergistic site, which can efficiently act as a catalysis zone at the copper dopant site, and thereby reduce CO_2 into the CO^* intermediate adsorbate and the dual Ti^{3+} defect site allows nitrogen adsorption followed by activation. The adjacent intermediate CO^* and

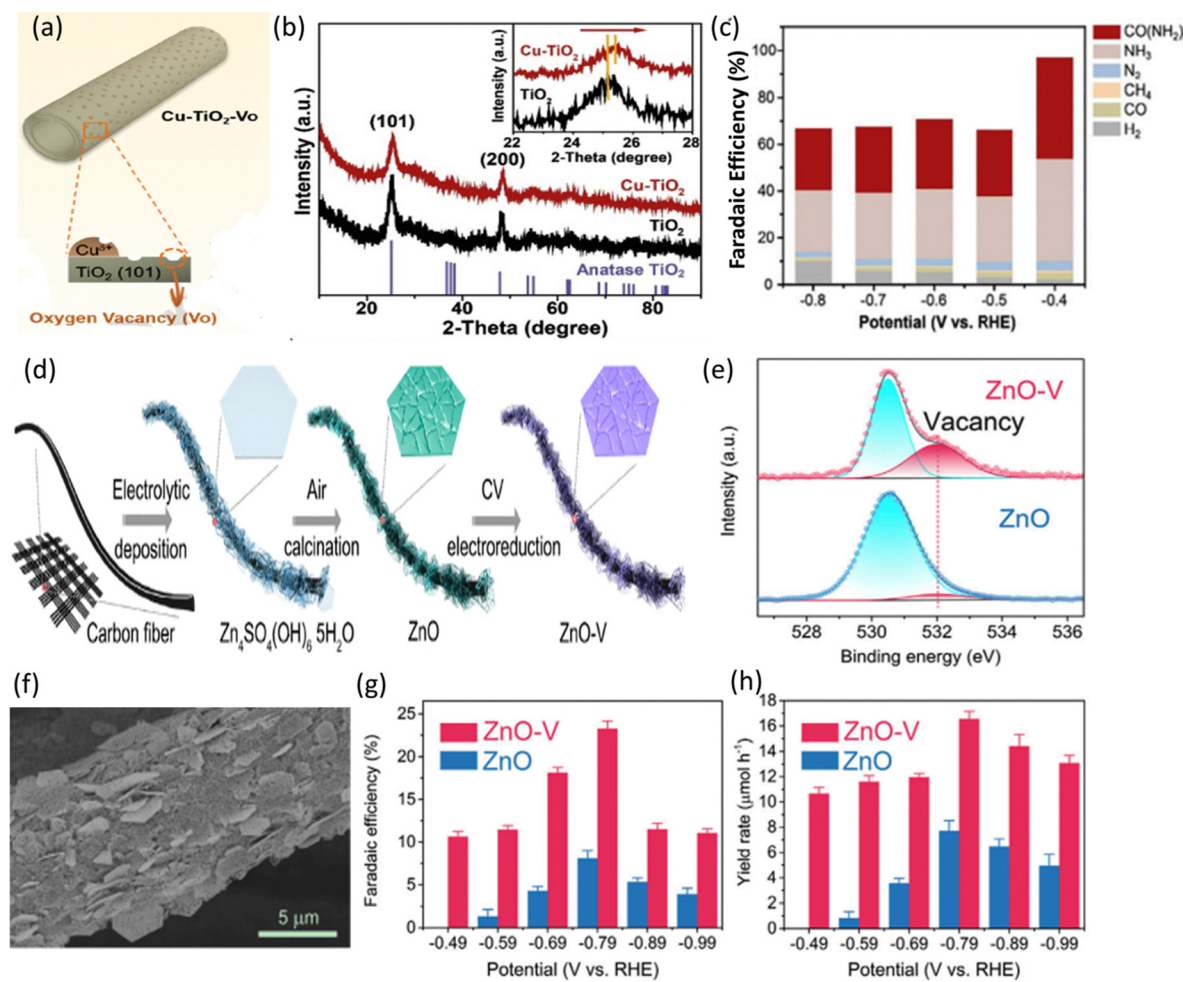


Fig. 11 (a) Diagrammatic illustration of the Cu doped TiO_2 (OV) catalyst.¹²⁷ Copyright 2020, Elsevier. (b) XRD spectra of undoped TiO_2 and Cu doped TiO_2 (OV).¹²⁷ Copyright 2020, Elsevier. (c) Faradaic efficiency of reaction products for the Cu doped TiO_2 (OV) system.¹²⁷ Copyright 2020, Elsevier. (d) Synthesis reaction scheme of ZnO (OV) porous sheets of nano order.¹²⁸ (e) O1s XPS spectra of ZnO and ZnO-V porous nanosheets.¹²⁸ (f) SEM image of ZnO (OV). (g and h) Faradaic efficiency and urea yield rate of ZnO (OV).¹²⁸

NH_2^* formation assists in C–N bond formation by a tandem reaction, to ultimately produce urea.¹²⁷

(c) *Oxygen vacancy rich ZnO porous nanosheets.* The oxygen vacant sites in the synthesized ZnO porous nanosheets can show electrochemical activity, and the synthesis reaction scheme is shown in Fig. 11d, and the oxygen vacant sites in ZnO were confirmed by an XPS study (Fig. 11e).¹⁰ The oxygen vacant ZnO has a hexagonal porous nanosheet morphology (Fig. 11f). The electrocatalyst is capable of converting nitrite contaminants and CO_2 to urea with a faradaic efficiency of 23.26% and a urea yield rate of $16.56 \mu\text{mol h}^{-1}$ at -0.79 V (vs. RHE), as shown in the bar charts in Fig. 11(g and h). The probable coupling of NH_2^* and COOH^* to produce urea has been studied by the conjoint use of *in situ* diffuse reflectance FTIR and differential electrochemical mass spectrometry.

3.3.2 Metal hydroxides. The electrocatalyst In(OH)_3 with explicitly designed {100} facets of nano-cubes in the range of 100–200 nm (Fig. 12a) *via* the solvothermal process resulted in a urea yield of $533.1 \mu\text{g h}^{-1} \text{ mg}_{\text{cat}}^{-1}$ (Fig. 12d) and a superior faradaic efficiency of 53.4% at -0.6 V vs. RHE with ultra-high nitrogen and carbon dioxide selectivity of 82.9% and $\sim 100\%$ respectively.¹²⁴ The electrocatalyst $\text{In(OH)}_3\text{-S}$ exhibits intrinsic n-type semiconductor behaviour as shown in Fig. 12(b and c); however a few interesting observations are made when argon gas is replaced with carbon dioxide. We find that the Mott–Schottky plot is divided into two regions, clearly showing the n-type region (positive slope) and the p-type region with the usual negative slope. The slope for the CO_2 purged system is much higher in comparison to the argon purged condition. The magnitude of the slope (in the linear region) is inversely related to the carrier concentrations. It is evident that electron population in n-type $\text{In(OH)}_3\text{-S}$ decreases in the CO_2 purged system.

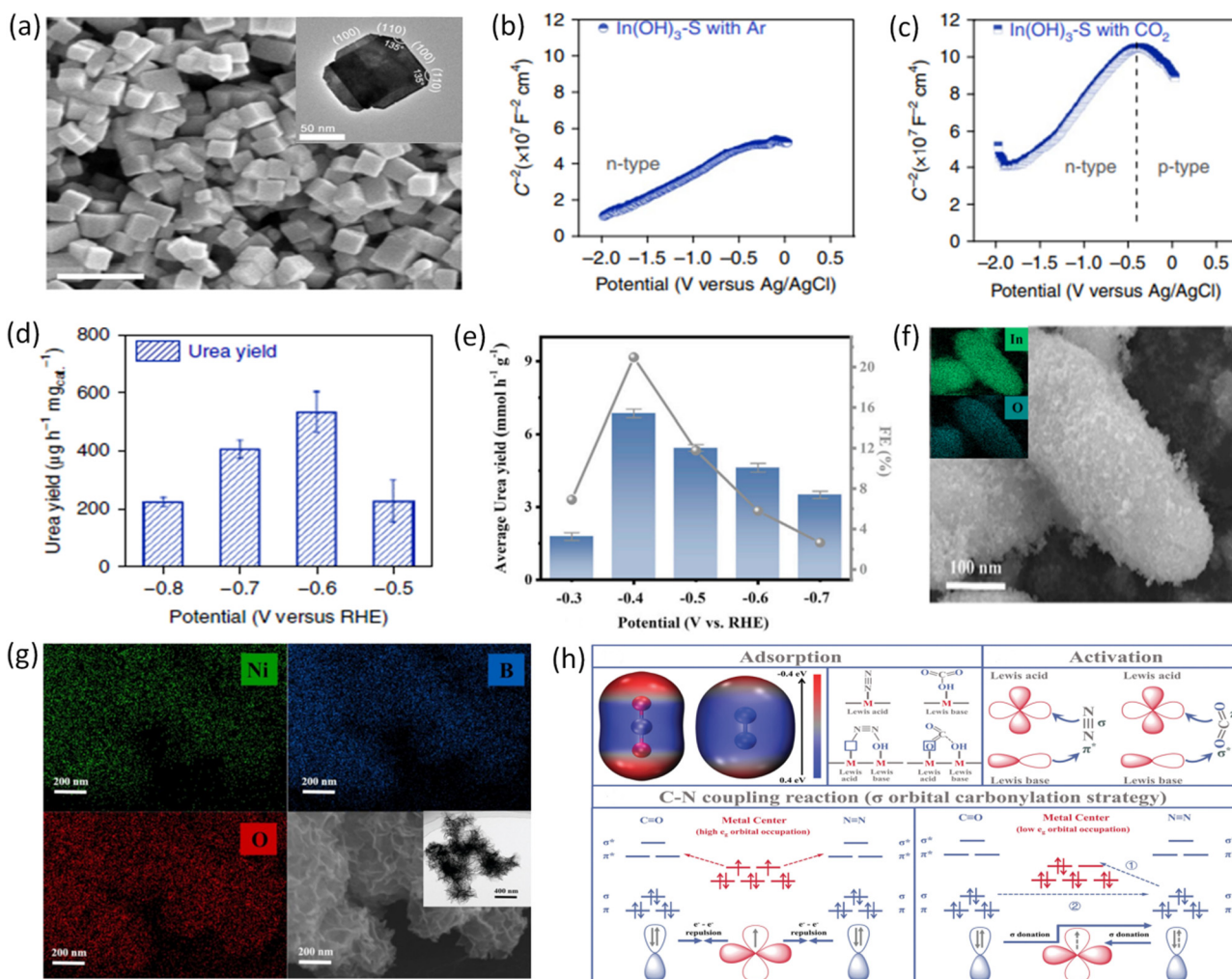


Fig. 12 (a) SEM image of $\text{In(OH)}_3\text{-S}$, scale bar, 500 nm (inset: TEM image).¹²⁴ (b and c) Mott Schottky plots measured in Ar and CO_2 for $\text{In(OH)}_3\text{-S}$.¹²⁴ (d) urea yield at different potentials for $\text{In(OH)}_3\text{-S}$.¹²⁴ (e) urea yield and faradaic efficiency at different potentials for In-O-O-H .¹³⁹ Copyright 2022, Elsevier. (f) SEM image and EDX mapping image of In-O-O-H .¹³⁹ Copyright 2022, Elsevier. (g) EDX elemental mapping of $\text{Ni}_3(\text{BO}_3)_2$ (inset: HRTEM image).¹⁴⁰ Copyright 2021, Royal Society of Chemistry. (h) Schematic illustration of artificial frustrated Lewis pairs in the adsorption, activation, and finally C–N coupling reaction steps during the urea electrosynthesis process.¹⁴⁰ Copyright 2021, Royal Society of Chemistry.

Therefore the synergistic effect of lower electron concentration and the p-type semiconducting behaviour of $\text{In(OH)}_3\text{-S}$ allows entrapment of electrons by CO_2 with the culmination of the hole layer on the surface of $\text{In(OH)}_3\text{-S}$. Thus due to the accumulation of the surface hole layer, n-type $\text{In(OH)}_3\text{-S}$ is transformed into p-type; therefore the catalyst can easily repel H^+ from its surface and effectively suppress the competitive HER.

3.3.3 Metal oxyhydroxides. This category includes a single reported electrocatalyst, namely, In-O-O-H nanocrystals,¹³⁹ which have a rice-like morphology as shown in Fig. 12f. The catalyst demonstrated a decent urea yield rate and a faradaic efficiency of $6.85 \text{ mmol h}^{-1} \text{ g}^{-1}$ and 20.97% at -0.4 (vs. RHE), as shown in Fig. 12e. In electrocatalytic urea synthesis, the activation step is the most challenging step which involves the rupture of the C=O bond and the $\text{N}\equiv\text{N}$ bond; the electron loss and gain process occurring in between the gaseous reactants and the catalytic sites results in the polarization of gas molecules and elongation of the chemical bonds until they break apart, thereby achieving the process of activation. Once the activation process is achieved, it results in the production of intermediates (like CO^* and N_2^*), and then the subsequent electrocatalytic coupling reaction occurs to form the vital C–N bond.

3.3.4 Metal borates. In this section we discuss the interesting electrocatalyst $\text{Ni}_3(\text{BO}_3)_2$,¹⁴⁰ which has a flower like morphology as shown in Fig. 12g. The electrochemical performance was brilliant with a urea yield of $9.75 \text{ mmol h}^{-1} \text{ g}^{-1}$ and an FE of 20.36% at -0.5 (vs. RHE). A unique strategy was adapted to prepare the catalyst system, in order to engineer an artificial frustrated Lewis pair (AFLP) in $\text{Ni}_3(\text{BO}_3)_2$. Briefly, a Lewis acid and a Lewis base possess such a stereochemical orientation due to precise molecular engineering such that the Lewis pair is prevented from any bond formation, thereby increasing the chemisorption capability and easier reaction with reactant gas molecules. The surface electrostatic potential analysis (Fig. 12h) proves that the carbon atom in the CO_2 molecule and the nitrogen atom in the N_2 molecule are electron deficient and electron rich, respectively. Thereafter, the lone pair electrons of the N atom in the N_2 molecule are donated to the Lewis acid sites coupled with the empty orbitals, while the C atom in the CO_2 molecule can easily accept electrons from the Lewis base sites having excess electrons. As a result, the AFLP can carry out the extremely important process of chemisorption of the dual gaseous reactants, namely N_2 and CO_2 molecules, *via* the unique orbital interaction. Yuan *et al.*¹⁴⁰ have used this strategy not only to address the major issue of adsorption and activation but also trigger the vital C–N coupling reaction by the σ orbital carbonylation technique; the schematic representation of the entire process of adsorption, activation and C–N coupling reaction is provided in Fig. 12h.

3.4 Metal alloy or bimetallic electrocatalytic systems

3.4.1 Te-doped Pd nanocrystals (NCs). This particular electrocatalytic system falls under the bimetallic system. Te-Pd NCs were prepared using the wet chemical technique; the HAADF-STEM image confirms the uniform size distribution

of synthesized Te-Pd NCs with a mean diameter of 20 nm (Fig. 13a and b).⁵⁴ The electrocatalyst displayed efficient electrochemical performance and showed activity towards the CO_2 and NO_2^- dual reduction reactions to produce urea at -1.1 V (vs. RHE) and achieved a faradaic efficiency of 12.2% and a N-atom efficiency of 88.7%, as shown in Fig. 13(d and e). The dual study of XPS, and XANES are complementary to one another, as the XPS study in Fig. 13c reveals that $3\text{d}_{3/2}$ and $3\text{d}_{5/2}$ peaks of Pd^0 undergo a small negative transposition for Te-doped Pd NC and the XANES study shows Pd to be in the metallic state and Te-Pd NC has lower intensity than Pd NC which implies that there is clear facilitation of electron transfer from Te to Pd. The precise fabrication of the electronic structure by judicious and strategic doping of Te in Pd NC enhanced the carbon dioxide adsorption and nitrite reduction to form urea.

3.4.2 Metal alloys. The Pd_1Cu_1 electrocatalytic system, as metal alloying enhances electronic interaction of a bimetal, promotes chemical adsorption and provides a greater number of active sites which are a necessity for electrocatalysis. TiO_2 nanosheets having oxygen vacancies are used as a catalyst support system which anchors the PdCu alloy nanoparticles, with a dimensional range of 2–4 nm (Fig. 13f).³⁵ The high-resolution XPS study reveals that the Pd $3\text{d}_{5/2}$ peak for $\text{Pd}_1\text{Cu}_1/\text{TiO}_2$ was shifted by 0.3 eV compared to that of Pd/TiO_2 , as shown in Fig. 13g. Similarly the Cu $2\text{p}_{3/2}$ peak for $\text{Pd}_1\text{Cu}_1/\text{TiO}_2$ was shifted negatively by 0.6 eV compared to that of Cu/TiO_2 (Fig. 13h) which confirms the promotion of interaction between the PdCu alloy and the TiO_2 –oxygen vacancy catalyst support. $\text{Pd}_1\text{Cu}_1/\text{TiO}_2$ displayed electrocatalytic urea synthesis at different potentials ranging from -0.3 to -0.8 V vs. RHE, as displayed in Fig. 13i. The maximum urea production rate of $3.36 \text{ mmol g}^{-1} \text{ h}^{-1}$ and a faradaic efficiency of 8.92% were reported at -0.4 V (vs. RHE).

3.5 Heterostructured catalyst

The heterostructural interface of $\text{Bi}-\text{BiVO}_4$ can assist in the specific adsorption and activation of the CO_2 and N_2 reactant molecules to form urea by the interplay of the electrochemical interface construction at the applied potential leading to the strategic design of the space charge region enhancing the formation of the mandatory C–N bond. Theoretical demonstration by electron density isosurface represented by the electrostatic potential scale, as shown in Fig. 14a, conceptualized the fact that the N atom has higher electron density in the N_2 molecule and the C atom has lower electron density in the CO_2 molecule and these atoms specifically target and adsorb on the electrophilic and nucleophilic zones of the heterostructured $\text{Bi}-\text{BiVO}_4$ catalyst due to the electronic interaction of the reactant molecule and the catalyst.¹⁴¹ The Mott Schottky (MS) analysis reveals about the transfer of electrons in the $\text{Bi}-\text{BiVO}_4$ catalytic system. BiVO_4 displays a positive slope in the MS plot (Fig. 14b), which represents the characteristic nature of the n-type semiconductor. In conjugation with metallic Bi, BiVO_4 gives rise to a fascinating MS heterostructure, in which electron movement can take place from BiVO_4 to the metallic Bi

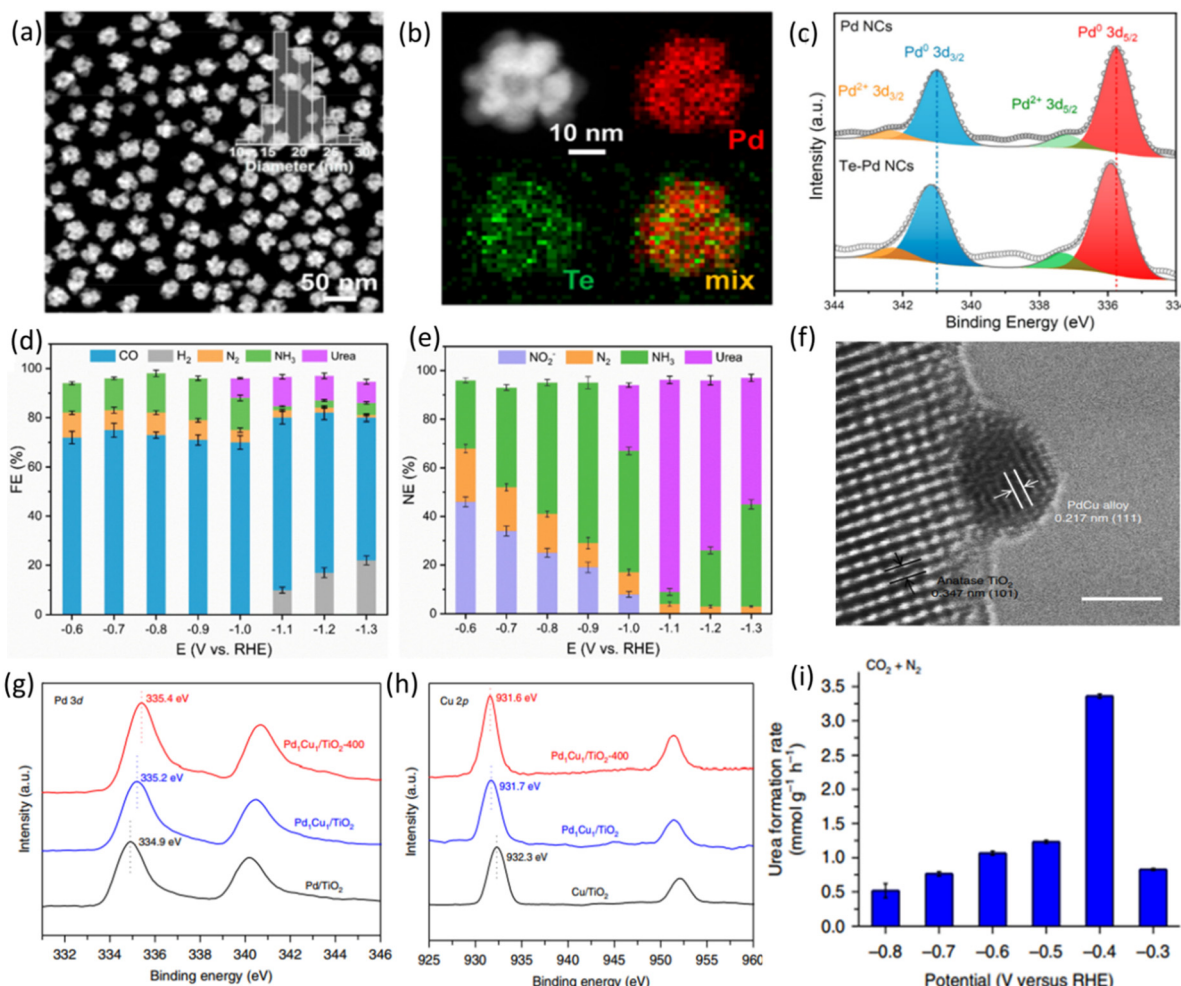


Fig. 13 (a and b) HAADF-STEM image and elemental mapping of Te–Pd NCs.⁵⁴ Copyright 2020, American Chemical Society. (c) Pd 3d XPS spectra of Te–Pd NCs.⁵⁴ Copyright 2020, American Chemical Society. (d and e) Faradaic efficiency and nitrogen efficiency at different potentials for urea synthesis of Te–Pd NCs.⁵⁴ Copyright 2020, American Chemical Society. (f) HRTEM image of Pd₁Cu₁ anchored on the TiO₂ substrate, scale bar 2 nm.³⁵ Copyright 2020, Springer Nature. (g and h) XRD spectra of Pd (3d) and Cu (2p) of the electro-catalyst system.³⁵ Copyright 2020, Springer Nature. (i) Urea formation rate at various potentials of Pd₁Cu₁/TiO₂.³⁵ Copyright 2020, Springer Nature.

counterpart, as displayed in the inset of Fig. 14b, owing to the unique space–charge orientation. The bar chart shown in Fig. 14c displays a urea yield rate of 5.91 mmol h⁻¹ g⁻¹ and a faradaic efficiency of 12.55% using a 0.1 M KHCO₃ electrolyte at -0.4 V vs. RHE.

Another catalytic system is represented by perovskite structured BiFeO₃/BiVO₄; this particular heterostructure gave rise to a unique p–n junction at the electrochemical interface which enhances the local charge redistribution *via* the localized nucleophilic and electrophilic interaction with the reactant molecules and also specific adsorption and co-activation of N₂ and CO₂, with exposed active sites and enhanced electrocatalytic kinetics facilitating the C–N bond formation by the specific *NCON* intermediate generation.⁵⁶ The FESEM image shown in Fig. 14d reveals that the BiFeO₃/BiVO₄ heterostructure has a distinctive feature of rice-like morphology with an average length of 1 mm and a diameter of approximately 400 nm. The relevant elemental mapping

demonstrates the evenly distributed Bi, Fe, V, and O elements (Fig. 14e). The Raman spectra (Fig. 14f) show the characteristic vibrational bands at 137 and 171 cm⁻¹ of Fe–O–Fe bonds in BiFeO₃; a small negative shift is observed with lowering of intensity when incorporated into the BiVO₄ system. The typical V–O stretching modes were present at 637, 702 and 826 cm⁻¹ and the VO₄³⁻ bending modes occurred at 327 and 367 cm⁻¹; the peaks also showed a distinct negative shift of the heterostructure in the space–charge zone. This broadening of vibrational modes and position shifting in the BiFeO₃/BiVO₄ electrocatalytic system clearly manifest the strong coupling interaction between BiFeO₃ and BiVO₄ heterostructures. The urea yield rate for the BiFeO₃/BiVO₄ system was found to be 4.94 mmol h⁻¹ g⁻¹ with a faradaic efficiency of 17.18% at -0.4 V vs. RHE (Fig. 14g); the performance was much better in comparison to those of BiFeO₃ (urea yield rate: 1.41 mmol h⁻¹ g⁻¹, FE: 4.35%) and the BiVO₄ system (urea yield rate: 2.50 mmol h⁻¹ g⁻¹, FE: 7.59%). The electrochemical

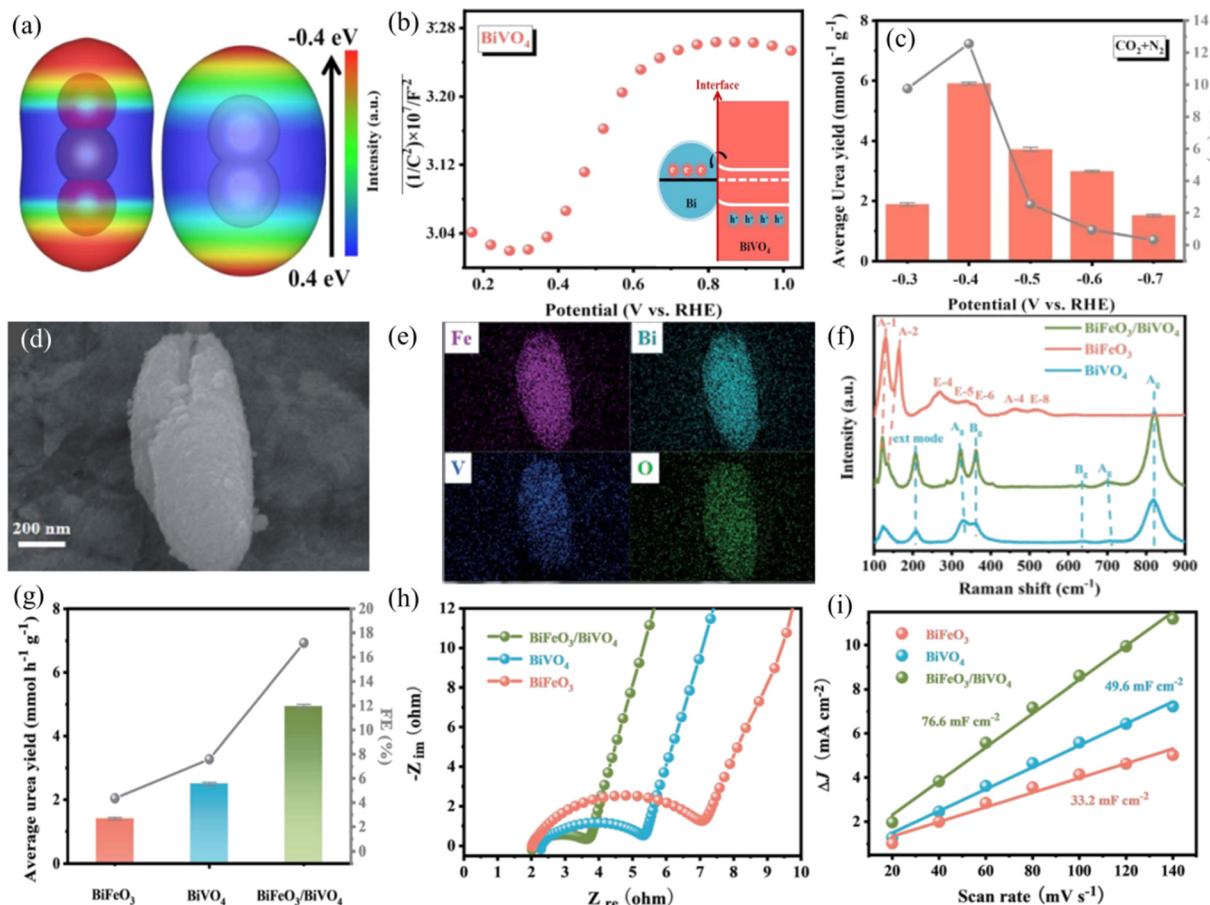


Fig. 14 (a) Electron-density isosurface of carbon dioxide (left) and nitrogen (right), the color bar represents the electrostatic potential scale.¹⁴¹ Copyright 2021, John Wiley & Sons, Ltd. (b) Mott–Schottky plot of BiVO₄ (inset: charge transfer process of Bi–BiVO₄).¹⁴¹ Copyright 2021, John Wiley & Sons, Ltd. (c) Urea formation rate and faradaic efficiency at various potentials for urea synthesis using Bi–BiVO₄.¹⁴¹ Copyright 2021, John Wiley & Sons, Ltd. (d and e) SEM and elemental mapping of the BiFeO₃/BiVO₄ heterostructure.⁵⁶ (f) Raman spectra of BiFeO₃/BiVO₄.⁵⁶ (g) Comparative urea yield.⁵⁶ (h) Nyquist plots of electrochemical impedance spectra (EIS) of BiFeO₃, BiVO₄ and BiFeO₃/BiVO₄.⁵⁶ (i) ΔJ of electrocatalysts plotted against the scan rate.⁵⁶

impedance spectroscopy (EIS) analysis (Fig. 14h) suggests that BiFeO₃/BiVO₄ shows a smaller semicircle and a higher slope than BiFeO₃ and BiVO₄, proving that the presence of local charge redistribution in the BiFeO₃/BiVO₄ heterostructure significantly promotes electron/ion transfer kinetics during the electrocatalytic process. The electrochemically active surface area (ECSA) results shown in Fig. 14i reveal that the BiFeO₃/BiVO₄ heterostructure (76.6 mF cm^{-2}) shows a greater electrochemical double-layer capacitance (C_{dl}) value than BiFeO₃ (33.2 mF cm^{-2}) and BiVO₄ (49.6 mF cm^{-2}), which signifies that local charge redistribution enhances the exposure of a greater number of active sites in the BiFeO₃/BiVO₄ heterostructure for gas molecule adsorption and activation. A ternary catalytic system was prepared based on the bimetal selenide heterostructure ($\text{Zn}_x\text{Ni}_{1-x}\text{Se}$ with NiSe/ZnSe) anchored on porous carbon nitride ($\text{g-C}_3\text{N}_4$). The photocatalytic activity remarkably improved for the ternary catalyst as compared to the binary system ($\text{ZnSe}/\text{g-C}_3\text{N}_4$ or $\text{NiSe}/\text{g-C}_3\text{N}_4$); furthermore the heterostructure showed decent performance with a urea yield rate of $1.12 \mu\text{mol h}^{-1} \text{ g}^{-1}$.¹⁴²

3.6 Carbon based electrocatalytic systems

3.6.1 Dual silicon doped graphitic carbon nitride sheet. The theoretical study using *ab initio* calculations proposed a novel non-hazardous metal free catalyst in the form of dual silicon doped graphitic carbon nitride sheets which can activate the nitrogen molecule followed by adsorption and addition of CO into the N–N bond forming the C–N bond and the intermediate $^{*}\text{NCON}^{*}$ to produce urea as the final product. The exclusivity of the work lies in the suppression of the ammonification reaction and hydrogen evolution reaction (HER) as the calculated onset potential of urea formation is much lower than that of HER and ammonia synthesis.¹⁴³

3.6.2 Metal-nitrogen-doped carbon (M–N–C) catalyst. Theoretical computations were done for different double transition metal(s) which are supported on corrole substrates.¹⁴⁴ Further investigations were done to find the carbon dioxide and nitrogen reduction capability to form urea using the electrocatalysis technique. From the list of metallic corrole catalysts, $\text{V}_2\text{N}_6\text{C}$ showed exceptional results with respect to urea synthesis

due to the unique electronic structure, strong interaction of the metal and the substrate and finally synergistic catalytic activity.

4. Strategies to combat competition reactions

As electrocatalytic urea synthesis involves the vital C–N bond formation, which involves the coupling reaction of carbon dioxide and nitrogenous intermediates, this often can give rise to different parallel reaction(s), thereby producing various products other than urea. This affects the overall process selectivity, so in order to combat and improve the selectivity performance the following strategies are exercised.

4.1 Suppression of HER formation

HER is the primary reaction which directly competes with the process of electrochemical urea synthesis. In order to combat the opponent, and finally dominate the HER process, we must understand the manner in which the HER process occurs. There are two distinct mechanisms of HER: (1) Tafel–Volmer and (2) Heyrovsky–Volmer mechanistic routes (Table 5).^{145–147} The Volmer step involves the reaction of a proton present in the electrolyte with an electron, in order to form an adsorbed hydrogen atom (H^*) on the catalytic surface. The next step proceeds *via* the Heyrovsky mechanism, in which the as-formed H^* directly combines with another proton and electron to produce H_2 . In the Tafel mechanism, another proton reacts with an electron to newly form H^* ; this nascent H^* reacts with the former H^* (produced *via* the Volmer reaction) to produce H_2 .

As we can find in the Tafel pathway, it is mandatory to have two adjoining active sites in order to adsorb two H^* species, so if we can tactfully design a catalyst in which such availability of adjoining active sites is less, like in the case of a single atom catalytic system, then we can effectively hinder the Tafel step and thus the HER process will be severely inhibited.

Now, the question remains how we can further restrict the HER process which may take place during the process of electrocatalytic urea synthesis. As CO is one of the vital intermediate species of urea formation, the above mentioned mechanism can also be applied during the reduction of the carbon dioxide molecule, as provided in Table 6.

Now, from the perspective of electrocatalyst design, the HER process can be further suppressed by the interplay between semiconductor switching and its effect on catalytic chemistry. The adsorbed CO_2 on the catalyst surface turns $In(OH)_3S$ into a p-type semiconductor;¹²⁴ furthermore the CO_2 can attract and seize the electrons to form a hole layer on the catalytic surface and thus the CO_2 instigated hole accumulation layer plays a

Table 5 The mechanistic route for the HER process

Chemical reaction	Mechanism
$H^+ + e^- \rightarrow H^*$	Volmer
$H^* + H^+ + e^- \rightarrow H_2$	Heyrovsky
$H^* + H^* \rightarrow H_2$	Tafel

Table 6 The mechanistic route for HER suppression via electrocatalytic urea synthesis

Chemical reaction	Mechanism
$CO_2 + H^+ + e^- \rightarrow COOH^*$	
$COOH^* + H^+ + e^- \rightarrow CO + H_2O$	Heyrovsky
$COOH^* + H^* \rightarrow CO + H_2O$	Tafel

pivotal role in repelling the protons effectively from the catalyst surface and thereby suppresses HER formation. It is important to note that transition metals' d orbital electrons with the appropriate symmetry help generate metal-H bonds, which has the effect of increasing the catalytic efficiency for the competitive HER while lowering the same for the urea synthesis process. In order to reduce hydrogen's propensity to bind to the chemical while also defeating the HER, a non-metallic equivalent could be added to transition metal compounds, and thus carbon, nitrogen, oxygen, or even boron containing groups can be bonded with the transition metal which in turn can suppress HER formation and promote urea yield. Apart from this technique, HER can be effectively suppressed by using transition metal phthalocyanines (CuPc);³⁶ they intrinsically possess multiple active sites, primarily nitrogen coordinated metal centres ($M-N_4$), and a non-metallic counterpart in CuPc, which provides a scope to decrease the adsorption capability of hydrogen to the catalyst and simultaneously suppress the HER. The abundant valence electrons in the non-metallic component of CuPc also provide a greater number of active sites for electrochemical urea synthesis.

Hence, for future application, we can strategically design various types of metal hydroxide(s), and engineer their properties in order to suppress the HER performance and increase the yield of electrochemical urea production.

4.2 Impeding ammonia production

In metal alloy systems³⁵ the parallel reaction of ammonia formation involves the energy input as it is highly endothermic in nature; hence ammonia production is highly impeded while $*NCON^*$ intermediate formation by nitrogen activation is kinetically as well as thermodynamically feasible which forms the basis of the C–N coupling reaction and thus enhances urea formation by increasing the selectivity of the catalytic system. It was also noted in perovskite hybrids⁵⁶ that the step of nitrogen reduction by proton addition forms the potential determining step of ammonia formation; the ΔG ($*NNH$) value was significantly higher than the ΔG ($*NCON^*$) value of the C–N coupling reaction, and due to the significantly high activation energy barrier the catalyst was inactive and did not produce ammonia at all.

4.3 Tuning CO production

The formation of CO can be precisely controlled by selecting a specific catalyst and judiciously optimizing and setting a specific threshold voltage for that particular catalytic system; for example in perovskite hybrids as well as in metal alloys the optimum voltage was set to be -0.4 V.^{35,56}

4.4 Selection of the electrolyte

The process of urea synthesis in an aqueous electrolyte under ambient conditions by a nucleophilic addition reaction between the molecular NH₃ and the CO₂⁻ intermediate during the CO₂RR process is an important avenue for urea production. In the field of electrocatalysis, the electrode–electrolyte interface plays a very important role with regard to the yield and efficiency of the electrosynthesis process.

As a protocol, the electrocatalyst which shows activity towards CO₂ reduction is primarily assessed by conducting linear sweep voltammetry experiment by saturating the electrolyte with CO₂ gas and comparing with respect to the inert gas (Ar). Thereafter the current density is assessed and the faradaic efficiency is reported. During the CO₂RR, a substantial number of CO₂⁻ intermediates are adsorbed onto the surface of the electrocatalyst; this is the key step in the nucleophilic addition process for the production of urea.

When using NH₄HCO₃ solution as the electrolyte for urea production rather than feeding NH₃ gas directly into the electrochemical system, after evaluating the CO₂ catalytic activity. This is due to the inevitable reaction between CO₂ and NH₃ at the electrode–electrolyte interface that produces a significant amount of NH₄HCO₃, which could compete with the generation of urea and eventually lead to a decrease in the urea yield. However, when NH₄HCO₃ plays the role of an electrolyte, the hydrolysis of NH₄⁺ (NH₄⁺ ⇌ NH₃ + H⁺) in an aqueous solution continuously supplies NH₃ for the synthesis of urea,

and thereby may promote the process of electrocatalytic urea synthesis.

5. Advancement of electrochemical cells and reactors

The electrochemical cell design is an essential component of the electrochemical urea synthesis process, as it plays the determining role with respect to the current density, faradaic efficiency, and stability. Since the first report about electrochemical urea synthesis in 1995, various kinds of cell design have been implemented in this field to enhance the performance. Presently, different kinds of electrochemical cells can be classified into the following categories: gas diffusion electrodes,^{22,23} H-type cells or two compartment cells,^{35,36,54} flow cells,^{35,54} and pressurized electrochemical cells.¹²¹ On the basis of reactors they can be categorized into two domains, namely, electromagnetic field induced reactors¹⁴⁸ and plasma assisted reactors.^{149–152} The following paragraphs explain the reactors and electrochemical cells in a detailed manner.

5.1 Pressurized electrochemical cell

In the electrochemical urea synthesis using a mixed atmosphere of CO₂ and N₂ under high pressure conditions of 30 bar for each gaseous component (Fig. 15a),¹²¹ the electrocatalysts of polyaniline and polypyrrole were painted over platinum electrodes

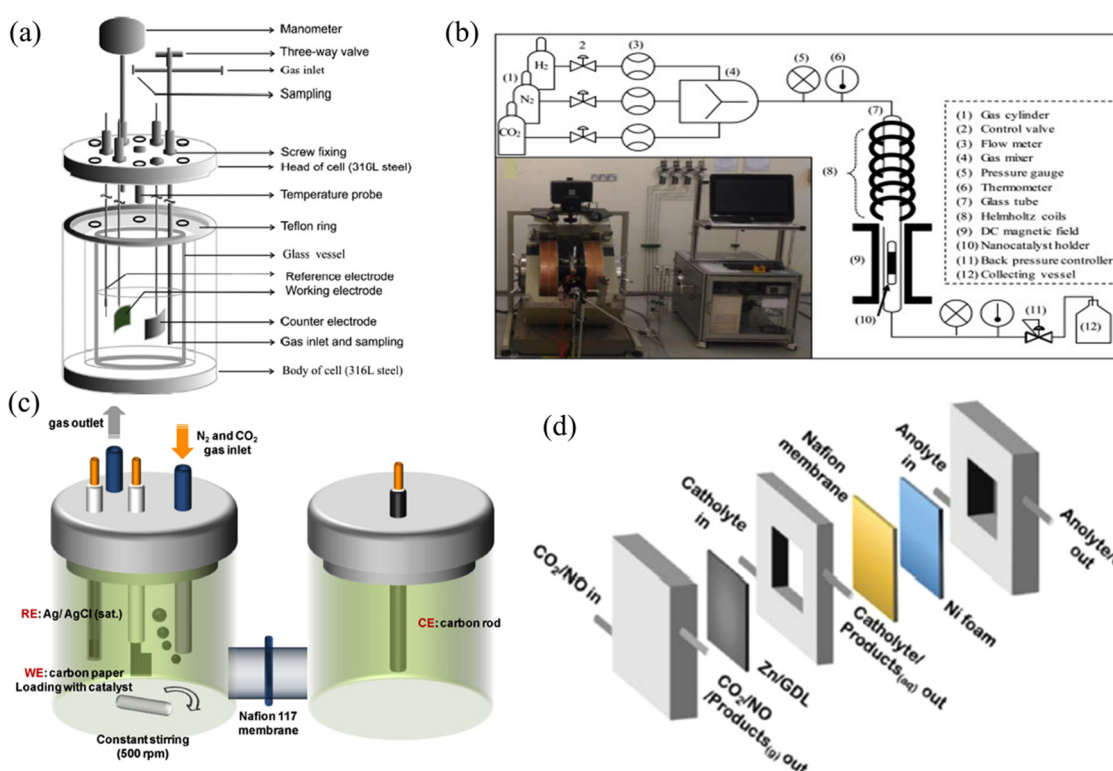


Fig. 15 (a) Pressurized electrochemical reactor.¹²¹ Copyright 2016, Elsevier. (b) Electromagnetic field induced reactor.¹⁴⁸ Copyright 2020, Elsevier. (c) Schematic representation of the H-type cell.³⁵ (d) Electrochemical flow cell reactor.¹²⁵ Copyright 2022, American Chemical Society.

and then the electrochemical reactions were carried out and the optimized potential was found to be -0.325 V which demonstrated a maximum urea yield of $21.2\text{ }\mu\text{mol}$ by polypyrrole and $12\text{ }\mu\text{mol}$ by polyaniline.

5.2 Electromagnetic field induced reactor

The electromagnetic field induced reactor (Fig. 15b) enhanced the kinetics of the urea synthesis in an efficient manner. The induced magnetic field effectively reduced the activation energy of the catalysts and weakened the chemical bonds present in the reactant molecules thereby enhancing the rate constant and increasing the urea yield. The two nanocatalysts considered for study, namely, Fe_3O_4 and ZnO , produced a maximum urea yield of 6500 ppm and 1000 ppm, respectively, at 0.5 MHz.¹⁴⁸

5.3 Gas diffusion electrode (GDE)

The first report on electrochemical urea synthesis using various metal loaded gas diffusion electrodes was published by Shibata *et al.*^{22,23} The nitrate ions and carbon dioxide were used as reagents to perform electrochemical reaction on various metal loaded GDEs to produce urea. Among different metals under study the best results were shown by the zinc loaded GDE with a faradaic efficiency of 35% at -1.75 V. In another study where the authors used feedstocks in the form of CO_2 and 0.02 M $\text{NO}_2^-/\text{NO}_3^-$ ions and a pressure of 1 bar was applied in the Cu-loaded GDE, a faradaic efficiency of 37% at -0.75 V (vs. RHE) was obtained.²²

5.4 Plasma assisted technology

The feasibility of urea production *via* gas-phase synthesis under ambient conditions by passing carbon dioxide and nitrogen gases under the influence of negative corona discharge was revealed, which resulted in the reaction of electronegative ammonia anions and CO_2 to form the vital C–N bond essential in urea formation. The study demonstrated urea synthesis without using any kind of metal catalyst yet with a conversion of 82.16% at 20 °C at 1 atm.¹⁴⁹ Recently, the plasma catalysis-integrated electrocatalysis has been widely demonstrated as an effective strategy to effectively activate nitrogen and the development of plasma techniques also promises to convert air to NO_3^- with low energy consumption and accelerate the process of electrochemical urea synthesis.^{150–152}

5.5 H-type cell

The H-type cell is the most common and conventional electrochemical cell^{35,36,54} employed for electrocatalytic urea synthesis; the two chambers of the H-type cell are separated by a selectively permeable membrane (Nafion membrane generally) which allows only proton exchange (Fig. 15c). The two electrodes are placed on two chambers separately; concerned gas or gases are purged in the chamber of the working electrode, and the catalyst mounted on the working electrode adsorbs the reactant molecules and the potential is applied to perform the electrochemical reaction. As the cathode chamber is separated from the anode chamber, it enhances the yield of urea formation by minimizing the oxidation of electrochemically

synthesized urea. As the process involves a selectively permeable membrane, it specifically allows proton exchange; hence the process shows high selectivity with respect to product formation.

5.6 Flow cell

The flow cell enhances the electrocatalytic performance as there is an increased electrode surface area which is exposed to the reactant molecules along with efficient mass transport;^{35,54} as a higher fraction of electrode area coverage can occur for gaseous reactants it shows enhanced performance towards gas-consumption reactions.³⁵ The flow cell is schematically shown in Fig. 15d.¹²⁵

5.7 Strategic design to optimize the electrochemical reactor

The experimental study confirms that in comparison to the H-type cell ($0.12\text{ mmol g}^{-1}\text{ h}^{-1}$ and faradaic efficiency of 0.66%) the flow cell ($3.36\text{ mmol g}^{-1}\text{ h}^{-1}$ and faradaic efficiency of 8.92%) performs clearly well in terms of the urea formation rate and faradaic efficiency.³⁵ Basically, the electrochemical cell is a reactor where the oxidation and reduction processes occur resulting in the redox reaction. The previous report suggests that current density, faradaic efficiency and yield not only depend upon the electrocatalyst but also on the electrochemical cell design. In the single cell the electrochemical cell design is simple, while in the H-type cell it involves a certain degree of complexity, as the two chambers of the H-type cell are joined *via* a membrane at the junction, which must have adequate gripping and not allow leakage of the electrolyte. The design of the H-type cell must involve necessary mass transfer and an optimized ion transport channel, as the Nafion membrane is a proton exchange membrane, which selectively allows protons to pass through the anode chamber to the cathode chamber. Urea produced during the process of electrocatalysis can undergo oxidation in the single cell while no such possibility exists in the H-type cell. Hence, the urea yield is expected to be higher in the case of the H-type cell as compared to the single cell. Finally, the industrial scaling and commercialization of the process of electrochemical urea synthesis can be addressed on process optimization terms. The economic perspective allows the single cell to have the upper hand over the H-type cell, as it does not involve design complexity and hence is less capital intensive. However, if sufficient capital is available for the setup of the H-type cell, for the cost of the Nafion membrane and the maintenance of the moving parts, then the H-type cell will surely be a better choice as the urea yield will be higher than in the single cell.

As proposed in the review article, the H-type cell^{35,36,54} is the most commonly used electrochemical cell to screen and evaluate the electrocatalytic performance in the electrolytic solution. However to overcome the limitation of mass transfer efficiency due to the low solubility of the dual gases, *i.e.*, CO_2 and N_2 , in aqueous electrolyte solutions, the flow cells are employed which show enhanced mass transfer efficiency as shown by the electrochemical study; the reason for the observation lies in the continuous transfer of reactants and products to

and away, respectively, from the electrode surface. It is clearly evident from the above discussion that the field of electrocatalytic urea synthesis is at the laboratory scale. In order to attain industrial maturity stage for this technology, some critical aspects like the yield, current density, and faradaic efficiency corresponding to the mass transport phenomena need to be addressed. Therefore, electrochemical cell design will play a crucial role in obliterating the present limitations suffered by the process. This review expects to trigger future research prospects in designing an efficient electrochemical reactor to serve the purpose of mass transfer, enhanced urea formation rate, and enhanced faradaic efficiency and ultimately present a practical application for electrochemical urea synthesis.

5.8 Advantages and disadvantages of different types of electrochemical cells/reactors

Cell type	Advantages	Disadvantages		
Gas diffusion electrode (GDE)	Gas diffusion electrodes (GDEs) incorporate a three-phase interface inside the electrode and significantly improve the kinetics of gas-related electrochemical reactions, such as O ₂ electroreduction, CO ₂ electroreduction, and N ₂ electroreduction	Two main challenges: flooding (infiltration of aqueous electrolytes into the GDE) and carbonation (interaction of CO ₂ with hydroxide, for CO ₂ RR). Flooding is challenging for all GDEs regardless of gaseous food and application, which causes HER through aqueous environment ¹⁵³	H-type cell	a cell reaction to high temperatures. As we cannot apply high temperature directly in a cell chamber, we can achieve that temperature by applying pressure Working electrode and counter electrode are separated by a chamber (with a membrane). The final product cannot interact with the counter electrode It is significantly easier for product separation and/or collection (especially gas)
Electromagnetic field induced reactor	The electromagnetic field-induced reactor enhances the kinetics of the reaction, and the induced magnetic field effectively reduces the activation energy of the catalysts and weakens the chemical bonds present in reactant molecules thereby enhancing the rate constant and increasing the electrolysis yield rate ¹⁴⁸	It requires more work area than other electrochemical cell reactions	Flow cell	The flow cell enhances the electrocatalytic performance as there is an increased electrode surface area which is exposed to the reactant molecules along with efficient mass transport
Pressurized electrochemical cell	A pressurized electrochemical cell is required to investigate the response of	It requires high pressure to operate		A membrane is required for separation of the cathode and anode chamber. That membrane is expensive as it is a proton exchange membrane and a perfect treatment is required before electrolysis

6. Qualitative and quantitative assessment of results

In order to avoid any “false positive” results of urea formation, isotope labelled experiments are performed to vehemently verify and produce a sanguine result regarding the source of urea formation. The qualitative tests like the FTIR study and NMR study have been conducted in order to verify the formation of urea as well as unveil its source (identification of the functional groups and the NMR peak assignment in isotope labelled experiments). In the quantitative experiment section the ¹H NMR study is also employed along with UV-vis spectroscopic measurements, to quantify the formation of urea and report about the yield.

6.1 Fourier transform infrared (FTIR) spectra

(a) The operando SR-FTIR experiment was conducted during the electrocatalysis experiment of carbon dioxide and nitrate ion reduction to underpin the electrokinetics and the specific potential at which the urea formation occurs. A broad infrared range of 1000–4000 cm⁻¹ was scanned for investigation, as

shown in Fig. 16a. Two characteristic regions were considered for the study: 1100–1800 cm⁻¹, where the rocking and bending of the NH₂ bond were noticed at 1170 and 1635 cm⁻¹, wagging of the NH₂ bond was found at 1307 cm⁻¹, C–N bond stretching was observed at 1419 cm⁻¹ and the O–C–O vibrational band was observed at 1396 cm⁻¹; 3000–3600 cm⁻¹, where N–H bending, N–H stretching and H–N–H stretching were observed at 3187, 3368 and 3440 cm⁻¹, respectively, as shown in Fig. 16b.¹²⁴

(b) Isotope labelled operando synchrotron radiation-based Fourier transform infrared (SR-FTIR) experiments were carried out during electrochemical studies of TiO₂ supported Pd–Cu.³⁵ The FTIR spectra displayed in Fig. 16c revealed that when isotope gases (¹⁵N₂ and ¹³CO₂) were purged, the corresponding stretching frequency of ¹⁵NH₂, ¹⁵NH and ¹³C = O underwent a shift of almost 20–30 cm⁻¹; the isotope effects were the cause of the shift towards a lower wavenumber implying the electrochemical reduction of ¹⁵N₂ and ¹³CO₂ purged gases.

(c) The relatively simple *in situ* attenuated total reflectance Fourier transform infrared spectroscopy (ATR-FTIR) technique gained prominence to investigate the formation of urea during electrocatalysis, as shown in Fig. 16d.¹²⁸ The analysis reveals that CO₂ electroreduction results in COOH* intermediate peaks at 1360 cm⁻¹ and 1210 cm⁻¹; the intensity of the peaks increases with the decrease of potential in a CO₂ environment. The reduction of NO₂⁻ results in the production of a signature NH₃ peak at 1100 cm⁻¹ and the remaining nitrite ions demonstrate the signal at 1220 cm⁻¹. The formation of urea is confirmed by the C–N bond formation having the characteristic peak at 1440 cm⁻¹.

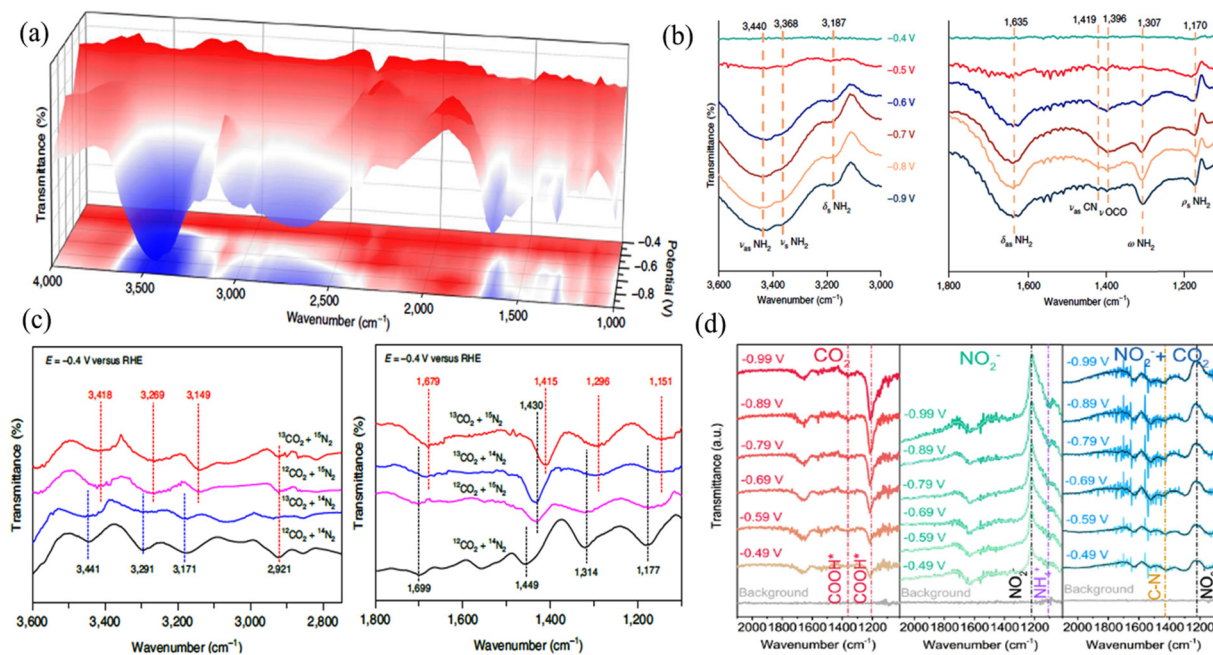


Fig. 16 (a) Three dimensional FTIR spectra.¹²⁴ Copyright 2021, Springer Nature. (b) IR signals spanning the range of 3000–3600 cm⁻¹ and 1100–1800 cm⁻¹ respectively.¹²⁴ Copyright 2021, Springer Nature. (c) FTIR signals in the range of 2750–3600 cm⁻¹ and isotope labelled FTIR signals in the range of 1100–1800 cm⁻¹ at -0.4 V using Pd₁Cu₁/TiO₂.³⁵ Copyright 2020, Springer Nature. (d) *In situ* ATR FTIR spectra for urea using CO₂, NaNO₂, and CO₂ + NaNO₂.¹²⁸

6.2 Nuclear magnetic resonance (NMR) spectra

(a) ¹H NMR spectral analysis. Generally NO_x as contaminants are predominantly present in chemicals and in the atmosphere, so it is extremely important to validate and prove that urea produced through the electrocatalysis technique arises due to the reduction reactions of the reactants and not due to the presence of unwanted contaminants. For this, the ¹H NMR spectra with signature peaks provide a real solution to the problem; so it is also used as a primary control experiment to find the nitrogen origin of urea formed. The simultaneous reduction of CO₂ and N₂ (not contaminants) can be verified by different ways: (I) by purging the non-isotopic form of the gas (¹⁴N₂ and ¹²CO₂), (II) feeding isotopic gases (¹⁵N₂ and ¹³CO₂), and (III) feeding a mixture of isotope and non-isotope gases (¹⁵N₂ and ¹²CO₂). The ¹H NMR spectra of non-isotopic urea (¹²CO(¹⁴NH₂)₂) with varying concentrations from 0 ppm to 4 ppm are shown in Fig. 17a. The calibration plot obtained from the ¹H NMR spectra establishes the relationship between the NMR integral area and the concentration of urea, as shown in Fig. 17b.

Similarly the ¹H NMR spectra of isotopic urea (¹³CO(¹⁵NH₂)₂) with different concentrations from 0 ppm to 4 ppm are shown in Fig. 17c. The standard calibration plot gives the quantitative relationship using the equation $y = 4878x - 122$, where 'y' denotes the NMR peak area and 'x' represents the urea concentration, as shown in Fig. 17d.

When non-isotopic gases were purged to form urea using electrocatalysis, the ¹H NMR responded with a single peak corresponding to the presence of ¹²CO(¹⁴NH₂)₂ in the

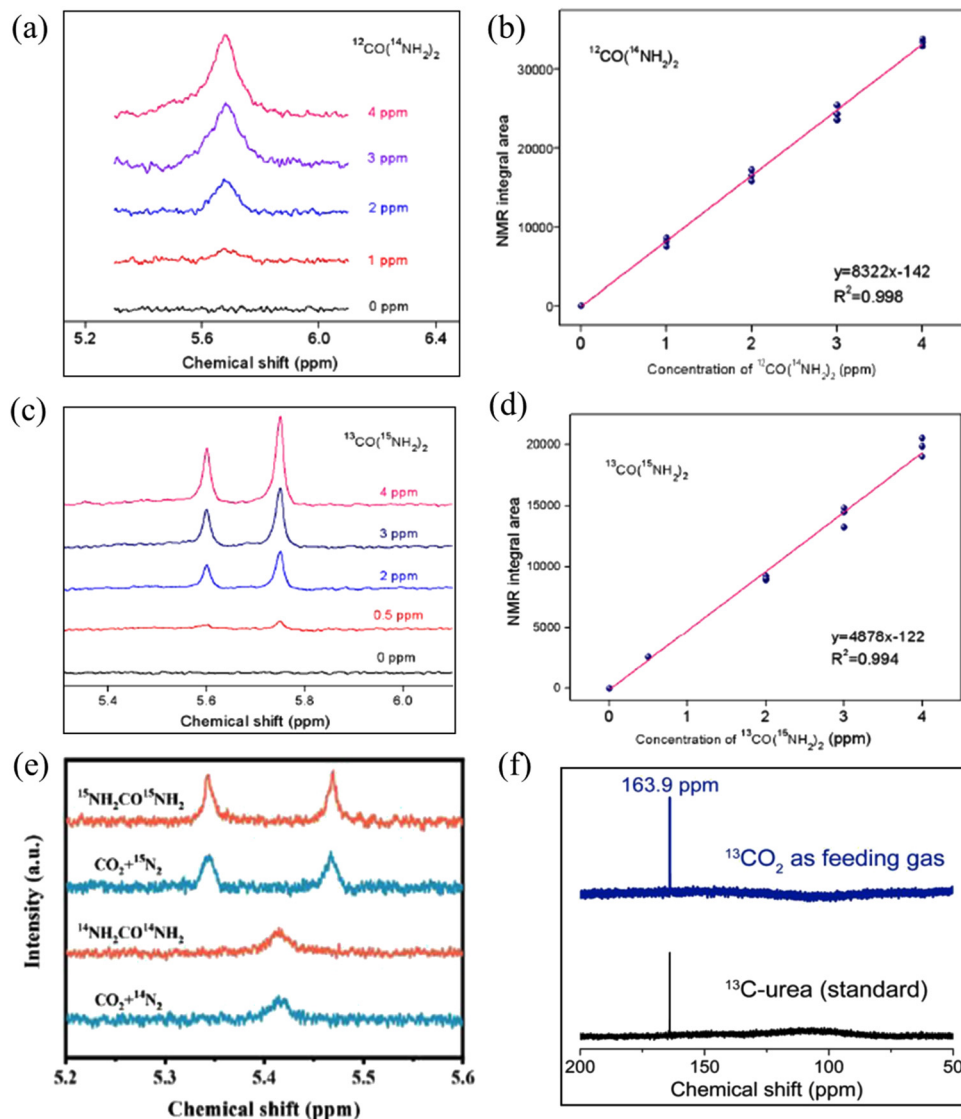


Fig. 17 (a) ^1H NMR spectra of $^{12}\text{CO}(\text{NH}_2)_2$ with different concentrations.³⁵ Copyright 2020, Springer Nature. (b) Calibration curve for $^{12}\text{CO}(\text{NH}_2)_2$.³⁵ Copyright 2020, Springer Nature. (c) ^1H NMR spectra of $^{13}\text{CO}(\text{NH}_2)_2$ with varying concentrations.³⁵ Copyright 2020, Springer Nature. (d) Calibration curve for $^{13}\text{CO}(\text{NH}_2)_2$.³⁵ Copyright 2020, Springer Nature. (e) ^1H NMR spectra of the electrolyte saturated with $^{15}\text{N}_2 + \text{CO}_2 / ^{14}\text{N}_2 + \text{CO}_2$ after 2 h electrolysis and standard $^{15}\text{NH}_2\text{CO}^{15}\text{NH}_2 / ^{14}\text{NH}_2\text{CO}^{14}\text{NH}_2$ solution.¹⁴¹ Copyright 2021, John Wiley & Sons, Ltd. (f) ^{13}C NMR spectra by feeding $^{13}\text{CO}_2$ (top) and standard ^{13}C -labelled urea (bottom).¹²⁴ Copyright 2021, Springer Nature.

electrolyte media.^{56,141} On the other hand, the feeding of isotopic gases resulted in two characteristic peaks in the ^1H NMR spectra which confirms the formation of urea of isotopic nature ($^{13}\text{CO}(\text{NH}_2)_2$) in the electrolyte (Fig. 17e).³⁵ In the last case where a mixture of isotopic and non-isotopic gases ($^{15}\text{N}_2$ and $^{12}\text{CO}_2$) was purged the corresponding signal of $^{12}\text{CO}(\text{NH}_2)_2$ was detected in the ^1H NMR spectra as inferred by the presence of a signature doublet peak.^{56,141}

(b) ^{13}C NMR spectral analysis. To search for the carbon origin of the electrocatalytically produced urea, experiments were performed by feeding isotopic carbon dioxide ($^{13}\text{CO}_2$) gas. The ^{13}C NMR spectra are displayed in Fig. 17f, which show that the technique has limited utility as it can only detect the presence of carbon isotope (^{13}C) labelled urea.¹²⁴

6.3 UV-visible spectroscopic analysis

Quantification of urea present in the electrolyte solution can be done by using a UV-vis spectrophotometer based on the diacetyl monoxime method (DAMO).^{35,36}

In this method, an acid ferric solution and a DAMO-TSC solution are required. The acid ferric solution can be prepared by mixing 300 mL of conc. H_2SO_4 and 100 mL of conc. phosphoric acid with 600 mL of distilled water. Mixing should be done in an ice bath. Then 100 mg of ferric chloride is added to the solution. The DAMO-TSC solution can be prepared by mixing 5 g of diacetyl monoxime (DAMO) and 100 mg of thiosemicarbazide (TSC) with 1000 mL of distilled water. Then 2 mL of acid ferric solution and 1 mL of DAMO-TSC solution are mixed with 1 mL of urea-containing electrolyte solution and the

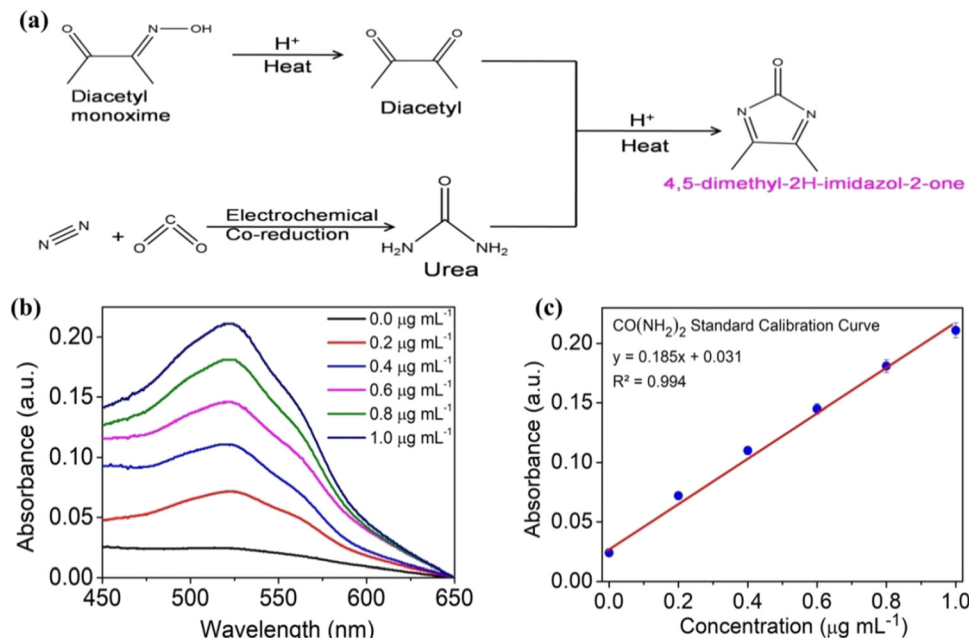


Fig. 18 Diacetyl monoxime method for urea quantification. (a) Scheme for the determination of urea concentration using the diacetyl monoxime method. (b) UV-vis absorption spectra at various urea concentrations. (c) Calibration curve used for quantifying urea solution.³⁶ Copyright 2022, John Wiley & Sons, Ltd.

solution mixture is heated to 100 °C for 15–20 min till a pink color is formed (Fig. 18a).

Then the solution is naturally cooled to room temperature. The maximum UV-vis absorption peak appears at 525 nm, which confirms the formation of urea in the electrolyte solution after the electrochemical reduction process. To calculate the concentration of urea present in the electrolyte solution, a standard urea calibration curve is plotted from where we can quantify the unknown urea concentration.

Fig. 18b shows the absorbance of 0.0, 0.2, 0.4, 0.6, 0.8, and 1.0 ppm urea solution(s). The UV-vis spectra show that the maximum absorbance occurs at 525 nm. From these curves (concentration vs. absorbance) a linear relation $y = 0.185x + 0.031$ was obtained with $R^2 = 0.994$ (Fig. 18c). Using this linear relation between absorbance and concentration, we can quantify the unknown urea concentration.

6.4 Yield rate and faradaic efficiency calculations

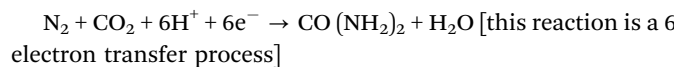
The formation of urea from electrochemical NO_x/N₂ and CO₂ reduction reaction, the urea yield rate and faradaic efficiency (FE) can be calculated using the following equations:

$$\text{Urea yield rate} = \frac{(C_{\text{urea}} \times V)}{(m_{\text{cat}} \times t \times 60.06)} \quad [\text{unit: } \mu\text{mol h}^{-1} \text{ mg}_{\text{cat}}^{-1}]$$

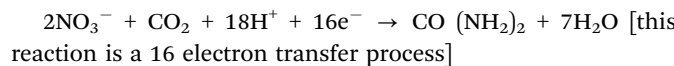
$$\text{Urea yield rate} = \frac{(C_{\text{urea}} \times V)}{(m_{\text{cat}} \times t)} \quad [\text{unit: } \mu\text{g h}^{-1} \text{ mg}_{\text{cat}}^{-1}]$$

$$\text{Urea yield rate} = \frac{(C_{\text{urea}} \times V)}{(S \times t)} \quad [\text{unit: } \mu\text{g h}^{-1} \text{ cm}^{-2}]$$

Faradaic efficiency can be calculated for the N₂ + CO₂ reduction to urea case:



$$\text{FE (\%)} = \frac{(6 \times F \times C_{\text{urea}} \times V)}{(60.06 \times Q)} \times 100\%$$



$$\text{FE (\%)} = \frac{(16 \times F \times C_{\text{urea}} \times V)}{(60.06 \times Q)} \times 100\%$$

where C_{urea} is the concentration of urea produced during the electrochemical reduction process, V is the volume of the electrolyte, t is the time duration for reduction, m is the catalyst mass, F is the faradaic constant (96 485 C mol⁻¹), Q is the total charge passing through the electrode, the molecular weight of urea is 60.06 g mol⁻¹, and S is the effective surface area of the catalyst.

Nitrogen selectivity can also be calculated using the equation

$$\text{N}_{\text{urea}}\text{-selectivity} = n_{\text{urea}}(\text{N})/n_{\text{total}}(\text{N})$$

where $n_{\text{urea}}(\text{N})$ is the moles of nitrogen in urea produced and $n_{\text{total}}(\text{N})$ is the moles of nitrogen in total products from NO_x/N₂.

Table 7 draws a comparison of the yield rate and faradaic efficiency for various investigated electrocatalysts in different electrochemical cells. The choice of the source of nitrogen (N₂, NO₂⁻, and NO₃⁻) plays a trade-off role in essence with respect to faradaic efficiency and the yield rate, as nitrogen gas

Table 7 Comparison of the electrochemical urea synthesis performance

Electrocatalyst [reference]	Active sites	Electrolyte	Applied potential (vs. RHE)	N ₂ source	Urea yield rate	FE (%)	Echem cell
Pd ₁ Cu ₁ /TiO ₂ ³⁵	PdCu surface	0.1 M KHCO ₃	-0.4 V	N ₂	0.12 mmol g ⁻¹ h ⁻¹ 3.36 mmol g ⁻¹ h ⁻¹	0.66 8.92	1. H-cell 2. Flow cell
CuPc ³⁶	CuN ₄ sites	0.1 M KHCO ₃	-0.6 V	N ₂	143.47 µg h ⁻¹ mg ⁻¹ cat	12.99	H-cell
BiFeO ₃ /BiVO ₄ ⁵⁶	BiFeO ₃ /BiVO ₄	0.1 M KHCO ₃	-0.4 V	N ₂	4.94 mmol h ⁻¹ g ⁻¹	17.18	H-cell
Bi-BiVO ₄ ¹⁴¹	Bi-BiVO ₄	0.1 M KHCO ₃	-0.4 V	N ₂	5.91 mmol h ⁻¹ g ⁻¹	12.55	H-cell
InOOH ¹³⁹	In and O sites	0.1 M KHCO ₃	-0.4 V	N ₂	6.85 mmol g ⁻¹ h ⁻¹	20.97	H-cell
Ni ₃ (BO ₃) ₂ ¹⁴⁰	Ni and O sites	0.1 M KHCO ₃	-0.5 V	N ₂	9.75 mmol g ⁻¹ h ⁻¹	20.36	H-cell
Zn ²³	Zn site	0.2 mol dm ⁻³ KHCO ₃ + 0.2 mol dm ⁻³ KNO ₃	-1.75 V	NO ₃ ⁻	NA	35	Gas diffusion cell
Cu ²²	Cu sites	0.2 mol dm ⁻³ KHCO ₃	-0.75 V	NO ₃ ⁻ + O ₂ ⁻	NA	37	Gas diffusion cell
Te-Pd ⁵⁴	Te-Pd(111) surface	0.1 M KHCO ₃ + 0.1 M KNO ₂	-1.1 V	NO ₂ ⁻	NA	12.2	1. H-cell 2. Flow cell
In(OH) ₃ ¹²⁴	In(OH) ₃ (100) surface	0.1 M KNO ₃	-0.6 V	NO ₃ ⁻	533.1 µg h ⁻¹ mg ⁻¹ cat	53.4	H-cell
Cu-TiO ₂ ¹²⁷	Cu sites and oxygen vacancy-rich TiO ₂	0.2 M KHCO ₃ + 0.2 M KNO ₂	-0.4 V	NO ₂ ⁻	20.8 µmol h ⁻¹	43.1	Single cell
OV-ZnO ¹²⁸	Oxygen vacancy-rich ZnO	0.2 M NaHCO ₃ + 0.1 M NaNO ₂	-0.79 V	NO ₂ ⁻	16.56 µmol h ⁻¹	23.26	H-cell
Nafion treated TiO ₂ ¹²⁹	Active TiO ₂	0.1 M KNO ₃	-0.4 V	NO ₃ ⁻	0.33 µmoles h ⁻¹	40	Single cell
Cu-N-C sac ¹³⁵	Cu-N ₄ sites	0.1 M K ₂ SO ₄ + 0.1 M KNO ₃	-0.9 V	NO ₃ ⁻	4.3 nmol s ⁻¹ cm ⁻²	28	H-cell
Fe-Ni ¹³⁸	FeNi-N ₆ site	0.1 M KHCO ₃	-1.5 V	NO ₃ ⁻	20.2 mmol g ⁻¹ h ⁻¹	17.8	H-cell

is inert in nature and has limited solubility in aqueous medium compared to the nitrite and nitrate ions which show greater solubility in water media. Hence, in general NO₂⁻ and NO₃⁻ show enhanced faradaic efficiency as the intensity of current density found during the chronoamperometry experiment is lower in comparison to the nitrogen gas purged system.

Presently, a maximum urea yield rate of 20.2 mmol g⁻¹ h⁻¹ has been reported for the Fe-Ni diatomic catalyst,¹³⁸ and the In(OH)₃¹²⁴ electrocatalytic system has shown the highest faradaic efficiency (53.4%) so far, among the investigated electrocatalysts. The active sites, reactant adsorption on the catalytic surface, specificity, selectivity of electrochemical reaction, and stability play a crucial role in the rate of urea formation. The line of comparison with respect to the urea yield can only be drawn if we have information on the mass loading of the catalyst on the substrate or the electrochemical surface area.

7. General protocol for electrocatalytic urea synthesis

Recently, an exclusive report has recommended the protocol of photo/electrocatalytic urea synthesis and quantification.¹⁵⁴ Inspired by this research, targeting the problem of reliability, accuracy and efficiency, we recommend a set of experimental protocols that researchers working on electrocatalytic urea synthesis can implement on a daily basis, as displayed in Fig. 19. The protocol is divided into four sequential steps, which are as follows:

Step 1: during the start of any experiment, the authors must ensure that the electrocatalytic system is free from any sort of contamination; impurities need to be entrapped and there should be complete absence of urea and ammonia from the system. Once the system is free from contamination, we shall move to the next step.

Step 2: this step consists of control experiments, which include the electrocatalytic tests (linear sweep voltammetry (LSV) and chronoamperometry (CA)) under inert gas conditions and then testing in the open circuit potential; simultaneously quantification of urea is done by the DAMO method (shown in Fig. 18). Then after completion of the mentioned tests, we shall move to the next step.

Step 3: this step is one of the crucial steps, as it involves the control tests which ensure about the purity of the reactant gases (¹⁴N₂, ¹⁵N₂, and ¹²CO₂) and verification of the nitrite/nitrate assay (¹⁴NO_x). Then we move to the next step.

Step 4: this is the most critical and vital step. In this step, electrocatalytic tests are carried out using the reactant sources (¹⁴N₂ + ¹²CO₂, or NO_x + ¹²CO₂), LSV and CA tests are done, and then estimation of urea is carried out. The authors should reproduce the same test(s) at least three times. Then they must include the error bars of the urea production at varying potential and also clearly state the method of error bar calculation. If a comparable amount of urea is produced, then the electrocatalyst under investigation qualifies as an active catalyst for urea synthesis. Then we proceed towards the next step.

Step 5: this step is an essential step, in which isotope labelling experiments are carried out to provide solid evidence

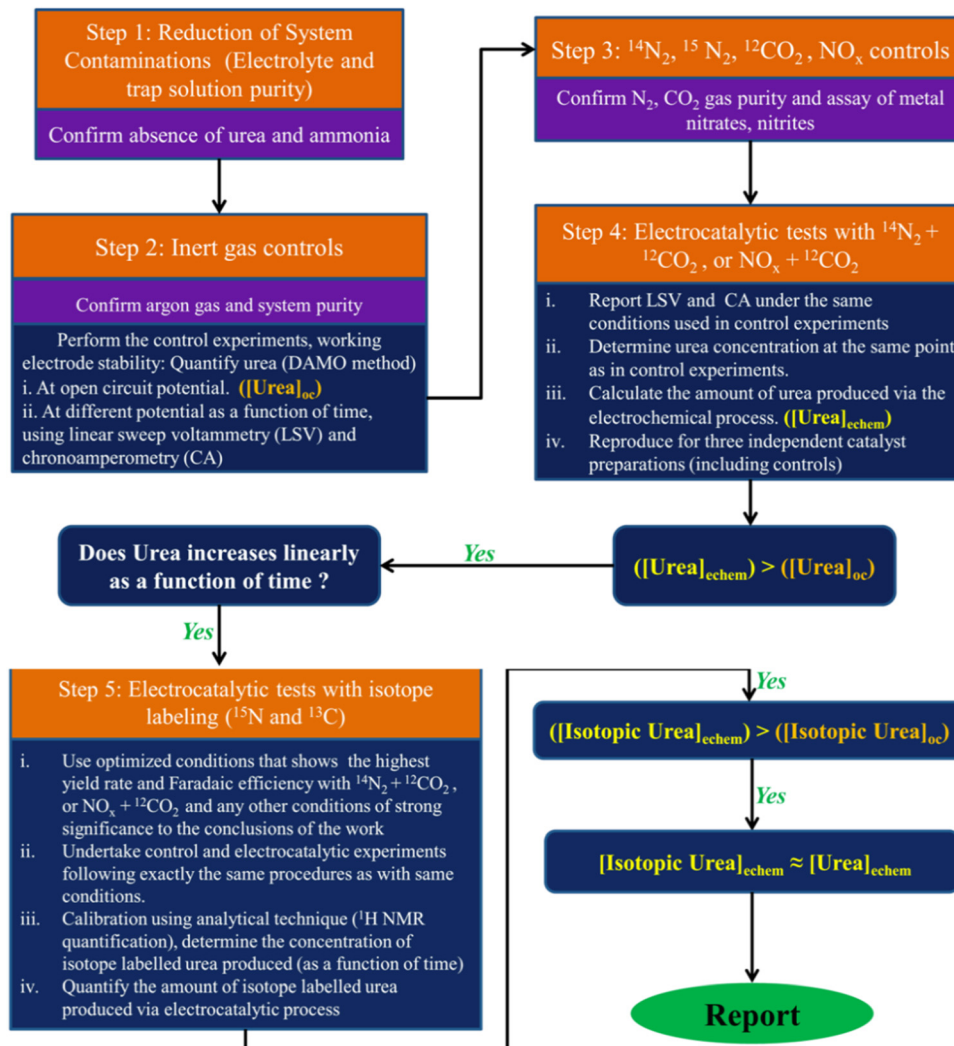


Fig. 19 Schematic illustration of the recommended experimental protocol for electrochemical urea synthesis.

regarding the formation of urea by the reactant sources only and not by any type of unwanted contaminants.

If the isotopic urea production is comparable to the non-isotopic urea produced *via* electrocatalysis, then the final report is made about the investigated electrocatalyst.

8. Challenges and techno-commercial roadmap analyses

The path of the scalability and commercialization of electrocatalytic urea synthesis is laden with a lot of hurdles in various forms which are as follows:

8.1 Efficiency of the overall process

The highest faradaic efficiency record of 53.4% was achieved by In(OH)_3 ,¹²⁴ however we must further increase the efficiency in order to challenge the present process of industrial urea production.

8.2 Selection of a potential catalyst

From a broad range of investigated catalysts we must choose the catalyst which produces a yield of the highest order; currently $\text{Ni}_3(\text{BO}_3)_2$ with $9.75 \text{ mmol g}^{-1} \text{ h}^{-1}$ is found to be the best. However, lot of research investigations need to be done specifically in this arena to find out a particular catalyst with paramount performance.

8.3 Technology readiness level (TRL)

Industrial upgradation requires different specifications to be addressed; only then a technology under investigation makes progress under the engineering scanner. As showcased in this article, currently this technology has surpassed the ideation level and the lab scale experimental level; technically its present position is at most TRL 3, as illustrated in Fig. 20. However, the NRR efficiency is far from satisfactory to meet the needs of the industrial production process.¹⁵⁵ The electrocatalytic refinery will be a mandatory step of the future in order to build a sustainable, ecofriendly yet economically feasible technique by

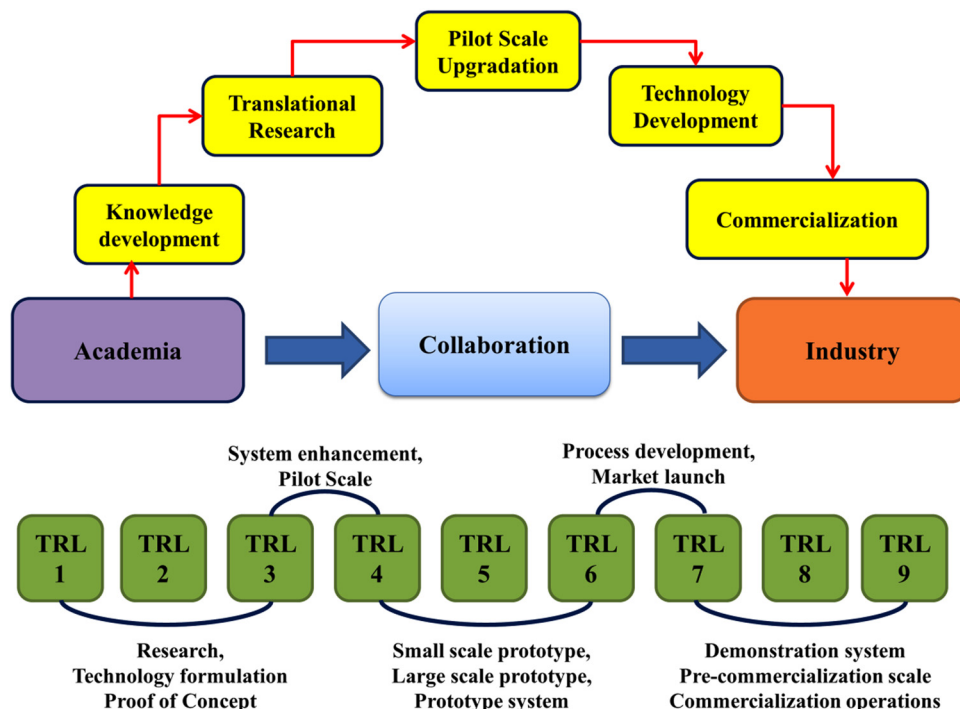


Fig. 20 Schematic representation of the technology readiness level.

leveraging the renewable energy and converting into value added products;¹⁵⁶ this can be achieved by strategically reinforcing the concept of well-defined reactions, mechanistic insights, rational design of electrocatalysts, electrode–electrolyte interaction and reactor design. The process of electrochemical urea synthesis can progress concerning the TRL, if the research fraternity can find the Holy Grail in the form of an electrocatalyst, which can exhibit enhanced performances in five key areas. First and foremost, it must be able to show faradaic efficiency performance which can compete with the existing industrial urea production process. Second, the urea yield rate needs improvement from the present yield. Third, stability is an important issue; the electrocatalyst must be sturdy enough to withstand a long-term electrochemical process. Fourthly, the specificity of product formation; the higher the specificity of the process, the better will be the urea yield. Finally, optimization of the entire electrochemical process (energy efficient process) will play a governing role in the pilot scale tests, prototype development, and the ultimate commercialization step.

8.4 Cost of operation and economic viability

In the field of economic viability, a techno-economic analysis of the biphasic reactant (CO_2 and NO) system has been reported.¹²⁵ The authors have considered the cost of urea to be \$ 0.41 per kg. They have found that 1 kg of urea can be produced by the consumption of 118.69 kW h of electricity; after considering industrial price of the reactants, the total operational cost translates to \$ 3.6 per kg of urea produced. This means that to date the cost of urea produced using the electrocatalytic technique has been 9 times higher than that of the present commercial urea.

From the Indian perspective, an exclusively agriculture based economy where the maximum retail price (MRP) is strictly regulated by the Government of India, presently the MRP of urea is set at Rs. 268 for 50 kg of urea.¹⁵⁷ This kind of valuation reveals that in India 1 kg of urea costs Rs. 5.36 (\$ 0.07), which implies that the cost of electrochemically produced urea is a whopping 51 times higher than that of the urea sold in the market. This is a serious economical speed breaker in the progress path of the aforementioned technology.

9. Conclusion

Presently there are a number of serious challenges in the path of electrocatalytic urea synthesis. These are as follows: non-development of a judicious catalysis synthesis strategy, a dissuasive mechanism of urea synthesis and inability to achieve the overall process efficiency to match the industrial urea synthesis process. The solution to the persisting problem can be addressed by performing extensive research to find the following key aspects of the electrocatalytic urea preparation:

- (1) In order to develop a well-established mechanism of urea synthesis, theoretical investigation with synergistic experimental verification (*in situ* study) is required to prove the concept, along with specific adsorption and active sites of the catalyst, realization of intermediate transient states, a preferred reaction route (distal or alternating), and identification of side reactions (carbon dioxide reduction reaction, nitrogen reduction reaction, and nitrite/nitrate reduction reaction) with experimental justification and finally selectivity of product formation.

(2) A salient feature of urea synthesis lies in the unison of carbon and nitrogen to form the vital C–N bond which depends on effective adsorption of nitrogen and carbon dioxide on the catalytic sites; hence the more catalytic active sites, the greater the adsorption. As the nitrogen molecule is inert in nature, it is very difficult to adsorb and activate N₂ as compared to CO₂. Then the formation of a transition state (NH₂^{*} or CO^{*}) followed by the achievement of highly specific spatial arrangement (adjacent intermediate state formation) in order to form the C–N bond on the catalyst surface.

(3) To improve the overall efficiency of the electrocatalytic process, tuning of the electrode/electrolyte interface, use of ionic liquids as the electrolyte to enhance the solubility of gas, rational engineering design of the catalyst and tailoring the active sites to promote electrocatalytic performance, and strategically designing the electrochemical cell in such a manner where the reactant gases can easily attack the electrode surface can be undertaken.

(4) HER is a direct competition of electrochemical urea synthesis, so HER needs to be impeded in an effective manner in order to enhance the urea formation rate. So, the strategy based on HER formation by the Tafel route can be inhibited by the use of single atom catalysts, the Mott–Schottky heterostructure can significantly impede the HER process, and the non-metallic part in the metal complex can also restrict the HER process by not assisting the formation of metal hydrides; the strategies are discussed with intricacy, so the catalyst of the future can be produced using the mentioned techniques, and thereby a greater degree of efficiency can be achieved with respect to HER suppression.

(5) The recommended protocol provided in Fig. 19 can be adapted by researchers in order to provide a reliable, reproducible, informative, and transparent research report which claims about the investigation of the electrocatalyst showing activity towards electrochemical urea synthesis.

The significance of the research on electrocatalytic urea synthesis is impeccable. We hope that the electrochemical urea production technology can run the gauntlet owing to the significant reduction in the price of renewable energy (solar and wind), development of optimum energy utilization and commissioning of the decarbonization strategy throughout the globe in order to create a sustainable future; the nascent yet growing technology can effectively be the alternate route of urea synthesis in the near future by culmination of facile adsorption and activation of reactants (carbon dioxide and nitrogen species) on the catalytic surface, followed by C–N bond formation and selectively producing urea as a dominant product.

Conflicts of interest

UKG, SP and AA have filed a US Patent application (17846753) and also an Indian Patent application (202131027290) regarding electrochemical green urea synthesis under ambient conditions.

Acknowledgements

A. A. thanks SERB for the fellowship. The authors acknowledge the financial support from the SERB-Core Research Grant (CRG/2022/009427), Govt. of India.

References

- B. Obama, The irreversible momentum of clean energy: Private-sector efforts help drive decoupling of emissions and economic growth, *Science*, 2017, **355**, 126–129.
- D. Lüthi, M. Le Floch, B. Bereiter, T. Blunier, J. M. Barnola, U. Siegenthaler, D. Raynaud, J. Jouzel, H. Fischer, K. Kawamura and T. F. Stocker, High-resolution carbon dioxide concentration record 650,000–800,000 years before present, *Nature*, 2008, **453**, 379–382.
- A. Alissandratos and C. J. Easton, Biocatalysis for the application of CO₂ as a chemical feedstock, *Beilstein J. Org. Chem.*, 2015, **11**, 2370–2387.
- J. C. Lee, J. H. Kim, W. S. Chang and D. Pak, Biological conversion of CO₂ to CH₄ using hydrogenotrophic methanogen in a fixed bed reactor, *J. Chem. Technol. Biotechnol.*, 2012, **87**, 844–847.
- Q. Yang, C. C. Yang, C. H. Lin and H. L. Jiang, Metal–Organic-Framework-Derived Hollow N-Doped Porous Carbon with Ultrahigh Concentrations of Single Zn Atoms for Efficient Carbon Dioxide Conversion, *Angew. Chem., Int. Ed.*, 2019, **58**, 3511–3515.
- J. Artz, T. E. Müller, K. Thenert, J. Kleinekorte, R. Meys, A. Sternberg, A. Bardow and W. Leitner, Sustainable Conversion of Carbon Dioxide: An Integrated Review of Catalysis and Life Cycle Assessment, *Chem. Rev.*, 2018, **118**, 434–504.
- E. C. Hann, S. Overa, M. Harland-Dunaway, A. F. Narvaez, D. N. Le, M. L. Orozco-Cárdenas, F. Jiao and R. E. Jinkerson, A hybrid inorganic–biological artificial photosynthesis system for energy-efficient food production, *Nat. Food*, 2022, **3**, 461–471.
- M. Liu, Y. Pang, B. Zhang, P. De Luna, O. Voznyy, J. Xu, X. Zheng, C. T. Dinh, F. Fan, C. Cao, F. P. G. De Arquer, T. S. Safaei, A. Mepham, A. Klinkova, E. Kumacheva, T. Filleteer, D. Sinton, S. O. Kelley and E. H. Sargent, Enhanced electrocatalytic CO₂ reduction via field-induced reagent concentration, *Nature*, 2016, **537**(7620), 382–386.
- J. Li, G. Chen, Y. Zhu, Z. Liang, A. Pei, C. L. Wu, H. Wang, H. R. Lee, K. Liu, S. Chu and Y. Cui, Efficient electrocatalytic CO₂ reduction on a three-phase interface, *Nat. Catal.*, 2018, **1**(8), 592–600.
- Z. Q. Liang, T. T. Zhuang, A. Seifitokaldani, J. Li, C. W. Huang, C. S. Tan, Y. Li, P. De Luna, C. T. Dinh, Y. Hu, Q. Xiao, P. L. Hsieh, Y. Wang, F. Li, R. Quintero-Bermudez, Y. Zhou, P. Chen, Y. Pang, S. C. Lo, L. J. Chen, H. Tan, Z. Xu, S. Zhao, D. Sinton and E. H. Sargent, Copper-on-nitride enhances the stable electrosynthesis of

- multi-carbon products from CO₂, *Nat. Commun.*, 2018, **9**, 1–8.
- 11 W. Ma, S. Xie, X. G. Zhang, F. Sun, J. Kang, Z. Jiang, Q. Zhang, D. Y. Wu and Y. Wang, Promoting electrocatalytic CO₂ reduction to formate via sulfur-boosting water activation on indium surfaces, *Nat. Commun.*, 2019, **10**, 1–10.
- 12 C. Qian, W. Sun, D. L. H. Hung, C. Qiu, M. Makaremi, S. G. Hari Kumar, L. Wan, M. Ghoussoub, T. E. Wood, M. Xia, A. A. Tountas, Y. F. Li, L. Wang, Y. Dong, I. Gourevich, C. V. Singh and G. A. Ozin, Catalytic CO₂ reduction by palladium-decorated silicon-hydride nano-sheets, *Nat. Catal.*, 2018, **2**(1), 46–54.
- 13 C. Li, T. Wang, B. Liu, M. Chen, A. Li, G. Zhang, M. Du, H. Wang, S. F. Liu and J. Gong, Photoelectrochemical CO₂ reduction to adjustable syngas on grain-boundary-mediated a-Si/TiO₂/Au photocathodes with low onset potentials, *Energy Environ. Sci.*, 2019, **12**, 923–928.
- 14 M. Schreier, F. Héroguel, L. Steier, S. Ahmad, J. S. Luterbacher, M. T. Mayer, J. Luo and M. Grätzel, Solar conversion of CO₂ to CO using Earth-abundant electrocatalysts prepared by atomic layer modification of CuO, *Nat. Energy*, 2017, **2**(7), 1–9.
- 15 B. Han, X. Ou, Z. Deng, Y. Song, C. Tian, H. Deng, Y. J. Xu and Z. Lin, Nickel Metal–Organic Framework Monolayers for Photoreduction of Diluted CO₂: Metal-Node-Dependent Activity and Selectivity, *Angew. Chem., Int. Ed.*, 2018, **57**, 16811–16815.
- 16 X. Li, J. Yu, M. Jaroniec and X. Chen, Cocatalysts for selective photoreduction of CO₂ into solar fuels, *Chem. Rev.*, 2019, **119**, 3962–4179.
- 17 I. H. Tseng, W. C. Chang and J. C. S. Wu, Photoreduction of CO₂ using sol–gel derived titania and titania-supported copper catalysts, *Appl. Catal., B*, 2002, **37**, 37–48.
- 18 P. De Luna, R. Quintero-Bermudez, C. T. DIInh, M. B. Ross, O. S. Bushuyev, P. Todorović, T. Regier, S. O. Kelley, P. Yang and E. H. Sargent, Catalyst electro-redeposition controls morphology and oxidation state for selective carbon dioxide reduction, *Nat. Catal.*, 2018, **1**(2), 103–110.
- 19 M. G. Kibria, J. P. Edwards, C. M. Gabardo, C. T. Dinh, A. Seifitokaldani, D. Sinton and E. H. Sargent, Electrochemical CO₂ Reduction into Chemical Feedstocks: From Mechanistic Electrocatalysis Models to System Design, *Adv. Mater.*, 2019, **31**, 1807166.
- 20 J. Li, K. Chang, H. Zhang, M. He, W. A. Goddard, J. G. Chen, M. J. Cheng and Q. Lu, Effectively Increased Efficiency for Electroreduction of Carbon Monoxide Using Supported Polycrystalline Copper Powder Electrocatalysts, *ACS Catal.*, 2019, **9**, 4709–4718.
- 21 J. E. Kim, S. Choi, M. Balamurugan, J. H. Jang and K. T. Nam, Electrochemical C–N Bond Formation for Sustainable Amine Synthesis, *Trends Chem.*, 2020, **2**, 1004–1019.
- 22 M. Shibata, K. Yoshida and N. Furuya, Electrochemical synthesis of urea on reduction of carbon dioxide with nitrate and nitrite ions using Cu-loaded gas-diffusion electrode, *J. Electroanal. Chem.*, 1995, **387**, 143–145.
- 23 M. Shibata, K. Yoshida and N. Furuya, Electrochemical Synthesis of Urea at Gas-diffusion Electrodes V. Simultaneous Reduction of Carbon Dioxide and Nitrite Ions with Various Boride Catalysts, *Denki Kagaku oyobi Kogyo Butsuri Kagaku*, 1998, **66**, 584–589.
- 24 M. D. Fryzuk, J. B. Love, S. J. Rettig and V. G. Young, Transformation of coordinated dinitrogen by reaction with dihydrogen and primary silanes, *Science*, 1997, **275**, 1445–1447.
- 25 H. P. Jia and E. A. Quadrelli, Mechanistic aspects of dinitrogen cleavage and hydrogenation to produce ammonia in catalysis and organometallic chemistry: relevance of metal hydride bonds and dihydrogen, *Chem. Soc. Rev.*, 2013, **43**, 547–564.
- 26 H. O. N. Tugaøen, S. Garcia-Segura, K. Hristovski and P. Westerhoff, Challenges in photocatalytic reduction of nitrate as a water treatment technology, *Sci. Total Environ.*, 2017, **599**, 1524–1551.
- 27 M. Aresta, A. Dibenedetto and A. Angelini, Catalysis for the valorization of exhaust carbon: From CO₂ to chemicals, materials, and fuels. technological use of CO₂, *Chem. Rev.*, 2014, **114**, 1709–1742.
- 28 Y. Liu, X. Zhao and L. Ye, A Novel Elastic Urea-Melamine-Formaldehyde Foam: Structure and Properties, *Ind. Eng. Chem. Res.*, 2016, **55**, 8743–8750.
- 29 H. M. Huang, J. J. W. McDouall and D. J. Procter, Radical Anions from Urea-type Carbonyls: Radical Cyclizations and Cyclization Cascades, *Angew. Chem., Int. Ed.*, 2018, **57**, 4995–4999.
- 30 L. Celleno, Topical urea in skincare: A review, *Dermatol. Ther.*, 2018, **31**, e12690.
- 31 F. Can, S. Berland, S. Royer, X. Courtois and D. Duprez, Composition-dependent performance of Ce_xZr_{1-x}O₂ mixed-oxide-supported WO₃ catalysts for the NO_x storage reduction-selective catalytic reduction coupled process, *ACS Catal.*, 2013, **3**, 1120–1132.
- 32 F. Barzaghi, F. Mani and M. Peruzzini, From greenhouse gas to feedstock: formation of ammonium carbamate from CO₂ and NH₃ in organic solvents and its catalytic conversion into urea under mild conditions, *Green Chem.*, 2011, **13**, 1267–1274.
- 33 T. M. Lenton, J. Rockström, O. Gaffney, S. Rahmstorf, K. Richardson, W. Steffen and H. J. Schellnhuber, Climate tipping points—too risky to bet against, *Nature*, 2019, **575**(7784), 592–595.
- 34 Emissions Gap Report 2021, <https://www.unep.org/resources/emissions-gap-report-2021>, (accessed 29 March 2023).
- 35 C. Chen, X. Zhu, X. Wen, Y. Zhou, L. Zhou, H. Li, L. Tao, Q. Li, S. Du, T. Liu, D. Yan, C. Xie, Y. Zou, Y. Wang, R. Chen, J. Huo, Y. Li, J. Cheng, H. Su, X. Zhao, W. Cheng, Q. Liu, H. Lin, J. Luo, J. Chen, M. Dong, K. Cheng, C. Li and S. Wang, Coupling N₂ and CO₂ in H₂O to synthesize urea under ambient conditions, *Nat. Chem.*, 2020, **12**(8), 717–724.
- 36 J. Mukherjee, S. Paul, A. Adalder, S. Kapse, R. Thapa, S. Mandal, B. Ghorai, S. Sarkar and U. K. Ghorai,

- Understanding the Site-Selective Electrocatalytic Co-Reduction Mechanism for Green Urea Synthesis Using Copper Phthalocyanine Nanotubes, *Adv. Funct. Mater.*, 2022, **32**, 2200882.
- 37 U. K. Ghorai, S. Das, S. Saha, N. Mazumder, D. Sen and K. K. Chattopadhyay, Efficient and persistent cold cathode emission from CuPc nanotubes: a joint experimental and simulation investigation, *Dalton Trans.*, 2014, **43**, 9260–9266.
- 38 S. H. Lee, J. C. Lin, M. Farmand, A. T. Landers, J. T. Feaster, J. E. Avilés Acosta, J. W. Beeman, Y. Ye, J. Yano, A. Mehta, R. C. Davis, T. F. Jaramillo, C. Hahn and W. S. Drisdell, Oxidation State and Surface Reconstruction of Cu under CO₂Reduction Conditions from in Situ X-ray Characterization, *J. Am. Chem. Soc.*, 2021, **143**, 588–592.
- 39 J. Mukherjee, A. Adalder, N. Mukherjee and U. K. Ghorai, Solvothermal synthesis of α -CuPc nanostructures for electrochemical nitrogen fixation under ambient conditions, *Catal. Today*, 2022, 113905.
- 40 S. Murmu, S. Paul, S. Kapse, R. Thapa, S. Chattopadhyay, N. Abharana, S. N. Jha, D. Bhattacharyya and U. K. Ghorai, Unveiling the genesis of the high catalytic activity in nickel phthalocyanine for electrochemical ammonia synthesis, *J. Mater. Chem. A*, 2021, **9**, 14477–14484.
- 41 S. D. Young, B. M. Ceballos, A. Banerjee, R. Mukundan, G. Pilania and B. R. Goldsmith, Metal Oxynitrides for the Electrocatalytic Reduction of Nitrogen to Ammonia, *J. Phys. Chem. C*, 2022, **126**, 12980–12993.
- 42 S. Murmu, S. Paul, A. Santra, M. Robert and U. K. Ghorai, Graphene wrapped nickel phthalocyanine nanohybrid: Efficient electrocatalyst for nitrogen reduction reaction, *Catal. Today*, 2022, 113938.
- 43 J. Fu, Y. Yang and J. S. Hu, Dual-Sites Tandem Catalysts for C-N Bond Formation via Electrocatalytic Coupling of CO₂ and Nitrogenous Small Molecules, *ACS Mater. Lett.*, 2021, 1468–1476.
- 44 A. Biswas, S. Kapse, R. Thapa and R. S. Dey, Oxygen Functionalization-Induced Charging Effect on Boron Active Sites for High-Yield Electrocatalytic NH₃ Production, *Nano-Micro Lett.*, 2022, **14**, 1–17.
- 45 Y. Luo, Q. Li, Y. Tian, Y. Liu and K. Chu, Amorphization engineered VSe_{2-x} nanosheets with abundant Se-vacancies for enhanced N₂ electroreduction, *J. Mater. Chem. A*, 2022, **10**, 1742–1749.
- 46 A. Banerjee, B. M. Ceballos, C. Kreller, R. Mukundan and G. Pilania, A first-principles investigation of nitrogen reduction to ammonia on zirconium nitride and oxynitride surfaces, *J. Mater. Sci.*, 2022, **57**, 10213–10224.
- 47 L. Merakeb, S. Bennaamane, J. De Freitas, E. Clot, N. Mézailles, M. Robert, L. Merakeb, J. De Freitas, M. Robert, S. Bennaamane, N. Mézailles and E. Clot, Molecular Electrochemical Reductive Splitting of Dinitrogen with a Molybdenum Complex, *Angew. Chem., Int. Ed.*, 2022, **61**, e202209899.
- 48 M. M. Shi, D. Bao, B. R. Wulan, Y. H. Li, Y. F. Zhang, J. M. Yan and Q. Jiang, Au Sub-Nanoclusters on TiO₂ toward Highly Efficient and Selective Electrocatalyst for N₂ Conversion to NH₃ at Ambient Conditions, *Adv. Mater.*, 2017, **29**, 1606550.
- 49 Y. Luo, P. Shen, X. Li, Y. Guo and K. Chu, Sulfur-deficient Bi₂S_{3-x} synergistically coupling Ti₃C₂T_x-MXene for boosting electrocatalytic N₂ reduction, *Nano Res.*, 2022, **15**, 3991–3999.
- 50 Q. Li, P. Shen, Y. Tian, X. Li and K. Chu, Metal-free BN quantum dots/graphitic C₃N₄ heterostructure for nitrogen reduction reaction, *J. Colloid Interface Sci.*, 2022, **606**, 204–212.
- 51 A. Biswas, S. Nandi, N. Kamboj, J. Pan, A. Bhowmik and R. S. Dey, Alteration of Electronic Band Structure via a Metal-Semiconductor Interfacial Effect Enables High Faradaic Efficiency for Electrochemical Nitrogen Fixation, *ACS Nano*, 2021, **15**, 20364–20376.
- 52 L. Merakeb and M. Robert, Advances in molecular electrochemical activation of dinitrogen, *Curr. Opin. Electrochem.*, 2021, **29**, 100834.
- 53 Y. Ding, L. Huang, J. Zhang, A. Guan, Q. Wang, L. Qian, L. Zhang and G. Zheng, Ru-doped, oxygen-vacancy-containing CeO₂ nanorods toward N₂ electroreduction, *J. Mater. Chem. A*, 2020, **8**, 7229–7234.
- 54 Y. Feng, H. Yang, Y. Zhang, X. Huang, L. Li, T. Cheng and Q. Shao, Te-Doped Pd Nanocrystal for Electrochemical Urea Production by Efficiently Coupling Carbon Dioxide Reduction with Nitrite Reduction, *Nano Lett.*, 2020, **20**, 8282–8289.
- 55 M. Jouny, J. J. Lv, T. Cheng, B. H. Ko, J. J. Zhu, W. A. Goddard and F. Jiao, Formation of carbon–nitrogen bonds in carbon monoxide electrolysis, *Nat. Chem.*, 2019, **11**(9), 846–851.
- 56 M. Yuan, J. Chen, Y. Bai, Z. Liu, J. Zhang, T. Zhao, Q. Shi, S. Li, X. Wang and G. Zhang, Electrochemical C–N coupling with perovskite hybrids toward efficient urea synthesis, *Chem. Sci.*, 2021, **12**, 6048–6058.
- 57 U. K. Ghorai, S. Paul, B. Ghorai, A. Adalder, S. Kapse, R. Thapa, A. Nagendra and A. Gain, Scalable Production of Cobalt Phthalocyanine Nanotubes: Efficient and Robust Hollow Electrocatalyst for Ammonia Synthesis at Room Temperature, *ACS Nano*, 2021, **15**, 5230–5239.
- 58 A. E. Shilov, Catalytic reduction of molecular nitrogen in solutions, *Russ. Chem. Bull.*, 2003, **52**, 2555–2562.
- 59 C. G. Zhan, J. A. Nichols and D. A. Dixon, Ionization Potential, Electron Affinity, Electronegativity, Hardness, and Electron Excitation Energy: Molecular Properties from Density Functional Theory Orbital Energies, *J. Phys. Chem. A*, 2003, **107**, 4184–4195.
- 60 T. A. Bazhenova and A. E. Shilov, Nitrogen fixation in solution, *Coord. Chem. Rev.*, 1995, **144**, 69–145.
- 61 C. J. M. Van Der Ham, M. T. M. Koper and D. G. H. Hettterscheid, Challenges in reduction of dinitrogen by proton and electron transfer, *Chem. Soc. Rev.*, 2014, **43**, 5183–5191.
- 62 S. G. Bratsch, Standard Electrode Potentials and Temperature Coefficients in Water at 298.15 K, *J. Phys. Chem. Ref. Data*, 2009, **18**, 1.

- 63 A. Adalder, S. Paul and U. K. Ghorai, Progress of electrochemical synthesis of nitric acid: catalyst design, mechanistic insights, protocol and challenges, *J. Mater. Chem. A*, 2023, **11**, 10125–10148.
- 64 M. B. Ross, P. De Luna, Y. Li, C. T. Dinh, D. Kim, P. Yang and E. H. Sargent, Designing materials for electrochemical carbon dioxide recycling, *Nat. Catal.*, 2019, **2**(8), 648–658.
- 65 A. Vasileff, C. Xu, Y. Jiao, Y. Zheng and S. Z. Qiao, Surface and Interface Engineering in Copper-Based Bimetallic Materials for Selective CO₂ Electroreduction, *Chem.*, 2018, **4**, 1809–1831.
- 66 Z. W. She, J. Kibsgaard, C. F. Dickens, I. Chorkendorff, J. K. Nørskov and T. F. Jaramillo, Combining theory and experiment in electrocatalysis: Insights into materials design, *Science*, 2017, **355**, eaad4998.
- 67 A. Rosas-Hernández, C. Steinlechner, H. Junge and M. Beller, Photo- and Electrochemical Valorization of Carbon Dioxide Using Earth-Abundant Molecular, *Catalysts*, 2017, 229–253.
- 68 G. Jones, T. Bligaard, F. Abild-Pedersen and J. K. Nørskov, Using scaling relations to understand trends in the catalytic activity of transitionmetals, *J. Phys.: Condens. Matter*, 2008, **20**, 064239.
- 69 I. Katsounaros, T. Chen, A. A. Gewirth, N. M. Markovic and M. T. M. Koper, Evidence for Decoupled Electron and Proton Transfer in the Electrochemical Oxidation of Ammonia on Pt(100), *J. Phys. Chem. Lett.*, 2016, **7**, 387–392.
- 70 A. J. Göttle and M. T. M. Koper, Proton-coupled electron transfer in the electrocatalysis of CO₂ reduction: prediction of sequential vs. concerted pathways using DFT, *Chem. Sci.*, 2016, **8**, 458–465.
- 71 C. V. S. Kumar and V. Subramanian, Can boron antisites of BNNTs be an efficient metal-free catalyst for nitrogen fixation? – A DFT investigation, *Phys. Chem. Chem. Phys.*, 2017, **19**, 15377–15387.
- 72 Y. Wang, C. Wang, M. Li, Y. Yu and B. Zhang, Nitrate electroreduction: mechanism insight, in situ characterization, performance evaluation, and challenges, *Chem. Soc. Rev.*, 2021, **50**, 6720–6733.
- 73 Q. Liu, L. Xie, J. Liang, Y. Ren, Y. Wang, L. Zhang, L. Yue, T. Li, Y. Luo, N. Li, B. Tang, Y. Liu, S. Gao, A. A. Alshehri, I. Shakir, P. O. Agboola, Q. Kong, Q. Wang, D. Ma and X. Sun, Ambient Ammonia Synthesis via Electrochemical Reduction of Nitrate Enabled by NiCo₂O₄ Nanowire Array, *Small*, 2022, **18**, 2106961.
- 74 Z. Li, Z. Deng, L. Ouyang, X. Fan, L. Zhang, S. Sun, Q. Liu, A. A. Alshehri, Y. Luo, Q. Kong and X. Sun, CeO₂ nanoparticles with oxygen vacancies decorated N-doped carbon nanorods: A highly efficient catalyst for nitrate electroreduction to ammonia, *Nano Res.*, 2022, **15**(10), 8914–8921.
- 75 Q. Liu, Q. Liu, L. Xie, Y. Ji, T. Li, B. Zhang, N. Li, B. Tang, Y. Liu, S. Gao, Y. Luo, L. Yu, Q. Kong and X. Sun, High-Performance Electrochemical Nitrate Reduction to Ammonia under Ambient Conditions Using a FeOOH Nanorod Catalyst, *ACS Appl. Mater. Interfaces*, 2022, **14**, 17312–17318.
- 76 L. Xie, Q. Liu, S. Sun, L. Hu, L. Zhang, D. Zhao, Q. Liu, J. Chen, J. Li, L. Ouyang, A. A. Alshehri, M. S. Hamdy, Q. Kong and X. Sun, High-Efficiency Electrosynthesis of Ammonia with Selective Reduction of Nitrate in Neutral Media Enabled by Self-Supported Mn₂CoO₄Nanoarray, *ACS Appl. Mater. Interfaces*, 2022, **14**(29), 33242–33247.
- 77 H. Wang, D. Zhao, C. Liu, X. Fan, Z. Li, Y. Luo, D. Zheng, S. Sun, J. Chen, J. Zhang, Y. Liu, S. Gao, F. Gong and X. Sun, FeS₂@TiO₂ nanobelts array enabled high-efficiency electrocatalytic nitrate reduction to ammonia, *J. Mater. Chem. A*, 2022, **10**, 24462–24467.
- 78 X. Zhang, Y. Wang, C. Liu, Y. Yu, S. Lu and B. Zhang, Recent advances in non-noble metal electrocatalysts for nitrate reduction, *Chem. Eng. J.*, 2021, **403**, 126269.
- 79 K. Chen, Y. Luo, P. Shen, X. Liu, X. Li, X. Li and K. Chu, Boosted nitrate electroreduction to ammonia on Fe-doped SnS₂ nanosheet arrays rich in S-vacancies, *Dalton Trans.*, 2022, **51**, 10343–10350.
- 80 Z. Deng, C. Ma, Z. Li, Y. Luo, L. Zhang, S. Sun, Q. Liu, J. Du, Q. Lu, B. Zheng and X. Sun, High-Efficiency Electrochemical Nitrate Reduction to Ammonia on a Co₃O₄Nanoarray Catalyst with Cobalt Vacancies, *ACS Appl. Mater. Interfaces*, 2022, **14**, 46595–46602.
- 81 A. J. Bard, R. Parsons and J. Jordan, *Standard Potentials in Aqueous Solution*, 2017, pp. 1–834.
- 82 Y. Zeng, C. Priest, G. Wang and G. Wu, Restoring the Nitrogen Cycle by Electrochemical Reduction of Nitrate: Progress and Prospects, *Small Methods*, 2020, **4**, 2000672.
- 83 S. Garcia-Segura, M. Lanzarini-Lopes, K. Hristovski and P. Westerhoff, Electrocatalytic reduction of nitrate: Fundamentals to full-scale water treatment applications, *Appl. Catal., B*, 2018, **236**, 546–568.
- 84 S. Paul, S. Sarkar, A. Adalder, S. Kapse, R. Thapa and U. K. Ghorai, Strengthening the Metal Center of Co-N4 Active Sites in a 1D–2D Heterostructure for Nitrate and Nitrogen Reduction Reaction to Ammonia, *ACS Sustainable Chem. Eng.*, 2023, **11**, 6191–6200.
- 85 Y. Abghoui and E. Skúlason, Onset potentials for different reaction mechanisms of nitrogen activation to ammonia on transition metal nitride electro-catalysts, *Catal. Today*, 2017, **286**, 69–77.
- 86 J. X. Liu, D. Richards, N. Singh and B. R. Goldsmith, Activity and Selectivity Trends in Electrocatalytic Nitrate Reduction on Transition Metals, *ACS Catal.*, 2019, **9**, 7052–7064.
- 87 M. T. De Groot and M. T. M. Koper, The influence of nitrate concentration and acidity on the electrocatalytic reduction of nitrate on platinum, *J. Electroanal. Chem.*, 2004, **562**, 81–94.
- 88 M. Fedurco, P. Kedzierzawski and J. Augustynski, Effect of Multivalent Cations upon Reduction of Nitrate Ions at the Ag Electrode, *J. Electrochem. Soc.*, 1999, **146**, 2569–2572.
- 89 V. N. Montesinos, N. Quici, H. Destaillats and M. I. Litter, Nitric oxide emission during the reductive heterogeneous photocatalysis of aqueous nitrate with TiO₂, *RSC Adv.*, 2015, **5**, 85319–85322.

- 90 R. Tenne, K. Patel, K. Hashimoto and A. Fujishima, Efficient electrochemical reduction of nitrate to ammonia using conductive diamond film electrodes, *J. Electroanal. Chem.*, 1993, **347**, 409–415.
- 91 M. C. P. M. Da Cunha, M. Weber and F. C. Nart, On the adsorption and reduction of NO_3^- ions at Au and Pt electrodes studied by in situ FTIR spectroscopy, *J. Electroanal. Chem.*, 1996, **414**, 163–170.
- 92 K. Y. Lee, D. J. Kuchynka and J. K. Kochi, Redox Equilibria of the Nitrosonium Cation and of Its Nonbonded Complexes, *Inorg. Chem.*, 1990, **29**, 4196–4204.
- 93 D. Xu, Y. Li, L. Yin, Y. Ji, J. Niu and Y. Yu, Electrochemical removal of nitrate in industrial wastewater, *Front. Environ. Sci. Eng.*, 2018, **12**, 9.
- 94 J. Gao, B. Jiang, C. Ni, Y. Qi and X. Bi, Enhanced reduction of nitrate by noble metal-free electrocatalysis on P doped three-dimensional Co_3O_4 cathode: Mechanism exploration from both experimental and DFT studies, *Chem. Eng. J.*, 2020, **382**, 123034.
- 95 A. C. A. De Vooys, R. A. Van Santen and J. A. R. Van Veen, Electrocatalytic reduction of NO_3^- on palladium/copper electrodes, *J. Mol. Catal. A: Chem.*, 2000, **154**, 203–215.
- 96 Y. Li, Y. K. Go, H. Ooka, D. He, F. Jin, S. H. Kim and R. Nakamura, Enzyme Mimetic Active Intermediates for Nitrate Reduction in Neutral Aqueous Media, *Angew. Chem., Int. Ed.*, 2020, **59**, 9744–9750.
- 97 R. Jia, Y. Wang, C. Wang, Y. Ling, Y. Yu and B. Zhang, Boosting Selective Nitrate Electroreduction to Ammonium by Constructing Oxygen Vacancies in TiO_2 , *ACS Catal.*, 2020, **10**, 3533–3540.
- 98 A. R. Cook, N. Dimitrijevic, B. W. Dreyfus, D. Meisel, L. A. Curtiss and D. M. Camaioni, Reducing Radicals in Nitrate Solutions. The NO_3^- -System Revisited, *J. Phys. Chem. A*, 2001, **105**, 3658–3666.
- 99 I. Katsounaros and G. Kyriacou, Influence of nitrate concentration on its electrochemical reduction on tin cathode: Identification of reaction intermediates, *Electrochim. Acta*, 2008, **53**, 5477–5484.
- 100 A. C. A. de Vooys, M. T. M. Koper, R. A. Van Santen and J. A. R. Van Veen, Mechanistic study of the nitric oxide reduction on a polycrystalline platinum electrode, *Electrochim. Acta*, 2001, **46**, 923–930.
- 101 A. S. Dutton, J. M. Fukuto and K. N. Houk, Theoretical reduction potentials for nitrogen oxides from CBS-QB3 energetics and (C)PCM solvation calculations, *Inorg. Chem.*, 2005, **44**, 4024–4028.
- 102 T. Yoshioka, K. Iwase, S. Nakanishi, K. Hashimoto and K. Kamiya, Electrocatalytic Reduction of Nitrate to Nitrous Oxide by a Copper-Modified Covalent Triazine Framework, *J. Phys. Chem. C*, 2016, **120**, 15729–15734.
- 103 J. Zheng, T. Lu, T. M. Cotton and G. Chumanov, Photo-induced Electrochemical Reduction of Nitrite at an Electrochemically Roughened Silver Surface, *J. Phys. Chem. B*, 1999, **103**, 6567–6572.
- 104 J. Yang, M. Duca, K. J. P. Schouten and M. T. M. Koper, Formation of volatile products during nitrate reduction on a Sn-modified Pt electrode in acid solution, *J. Electroanal. Chem.*, 2011, **662**, 87–92.
- 105 M. D. Bartberger, W. Liu, E. Ford, K. M. Miranda, C. Switzer, J. M. Fukuto, P. J. Farmer, D. A. Wink and K. N. Houk, The reduction potential of nitric oxide (NO) and its importance to NO biochemistry, *Proc. Natl. Acad. Sci. U. S. A.*, 2002, **99**, 10958–10963.
- 106 F. T. Bonner and M. N. Hughes, The Aqueous Solution Chemistry of Nitrogen in Low Positive Oxidation States, *Comments Inorg. Chem.*, 2006, **7**, 215–234, DOI: [10.1080/02603598808072309](https://doi.org/10.1080/02603598808072309).
- 107 J. F. E. Gootzen, P. G. J. M. Peeters, J. M. B. Dukers, L. Lefferts, W. Visscher and J. A. R. Van Veen, The electrocatalytic reduction of NO_3^- on Pt, Pd and Pt + Pd electrodes activated with Ge, *J. Electroanal. Chem.*, 1997, **434**, 171–183.
- 108 V. Rosca and M. T. M. Koper, Electrocatalytic oxidation of ammonia on Pt(111) and Pt(100) surfaces, *Phys. Chem. Chem. Phys.*, 2006, **8**, 2513–2524.
- 109 M. Duca, M. O. Cucarella, P. Rodriguez and M. T. M. Koper, Direct reduction of nitrite to N_2 on a Pt(100) electrode in alkaline media, *J. Am. Chem. Soc.*, 2010, **132**, 18042–18044.
- 110 Y. Hori, H. Wakebe, T. Tsukamoto and O. Koga, Electrocatalytic process of CO selectivity in electrochemical reduction of CO_2 at metal electrodes in aqueous media, *Electrochim. Acta*, 1994, **39**, 1833–1839.
- 111 B. A. Rosen, A. Salehi-Khojin, M. R. Thorson, W. Zhu, D. T. Whipple, P. J. A. Kenis and R. I. Masel, Ionic liquid-mediated selective conversion of CO_2 to CO at low overpotentials, *Science*, 2011, **334**, 643–644.
- 112 D. D. Zhu, J. L. Liu and S. Z. Qiao, Recent Advances in Inorganic Heterogeneous Electrocatalysts for Reduction of Carbon Dioxide, *Adv. Mater.*, 2016, **28**, 3423–3452.
- 113 W. Zhang, Y. Hu, L. Ma, G. Zhu, Y. Wang, X. Xue, R. Chen, S. Yang and Z. Jin, Progress and Perspective of Electrocatalytic CO_2 Reduction for Renewable Carbonaceous Fuels and Chemicals, *Adv. Sci.*, 2018, **5**, 1700275.
- 114 S. Zhang, Q. Fan, R. Xia and T. J. Meyer, CO_2 Reduction: From Homogeneous to Heterogeneous Electrocatalysis, *Acc. Chem. Res.*, 2020, **53**, 255–264.
- 115 W. H. Wang, Y. Himeda, J. T. Muckerman, G. F. Manbeck and E. Fujita, CO_2 Hydrogenation to Formate and Methanol as an Alternative to Photo- and Electrochemical CO_2 Reduction, *Chem. Rev.*, 2015, **115**, 12936–12973.
- 116 J. Shen, R. Kortlever, R. Kas, Y. Y. Birdja, O. Diaz-Morales, Y. Kwon, I. Ledezma-Yanez, K. J. P. Schouten, G. Mul and M. T. M. Koper, Electrocatalytic reduction of carbon dioxide to carbon monoxide and methane at an immobilized cobalt protoporphyrin, *Nat. Commun.*, 2015, **6**(1), 1–8.
- 117 Y. Y. Birdja, E. Pérez-Gallent, M. C. Figueiredo, A. J. Göttle, F. Calle-Vallejo and M. T. M. Koper, Advances and challenges in understanding the electrocatalytic conversion of carbon dioxide to fuels, *Nat. Energy*, 2019, **4**, 732–745.
- 118 J. Shen, M. J. Kolb, A. J. Göttle and M. T. M. Koper, DFT Study on the Mechanism of the Electrochemical Reduction

- of CO₂ Catalyzed by Cobalt Porphyrins, *J. Phys. Chem. C*, 2016, **120**, 15714–15721.
- 119 H. A. Schwarz and R. W. Dodson, Reduction potentials of CO₂[·] and the alcohol radicals, *J. Phys. Chem.*, 1989, **93**, 409–414.
- 120 Z. Tao, C. L. Rooney, Y. Liang and H. Wang, Accessing Organonitrogen Compounds via C–N Coupling in Electrocatalytic CO₂ Reduction, *J. Am. Chem. Soc.*, 2021, **143**, 19630–19642.
- 121 D. B. Kayan and F. Köleli, Simultaneous electrocatalytic reduction of dinitrogen and carbon dioxide on conducting polymer electrodes, *Appl. Catal., B*, 2016, **181**, 88–93.
- 122 S. Paul, S. Sarkar, A. Adalder, A. Banerjee and U. K. Ghorai, Dual metal site-mediated efficient C–N coupling toward electrochemical urea synthesis, *J. Mater. Chem. A*, 2023, **11**, 13249–13254.
- 123 X. Wei, X. Wen, Y. Liu, C. Chen, C. Xie, D. Wang, M. Qiu, N. He, P. Zhou, W. Chen, J. Cheng, H. Lin, J. Jia, X. Z. Fu and S. Wang, Oxygen Vacancy-Mediated Selective C–N Coupling toward Electrocatalytic Urea Synthesis, *J. Am. Chem. Soc.*, 2022, **144**, 11530–11535.
- 124 C. Lv, L. Zhong, H. Liu, Z. Fang, C. Yan, M. Chen, Y. Kong, C. Lee, D. Liu, S. Li, J. Liu, L. Song, G. Chen, Q. Yan and G. Yu, Selective electrocatalytic synthesis of urea with nitrate and carbon dioxide, *Nat. Sustainable*, 2021, **4**(10), 868–876.
- 125 Y. Huang, R. Yang, C. Wang, N. Meng, Y. Shi, Y. Yu and B. Zhang, Direct Electrosynthesis of Urea from Carbon Dioxide and Nitric Oxide, *ACS Energy Lett.*, 2022, **7**, 284–291.
- 126 X. Liu, Y. Jiao, Y. Zheng, M. Jaroniec and S. Z. Qiao, Mechanism of C–N bonds formation in electrocatalytic urea production revealed by ab initio molecular dynamics simulation, *Nat. Commun.*, 2022, **13**(1), 1–9.
- 127 N. Cao, Y. Quan, A. Guan, C. Yang, Y. Ji, L. Zhang and G. Zheng, Oxygen vacancies enhanced cooperative electrocatalytic reduction of carbon dioxide and nitrite ions to urea, *J. Colloid Interface Sci.*, 2020, **577**, 109–114.
- 128 N. Meng, Y. Huang, Y. Liu, Y. Yu and B. Zhang, Electrosynthesis of urea from nitrite and CO₂ over oxygen vacancy-rich ZnO porous nanosheets, *Cell Rep. Phys. Sci.*, 2021, **2**, 100378.
- 129 D. Saravanakumar, J. Song, S. Lee, N. H. Hur and W. Shin, Electrocatalytic Conversion of Carbon Dioxide and Nitrate Ions to Urea by a Titania–Nafion Composite Electrode, *ChemSusChem*, 2017, **10**, 3999–4003.
- 130 X. Zhu, X. Zhou, Y. Jing and Y. Li, Electrochemical synthesis of urea on MBenes, *Nat. Commun.*, 2021, **12**(1), 1–9.
- 131 L. Zailun, S. Like, Z. Qitao, T. Zhenyuan, S. Hongli and S. Chenliang, TiO₂-supported Single-atom Catalysts: Synthesis, Structure, and Application, *Chem. Res. Chin. Univ.*, 2022, **38**, 1123–1138.
- 132 X. Zhang, S. Guo, Y. Qin and C. Li, Functional Electrospun Nanocomposites for Efficient Oxygen Reduction Reaction, *Chem. Res. Chin. Univ.*, 2021, **37**(3), 379–393.
- 133 L. Kong, D. Jiao, Z. Wang, Y. Liu, Y. Shang, L. Yin, Q. Cai and J. Zhao, Single metal atom anchored on porous boron nitride nanosheet for efficient collaborative urea electrosynthesis: A computational study, *Chem. Eng. J.*, 2023, **451**, 138885.
- 134 Y. Xiao, C. Shen and T. Long, Theoretical Establishment and Screening of an Efficient Catalyst for N₂ Electroreduction on Two-Dimensional Transition-Metal Borides (MBenes), *Chem. Mater.*, 2021, **33**, 4023–4034.
- 135 J. Leverett, T. Tran-Phu, J. A. Yuwono, P. Kumar, C. Kim, Q. Zhai, C. Han, J. Qu, J. Cairney, A. N. Simonov, R. K. Hocking, L. Dai, R. Daiyan and R. Amal, Tuning the Coordination Structure of Cu–N–C Single Atom Catalysts for Simultaneous Electrochemical Reduction of CO₂ and NO₃[–] to Urea, *Adv. Energy Mater.*, 2022, **12**, 2201500.
- 136 S. Paul, A. Adalder, S. Saha, U. K. Ghorai, K. K. Chattopadhyay and S. Das, Alq₃-Graphene Bi-Functional Nanocomposite for Cold Cathodes and Luminescent Anodes in Field Emission Display Applications, *J. Electron. Mater.*, 2023, **52**, 1662–1667.
- 137 Y. Zhao, J. Wan, N. Yang, R. Yu and D. Wang, sp-Hybridized nitrogen doped graphdiyne for high-performance Zn-air batteries, *Mater. Chem. Front.*, 2021, **5**, 7987–7992.
- 138 X. Zhang, X. Zhu, S. Bo, C. Chen, M. Qiu, X. Wei, N. He, C. Xie, W. Chen, J. Zheng, P. Chen, S. P. Jiang, Y. Li, Q. Liu and S. Wang, Identifying and tailoring C–N coupling site for efficient urea synthesis over diatomic Fe–Ni catalyst, *Nat. Commun.*, 2022, **13**(1), 1–9.
- 139 M. Yuan, H. Zhang, Y. Xu, R. Liu, R. Wang, T. Zhao, J. Zhang, Z. Liu, H. He, C. Yang, S. Zhang and G. Zhang, Artificial frustrated Lewis pairs facilitating the electrochemical N₂ and CO₂ conversion to urea, *Chem Catal.*, 2022, **2**, 309–320.
- 140 M. Yuan, J. Chen, Y. Xu, R. Liu, T. Zhao, J. Zhang, Z. Ren, Z. Liu, C. Streb, H. He, C. Yang, S. Zhang and G. Zhang, Highly selective electroreduction of N₂ and CO₂ to urea over artificial frustrated Lewis pairs, *Energy Environ. Sci.*, 2021, **14**, 6605–6615.
- 141 M. Yuan, J. Chen, Y. Bai, Z. Liu, J. Zhang, T. Zhao, Q. Wang, S. Li, H. He and G. Zhang, Unveiling Electrochemical Urea Synthesis by Co-Activation of CO₂ and N₂ with Mott–Schottky Heterostructure Catalysts, *Angew. Chem., Int. Ed.*, 2021, **60**, 10910–10918.
- 142 Y. Tian, Y. Wu, H. Liang, B. Zhao, Y. Jin, J. Liu and Z. Li, Bimetal selenide NiSe/ZnSe heterostructured nanoparticles decorated porous g-C₃N₄ nanosheets to boost H₂ evolution and urea synthesis, *Appl. Surf. Sci.*, 2022, **602**, 154329.
- 143 P. Roy, A. Pramanik and P. Sarkar, Dual-Silicon-Doped Graphitic Carbon Nitride Sheet: An Efficient Metal-Free Electrocatalyst for Urea Synthesis, *J. Phys. Chem. Lett.*, 2021, **12**, 10837–10844.
- 144 Z. Zhang and L. Guo, Electrochemical reduction of CO₂ and N₂ to synthesize urea on metal–nitrogen-doped carbon catalysts: a theoretical study, *Dalton Trans.*, 2021, **50**, 11158–11166.
- 145 J. O. Bockris and E. C. Potter, The Mechanism of the Cathodic Hydrogen Evolution Reaction, *J. Electrochem. Soc.*, 1952, **99**, 169.
- 146 Y. Zheng, Y. Jiao, M. Jaroniec and S. Z. Qiao, Advancing the Electrochemistry of the Hydrogen-Evolution Reaction

- through Combining Experiment and Theory, *Angew. Chem., Int. Ed.*, 2015, **54**, 52–65.
- 147 P. C. K. Vesborg, B. Seger and I. Chorkendorff, Recent development in hydrogen evolution reaction catalysts and their practical implementation, *J. Phys. Chem. Lett.*, 2015, **6**, 951–957.
- 148 B. Alqasem, S. Sikiru, E. M. Ali, K. A. Elraies, N. Yahya, A. Rostami, M. Ganeson, C. M. Nyuk and S. Qureshi, Effect of electromagnetic energy on net spin orientation of nanocatalyst for enhanced green urea synthesis, *J. Mater. Res. Technol.*, 2020, **9**, 16497–16512.
- 149 X. Xiang, L. Guo, X. Wu, X. Ma and Y. Xia, Urea formation from carbon dioxide and ammonia at atmospheric pressure, *Environ. Chem. Lett.*, 2012, **10**, 295–300.
- 150 J. Sun, D. Alam, R. Daiyan, H. Masood, T. Zhang, R. Zhou, P. J. Cullen, E. C. Lovell, A. Jalili and R. Amal, A hybrid plasma electrocatalytic process for sustainable ammonia production, *Energy Environ. Sci.*, 2021, **14**, 865–872.
- 151 L. Li, C. Tang, X. Cui, Y. Zheng, X. Wang, H. Xu, S. Zhang, T. Shao, K. Davey and S. Z. Qiao, Efficient Nitrogen Fixation to Ammonia through Integration of Plasma Oxidation with Electrocatalytic Reduction, *Angew. Chem., Int. Ed.*, 2021, **60**, 14131–14137.
- 152 Y. Ren, C. Yu, L. Wang, X. Tan, Z. Wang, Q. Wei, Y. Zhang and J. Qiu, Microscopic-Level Insights into the Mechanism of Enhanced NH₃Synthesis in Plasma-Enabled Cascade N₂Oxidation-Electroreduction System, *J. Am. Chem. Soc.*, 2022, **144**, 10193–10200.
- 153 H. Rabiee, L. Ge, X. Zhang, S. Hu, M. Li and Z. Yuan, Gas diffusion electrodes (GDEs) for electrochemical reduction of carbon dioxide, carbon monoxide, and dinitrogen to value-added products: a review, *Energy Environ. Sci.*, 2021, **14**, 1959–2008.
- 154 D. Li, N. Xu, Y. Zhao, C. Zhou, L. P. Zhang, L. Z. Wu and T. Zhang, A Reliable and Precise Protocol for Urea Quantification in Photo/Electrocatalysis, *Small Methods*, 2022, **6**, 2200561.
- 155 D. Yao, C. Tang, P. Wang, H. Cheng, H. Jin, L. X. Ding and S. Z. Qiao, Electrocatalytic green ammonia production beyond ambient aqueous nitrogen reduction, *Chem. Eng. Sci.*, 2022, **257**, 117735.
- 156 C. Tang, Y. Zheng, M. Jaroniec and S. Z. Qiao, Electrocatalytic Refinery for Sustainable Production of Fuels and Chemicals, *Angew. Chem., Int. Ed.*, 2021, **60**, 19572–19590.
- 157 Annual Report 2019–20 Government of India Ministry of Chemicals and Fertilizers Department of Fertilizers.